Commissioning and validation of the underlying model of a test rig analyzing rotation and expansion performing assemblies in parabolic trough collector power plants

MASTER-THESIS

presented by
Müller, Thore
Sustainable Energy Supply (M.Sc.)

Supervision and Assessment
1st Examiner: **Univ.-Prof. Dr.-Ing. Bernhard Hoffschmidt**
2nd Examiner: **Univ.-Prof. Dr.-Ing. Robert Pitz-Paal**
Tutor: **Dipl.-Ing. Christoph Hilgert**

Almería, January 27, 2017

Declaration of Academic Honesty / Eidesstattliche Erklärung

I hereby declare to have written the present master's thesis on my own, having used no other resources and tools than the listed. All contents cited from published or nonpublished documents are indicated as such.

Hiermit erkläre ich, dass ich die vorliegende Masterarbeit selbständig verfasst und keine anderen als die angegebenen Hilfsmittel verwendet habe. Alle Inhalte, die wörtlich oder sinngemäß aus veröffentlichten oder nicht veröffentlichten Schriften entnommen sind, sind als solche kenntlich gemacht.

_____
Place, Date

_____
Signature

Abstract

In parabolic through power plants, Rotation and Expansion Performing Assemblies (REPAs) compensate for the rotational movement of the absorber tube while tracking the sun to optimize optical efficiency. This movement as well as hostile working conditions, e.g. high pressure and temperature, cause stress that makes REPAs one of the main reasons for leakage of potentially toxic Heat Transfer Fluids (HTFs). A new test rig, that will reproduce accelerated aging under typical operational conditions, is being constructed at the Plataforma Solar de Almería (PSA) under the surveillance of the German Aerospace Center (DLR) and Centro de Investigaciones Energéticas, Medioambientales y Tecnológicas (CIEMAT). It's purpose is to understand and qualify the mechanisms that lead to REPA-failure.

The first part of this work deals with the commissioning of the main measurement assembly, the kinematic unit that will replicate all motion responsible for REPA-aging and the first of later four dynamo-meters that will measure all forces and moments that affect the REPA. This work discusses taken actions and possibilities to reduce the uncertainties of these measurements. This includes a photogrammetric survey of the piping system and test rig machinery in order to verify compliance with the allowed tolerances as well as optimal testing conditions.

The second part describes the validation process of the (ROHR2-) model, that estimates the piping system behavior. The operating behavior of the piping system is examined experimentally, in order to validate the model and to account for manufacturing inaccuracies. Results from simulation and experiment are then compared and statements about the measurement uncertainty will be deduced. In order to reduce said uncertainty, the dynamo-meter has been re-calibrated and it's temperature related behavior has been tested. Further more the sensor- and piping insulation has been improved. Important aspects of continued efforts to improve measurement accuracy are given.

Contents

List of Figures

List of Tables

1   Introduction

At the Paris climate conference (COP21) in December 2015, 195 countries agreed to limit global mean temperature increase to well below 2 °C. This implies significant reductions of global carbon dioxide emissions. The European Union for example targets to reduce emissions by at least 40% by 2030 [1]. Concentrated Solar Power (CSP) strives to be part of the key to reach that goal. At the same time CSP promises to provide cheap energy that ensures economic growth and wealth.

For theses purposes it is indispensable that CSP proves to be a fail-safe and competitive source of energy. Parabolic Trough Collector (PTC) power plants, next to Solar Tower Collector (STC) power plants, appear to be the most promising CSP technology so far. Their success however will depend on improvements regarding cost and safety. One of the most critical parts are the Rotation and Expansion Performing Assemblies (REPAs), flexible tube connections, that link the absorber tubes in the focal lines of the parabolic mirrors and the fixed pipes on the ground, leading to the power block. In a typical solar field there are eight REPAs per collector loop with a cost of approx. 1000 Euro each. [2]. A report of the International Renewable Energy Agency (IRENA) states that for a 50 MW PTC power plant 2.6 Million USD or 0.7% of the investment is needed for swivel joints (i.e. REPAs) [3]. But this is the investment only. Beyond the investments REPA wear requires maintenance during operation and often expensive replacements and repair. The latter require an operation stop and oil discharge of the whole loop which means costly production losses. REPA leakage due to spillage of potentially very toxic HTFs is a severe threat to the environment. REPA failures, which have to be avoided by all means, may lead to fires and explosions, as shown in figure 1.1c, that may also damage other parts of the power plant. It can therefore be concluded that REPAs are an important, expensive and safety relevant part that needs to be well understood.

Currently there are two main types of REPAs: Rotary Flex Hose Assemblies (RFHAs) which consist of a flexible tube and a swivel joint, and Ball Joint Assemblies (BJAs) which are made from three swivel joints connected by two rigid pipes. Examples are shown in figures 1.1a and 1.1b. Regardless of the type used, REPAs have to endure high temperatures and pressures while compensating for rotational and translational motion between the two pipes they connect.

Improvements to the current designs are limited by the fact that the causes of wear and failure, i.e. the pressures, forces and temperatures are not really understood. In fact no test-rig exists yet that reproduces the interaction of all important parameters that occur in daily REPA life. To increase efficiency and thus lower costs in PTC power plants, higher fluid temperatures and pressures are aimed for. This further increases operational loads and the necessity of a better understanding of wear mechanisms. Against this background REPA manufacturers have approached the German Aerospace Center (DLR) to build a test-rig and further investigate REPA wear and failure mechanisms.

(a) Rotary Flex Hose Ass. (RFHA)   **(b)** Ball Joint Assembly (BJA)   **(c)** REPA Failure
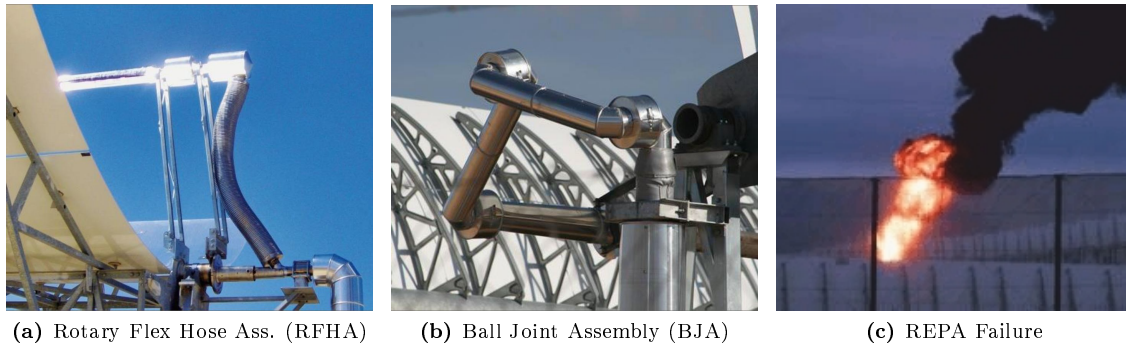
Figure 1.1: Left: RFHA (insulated) with swivel joint connection (here not insulated). Middle: BJA (insulated) [2], Right: Consequences of REPA-failure: fire in an Andasol PTC power plant, 2009 [4].

The DLR and the Centro de Investigaciones Energéticas, Medioambientales y Tecnológicas (CIEMAT) are therefore currently building a new test rig at the Plataforma Solar de Almería (PSA) in Tabernas, Almería, Spain for investigating all different types of REPAs under representative and complete operational conditions. This thesis documents efforts undertaken to accompany the mounting and commissioning process of the test-rig. The main focus is on the validation of the principle behind the REPA-force measurements. A correct measurement of the static and dynamic forces acting on and in the REPA is the key to understanding REPA wear under authentic working conditions.

1.1   REPA working conditions and operational loads

PTC power plants consist of long parabolic troughs that collect and focus sunlight to heat the HTF inside the absorber tubes in their focal lines. The hot HTF is then used as heat source in a steam cycle. Usually troughs, also called Solar Collector Assemblies (SCAs), such as the EuroTrough, are of modular built, consisting of twelve Solar Collector Elements (SCEs) each. One SCE contains 28 mirrors and three absorber tubes. SCEs itself are usually organized in loops of four (or six), connected by eight (or twelve) REPAs. Figure 1.2 shows a standard loop assembly and the positions of the REPAs: two are placed on each 'shared pylon' that interconnects two SCAs and one on each 'end pylon' that supports the free end of each SCA. As HTF temperature rises on its path through the absorber tubes and as pressure drops due to friction losses, every REPA experiences different working conditions.

In all commercial PTC power plants SCAs are oriented in north-south direction, allowing the collector to track the sun on its path from east to west. At every sunrise collectors rotate from their stow position φ_{stow} to the sunrise position φ_r, then while tracking the sun, slowly rotate to φ_s at sunset and back to φ_{stow} at which the collector rests at night. A typical day cycle of a REPA therefore consists of a slow rotation from east to west, followed by a quick rotation back and a longer standstill at rest position during night. During the day HTF temperatures typically rise from 293 °C to 393 °C in

1)

Solar collector assembly (SCA) (e.g.: EuroTrough) composed of twelve **solar collector elements (SCEs)**, six to each side of the drive pylon and with 28 mirrors and 3 absorber tubes per SCE. A U-Shaped loop contains 4 (sometimes 6) SCEs plus 8 (sometimes 12) REPAs

2)

Inlet and Outlet, called cold and hot Headers connect the loop to the grid.

3)

Shared pylon connecting two SCAs and thus carrying two **rotation and expansion performing assemblies (REPAs)**. The respective pylon at the ends is called end pylon, carrying only one REPA.

4)

The **drive pylon** contains the hydraulic system which rotates all 12 SCEs of an SCA at a time. As the whole SCA has a length of 150m, each end, thus each REPA is situated 75m away from the drive pylon. Due to torsion of the whole trough the ends of the SCA do notexperience the same rotational movement as the most inner parts.

Figure 1.2: Schematic description of a typical loop in a PTC power plant and the typical positions of REPAs (black circles) and drive pylons (small black squares). The HTF is heated between inlet and outlet, inside four SCAs (e.g.: EuroTrough) before being brought back to the power block in order to fuel the steam cycle. Sources: Photos 1) and 2), as well as the basis for the drawing and information from [5] and photos 3) and 4) taken at Andasol Power Plant by DLR.

the absorber tubes between inlet and outlet of a loop. At the same time HTF pressure usually drops from 30 bar at the inlet to 20 bar at the outlet. Consequently average operational conditions are 350 °C and 25 bar. During night HTF temperatures usually do not fall below 110 °C [6]. During its 25 year lifetime a REPA is set to execute approximately 10.000 of such hot-cold rotation cycles [7].

Every day the collector tracks the sun on it path between sunrise and sunset. This motion appears to be identical every day and continous at macro level, omitting the seasonal influences. This however is not true for the micro-level: The tracking algorithm usually recalculates the exact position of the sun every 20-40 seconds. The two hydraulic cylinders of the drive pylon then rotate the whole trough according. In order to control and stabilize the overall power generation process it is common practice to eventually delay optimal tracking to lower the heat intake [8]. This practice is called *dumping* and leads to additional rotational motion. Time-discrete tracking and superimposed dumping lead to small intermittent movements of the cylinder pistons that adjust the rotation
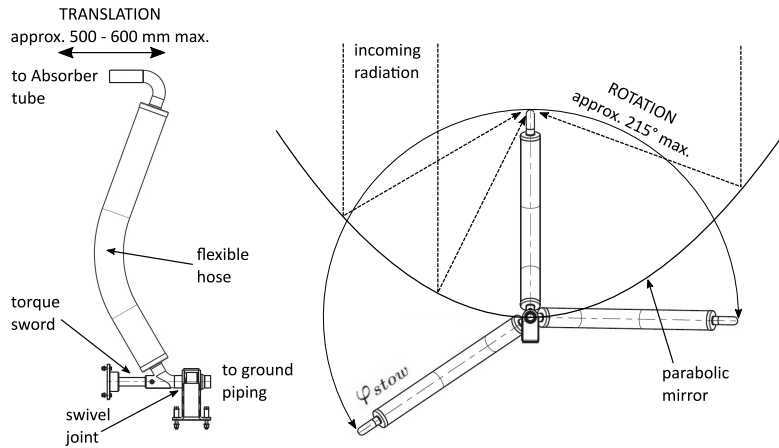
Figure 1.3: REPA translation and rotation at the example of a RFHA: due to absorber tube heat dilatation, the upper end experiences up to 600 mm of translational motion which is compensated for by the flexible hose. During one day a REPA experiences up to 215° of rotational motion which is compensated for by the swivel joint. The necessary torque that is needed to move the swivel drive is transduced by the torque sword, which forms a rigid connection to the collector structure.

angle φ of receiver and REPA. Consequently operational motion itself is discontinuous, even at drive pylon level. Additional *breakaway torques* apply. They delay the rotation experienced by the outer ends of each SCA and thus by each REPA. Once the torque applied by the drive pylon exceeds the combined static friction of all bearings, the rotation breaks free and the REPAs perform a swift rotation step.

In addition to the rotational motion REPAs also experience translational motion depending on the average absorber tube temperature which causes heat dilatation. The maximum change in length of all combined absorber tubes on one side of the drive pylon is ≈ 600 mm. REPAs have to compensate for this translational motion at the outermost end of the collector. In real-life applications absorber tube temperature fluctuations due to clouds and dumping superimpose additional mini-cycles, that make "approx. 13% of the total dilatation"[8, p.37] and that have to be considered as well.

The REPA test-rig at Tabernas will be the first of its kind to a) reproduce all loads previously mentioned and b) do this in an accelerated manner. The only loads that can not be tested are those from weather and spillage. Weather effects, such as wind and rain are believed to be negligible concerning REPA lifetime and would hurt the measurement equipment. Spillage is direct irradiation of concentrated sunlight which misses the absorber tubes and occurs at lower elevation angles, usually at the northern end of a SCA (northern hemisphere). It leads to increased temperatures of the insulation material covering the REPA. The effect on REPA lifetime is still unknown. For more details on REPA loads and typical day cycles, please have a look at the master's thesis of Andreas Plumpe [8]. Knowing all the parameters to be measured the appropriate test-rig design was developed.

2 REPA test-rig

The concept of the REPA test-rig is to simultaneously rotate two REPAs in various translational positions, while hot and pressurized HTF is flowing through them. This task requires the work of three mayor sub-units: The Kinematic Unit (KU) is responsible for all mechanical stress simulation, the HTF-Cycle assures correct and representative HTF-temperatures, -pressures and -mass flow rates and finally the Supervisory Control and Data Acquisition (SCADA)-System and monitors correct functioning of the two previously named sub-units and at the same time gathers all of the required data. Figure 2.1 shows a sketch of the test-rig: Kinematic Unit (KU), HTF-Cycle and both electrical cabinets that contain the SCADA-System.

The *main assembly* is a term to describe the KU, the traverse and the two tables the REPAs are placed upon. Figure 2.2 shows the state of the test-rig end of January 2017. The KU consists of the hydraulic system, which actuates the four hydraulic cylinders inside and on top of the drive pylon. The traverse that connects the upper ends of both REPAs is carried and rotated by the inner two drive pylon arms. The outer swivel drive arms solely serve to transfer the rotational motion to the swivel drives of the REPA (compare figure 1.3).

The HTF-Cycle consists of a pump, that generates makes the HTF flow circular and six electric band heaters. Further more there is an expansion vessel that compensates for the thermal expansion of the HTF by introducing nitrogen into or evacuating nitrogen from the expansion vessel. The nitrogen system is also responsible for the system pressure. A bypass that shortcuts the main assembly guarantees quick separation of pump and main assembly in case of any failure.

The SCADA-System is divided into five main areas (Observe System / Check Status, Operate HTF cycle, Operate Kinematics Unit, Data Acquisition and Human-Machine Interface). It's subsystems are the Programmable Logic Controller (PLC) that carries out most basic operations such as cylinder movements that require safe and fault-free running, the Graphical User Interface (GUI) done in LabVIEW (LV) that shows results and offers more sophisticated tools for evaluation and finally the Open Platforms Communications Server (OPC-Server) that is the interface between LV and PLC. Please refer to the work of Tobias Hilbel for more information [9].

2.1 Reproducing representative REPA working conditions

All three sub-units work together to reproduce all important REPA working conditions: rotational and translational motion as well as HTF-temperature, pressure and mass-flow rate.

The life of a REPA can be seen as a sequence of many day-cycles. These day-cycles are mainly defined by the rotational motion. The test-rig is designed to perform a
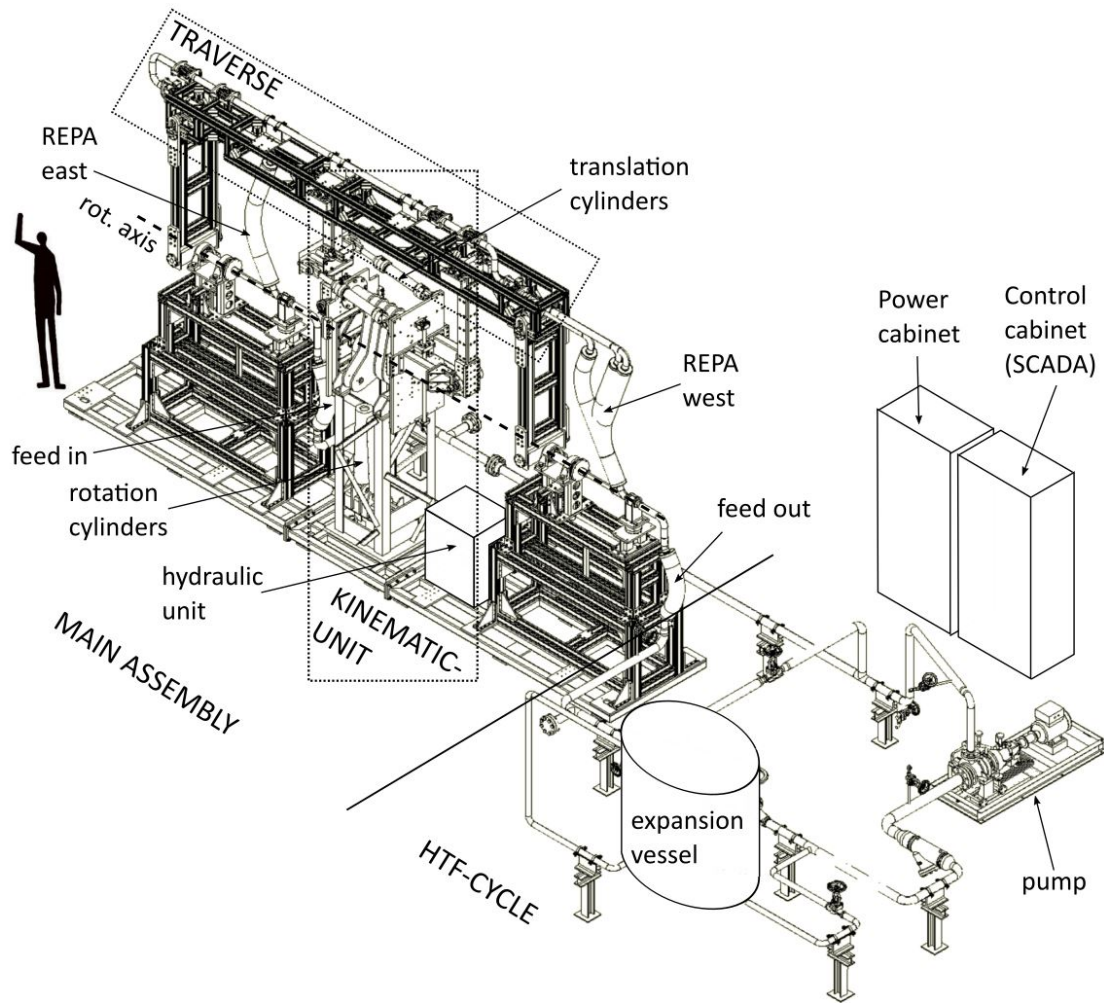
Figure 2.1: A sketch of the REPA test-rig with its sub-units and REPA positions. The hydraulic control unit that actuates both rotation and translation cylinders is situated in the space between drive pylon and the right table. The only part missing in the sketch is the nitrogen system which compensates for the change in volume of the HTF when heated. More detailed sketches of all main parts with indications and names of all parts can be found in appendix A.2.

rotational motion from stow position $\varphi = -120°$ to end position $\varphi = 90°$. This means a total rotation of 210°. The hydraulic system that is responsible for all motion has been specifically chosen to be able to perform swift rotation steps to approximate dumping and break-away torques. In the test-rig this is facilitated by an hydraulic system. In order to reduce the influence of hydraulic damping in this system the hydraulic unit has been placed as close to the cylinders as possible. All hydraulic connections are done with rigid tubes where possible.

The translational motion is executed by two parallel cylinders that rotate the drive pylon arms, altering the horizontal distance between traverse and HTF-cycle connection of each REPA. The piston movement translates to a translational motion which really is

Figure 2.2: The main assembly as built including insulation and REPAs with the traverse still resting on additional supports at stow position.

a rotational motion and therefore measured by a translation angle θ. Even though the design of the test-rig allows up to 45° of such rotation, only a fraction of this range will actually be used to reproduce the 500-600 mm of heat dilatation at maximum temperature. Therefore the small angle approximation applies, meaning that a linear relation between θ and absorber pipe temperature can be assumed. According to the manufacturer the small change in focal length is negligible for REPA lifetime.

The HTF temperature ϑ_{HTF} is maintained by six high performance band heaters with 3.500 W of power each, put around pipes leading to the traverse. All tubes are covered in 120 mm of insulation material allowing HTF temperatures up to 450 °C to also test new silicone oils with higher maximum temperatures. The maximum design temperature was set to 500 °C. The pump as the heart of the HTF-cycle is responsible for the hydraulic loads: HTF mass flow rate $\dot{m}_{HTF}$ with a range of 6 to 60 m/h^3 and HTF pressure p_{HTF} up to 40 bar. HTF density ϱ_{HTF} usually depends on HTF temperature ϑ_{HTF} and the fluid used (HELISOL©for commissioning).

Next to this operating parameters is is also possible to investigate the effect of exceeded mounting tolerances. A photogrammetric setup has been provided, making it possible to accurately determine and set REPA installation position and orientation in order to test the effect of tolerances and ill-positioning. A detailed list of all REPA parameters and specifications as well as some remarks on limitations and problems can be found in appendix A.1.

Once put in operation the test-rig will will perform up to 400 cycles a day, trying to represent a whole REPA life-span of 25 years (approx. 10000 day-cycles) in only a few weeks or months [7]. In an actual power-plant REPAs slowly rotate from $\varphi_r \approx 90°$ at sunrise to $\varphi_s \approx -90°$ at sunset. After that they are quickly rotated to their stow position φ_{stow} where they are left during the night. Usually $\varphi_{stow} \approx \varphi_r$ meaning that the quick rotation is done while the system is still hot. If $\varphi_{stow} \approx \varphi_s$ the rotation back

7

happens just a few moments before sunrise, i.e. in cold state. Due to the thermal inertia of the system, it will be impossible to perform an alternating sequence of 'hot' and 'cold' rotations. Instead there will probably be some 'hot' followed by the same number of 'cold' rotations. The question whether this approach leads to results comparable to real-life wear is not part of this thesis, but will be subject to future research. The same applies to the maximum acceleration ratio[1] which will depend on how accurate the typical operational conditions have to be reproduced in order to recreate failure scenarios.

Although similar in appearance, the traverse does not represent the absorber tubes, meaning that one side experiences 'inlet'-conditions, while the other experiences 'outlet'-conditions. Both REPAs always represent the same of the eight possible positions inside the a loop (compare figure 1.2). That way both experience similar stresses and their results can be directly compared to each other.

2.2   REPA force measurement

In order to understand the reasons and mechanisms that lead to REPA-wear and finally to its failure, there are four dynamo-meters that measure the forces and moments each REPA exerts onto its bearings. Both REPAs, called 'west' and 'east', rest on two dynamo-meters each, one on top and one at the bottom. The dynamo-meters are therefore referred to as 'top-west', 'bottom-west', 'top-east' and 'bottom-east'. Figure 2.3 indicates test-rig motion and dynamo-meter positions. Dynamo-meters are measurement devices based on strain gauges that transduce forces and moment into signals. For all force and torque measurements a K6D175 - dynamo-meter from 'ME-Messsysteme' is used. This sensor measures x-, y- and z- components of the forces and moments the bearing supports that is placed on top of the K6D175. A measurement amplifier then transforms these voltages into three forces and three moments, here called the dynamo-meter reading F_{dyn}.

---

[1]The actual acceleration ratio is the life span divided by time needed to represent life span
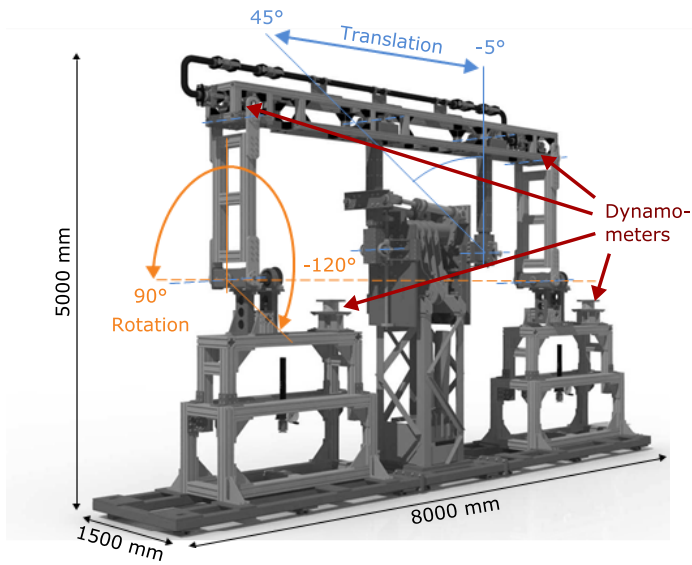
Figure 2.3: A sketch of the REPA test-rig main assembly: the Kinematic Unit (KU) and the traverse chapter of the HTF-Cycle, without REPAs. The dotted orange line represents the axis of rotation, the dotted blue line represents the axis of translation. The red arrows indicate the positions of the four dynamometers. Graphic taken from [8, p.66]

REPAs and the adjacent traverse piping system are directly mounted onto the dynamo-meters and held in place by a location bearing/ floating bearing combination. This is shown in figure 2.4. During test-rig operation the dynamo-meters therefore measure the **sum of forces** and moments stemming from the respective adjacent piping system and the REPAs. To be able to subtract the effect of the adjacent piping system from the dynamometer reading, it has to be approximated with a simulation. The simulation is done with ROHR2 pipe system simulation software, the model will be referred to as the *ROHR2-model*.

Naturally every model is a simplification of the actual technical system and thus has to be erroneous to some extend. To keep the relative error made by the simulation as small as possible, the heat dilatation of the traverse piping system is compensated by two angular and one gimbal compensators, also reducing the resulting forces onto the the dynamo-meter bearing.

Top Position:

$$h_{fix} = \begin{pmatrix} 0 \\ -102,5 \ mm \\ 136,7 \ mm \end{pmatrix}$$

$$h_{float} = \begin{pmatrix} 0 \\ 133 \pm 2,5 \ mm \\ 136,7 \ mm \end{pmatrix}$$

$$h_{REPA} = \begin{pmatrix} 0 \\ -102,5 - 496,8 \ mm \\ 136,7 \ mm \end{pmatrix}$$

$$h_{dyn} = h_{ROHR2} = \begin{pmatrix} 0 \\ 0 \\ 0 \end{pmatrix}$$

Bottom Position:

$$h_{float} = \begin{pmatrix} 0 \\ 0 \\ 156,8 \ mm \end{pmatrix}$$

$$h_{dyn} = h_{ROHR2} = \begin{pmatrix} 0 \\ 0 \\ 0 \end{pmatrix}$$
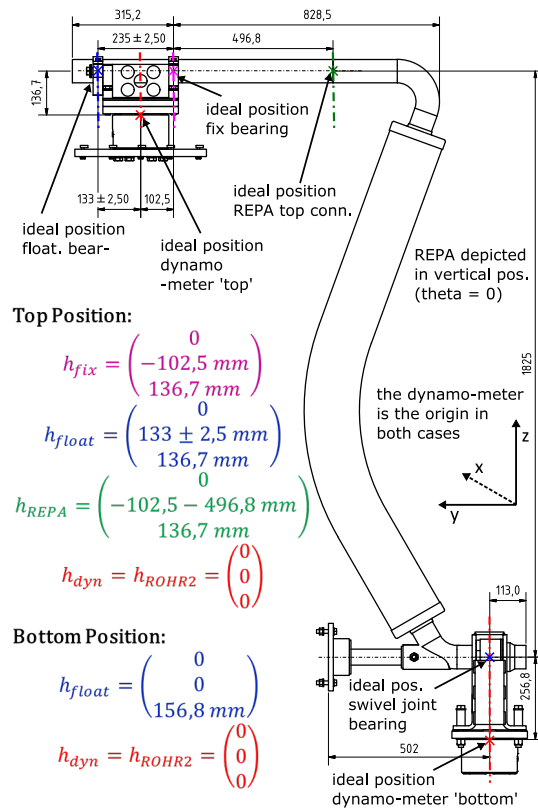
Figure 2.4: The graphic shows a technical drawing of one of both REPAs 'as build' for translation angle $\theta = 0°$.

The dynamo-meter reading F_{dyn} can be represented as the sum of forces and

moments exerted by fix and floating part of the dynamo-meter bearing.

$$F_{dyn} = F_{fix} + F_{float} \tag{2.1}$$

As the effect of the piping system is known from the ROHR2 model, the REPA forces and moments can be calculated using a simple substraction, as shown in equation 2.2.

$$F_{dyn} = F_{piping\ sys} + F_{REPA}$$
$$F_{piping\ sys} = F_{ROHR2} \tag{2.2}$$
$$F_{REPA} = F_{dyn} - F_{ROHR2}$$

The ideal positions of bearings, dynamo-meters and REPAs are not identical, levers have to be taken into account when calculating the resulting moment. Ideal positions and levers h are shown in figure 2.4.

$$M_{ROHR2} = M_{fix} + M_{float} + F_{fix} \times h_{fix} + F_{float} \times h_{float}$$
$$M_{REPA} = M_{dyn} - M_{ROHR2} - F_{REPA} \times h_{REPA} + F_{ROHR2} \times h_{ROHR2} \tag{2.3}$$

So far only the top-west position is equipped with a *K6D1175 - 10kN/1kNm* dynamo-meter from ME-Messsysteme. The other three positions are filled with 'dummies' (simple blocks of steel with matching dimensions). Dynamo-meter positions and their motion and rotation during test-rig operation is indicated in figure 2.5.
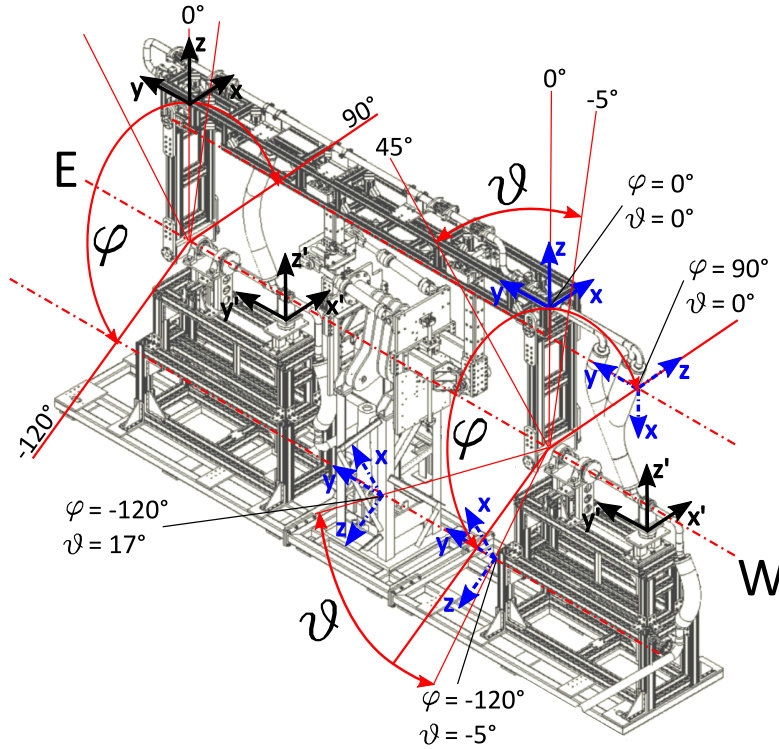
Figure 2.5: Dynamo-meter positions during operation: both rotation φ and translation ϑ lead to dynamo-meter displacement. In blue: a few positions of dynamo-meter top-west. Dynamo-meters top-east, bottom-east and bottom-west indicated in black.

As the implementation and mounting of the test-rig continues, the three vacant positions will be equipped with dynamo-meters. Due to more detailed knowledge about future measurement circumstances, another dynamo-meter model might yield better results. The same applies for the ROHR2-model: For the lower position no such model exists yet and thus will have to be created. The experiences made during this thesis will help to do this in an efficient manner.

2.3   Content of this work

This thesis aimed to support the mounting and commissioning process of the REPA test-rig. First chapter 3 explains the dynamo-meter measurements and investigates the expected measurement error. Chapter 4 then deals with the two photogrammetrics that were done to align all rotation axes to the main rotation axis as an important step during mounting and to derive the exact dimensions of the traverse piping system for the ROHR2 model. This thesis further deals with the validation of the ROHR2 model. Chapter 5 presents chosen parameters and discusses results. Chapter 6 compares model and experiment in order to evaluate the predictions made and make improvements to the model. Validation experiments also led to improvements at the test-rig, mainly concerning insulation and sensor cooling. These are presented in chapter A.9. Finally the whole work is then summed up and evaluated in chapter 7.

3 Dynamo-meter measurements and uncertainty

Every force measurement chain consists of a sensor that transduces the physical forces and moments into a measurement signal, a signal amplifier and some indication device. At the REPA test-rig the first dynamo-meter is a K6D175 from ME-Messsysteme, shown in figure 3.1.

Figure 3.1: Right: Dynamo-meter K6D175 10kN/1kNm; Center: Measurement amplifier GSV-1A16USB K6D/M16; Left: Computer with measurement software GSV-multi running.

Figure 3.2 depicts a graphical representation. Normally we assume a linear behavior for both sensor and measurement amplifier, which means that the whole chain has a linear dependency of amplifier output voltage U on the forces (and moments) applied F. We will call the result displayed the dynamo-meter reading F_{dyn}.
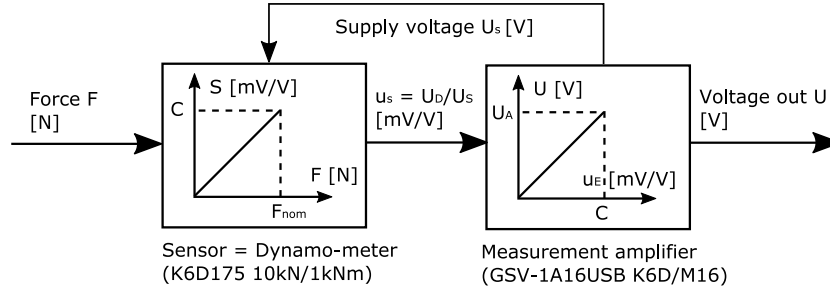
Figure 3.2: A scematic representation of the measuerment chain, transducing a physical quantitiy into an output voltage. Source: [10]. As the bridge voltage U_D is proportional to the supply voltage U_s, that is provided by the measuring amplifier, the output signal u_S is usually given in relation to the supply voltage.

This linear behavior can be expressed by a simple expression using the calibration matrix K:

$$F_{dyn} = K \cdot U \tag{3.1}$$

K is fully equipped, 6x6 matrix. Therefore all six channels of U have an influence on each of the three forces and three moments of F_{dyn}. If only one of the channels is defect, none of the results displayed is accurate. For detailed information on the linearity of

both dynamo-meter and measurement amplifier as well as other useful information please read the appendix A.3 and have a look at the glossary.

3.1 Measurement Uncertainties

Generally speaking, equation 3.1 is never fully valid. Even at calibration loads and calibration temperature, uncertainties have to be taken into account when interpreting the results. These can be split in three groups:

- **Measurement uncertainties that affect the zero-signal:**
  - zero signal when mounted S_{F0}
  - rel. reversibility error (hysteresis error) μ
  - rel. creep d_{cr}

- **Measurement uncertainties that affect the characteristic:**
  - rel. linearity error d_{lin}
  - rel. repeatability error b_{rg}
  - uncertainties from calibration on basis of an inappropriate load scenario

- **Temperature related uncertainties:**
  - temperature effect on zero signal TK_0
  - temperature effect on characteristic value TK_C
  - difference in zero signal due to increased sensor temperature $U_{0,\vartheta}$
  - difference in zero signal after complete heating cycle $\Delta U_{0,20C}$

In order to keep the measurement uncertainties as low as possible all dynamo-meters should be comissioned according to the document 'Inbetriebnahme von Sensoren' published by ME-Messsysteme [11]. Information about uncertainties are taken from the FAQ and documentation chapter of www.me-systeme.de (20.11.2016), as well as VDI2638 [12].

Effects on Zero Signal

The *Zero signal* is the output signal of the unloaded sensor. A distinction is made between the zero signal when removed S_0 (no mounting parts) and the zero signal when mounted S_{F0} (not mechanically loaded, with mounting parts, at the beginning of a loading cycle) [12]. Values are given in appendix A.3.

S_0 itself, or its expression U_0 in Volt are far from being zero. The multiplication with K yields forces as high as $-400\,\mathrm{N}$ (Compare equations A.10 and A.12 in the appendix.) Therefore no measurement is valid if neither a) the zero signal stated in the calibration certificate is subtracted from the output signal before being multiplied with K, or b) the dynamo-meter reading is defined to be zero at the beginning of a measurement (offset compensation). On the one hand b) has advantages over a) as regular offset compensation ensures that possible changes to the zero signal are accounted for as well. On the other hand a) is an absolute measurement, while b) is only relative.

Looking at figure 3.3 we can see that S_{F0} possibly differs from S_0. This is due to the effect of mounting the sensor on an uneven surface or onto soft material such that tightening the sensor screws leads to its deformation. During sensor mounting the change of zero signal should therefore be measured and evaluated. This effect constitutes another reason to choose b) over a).
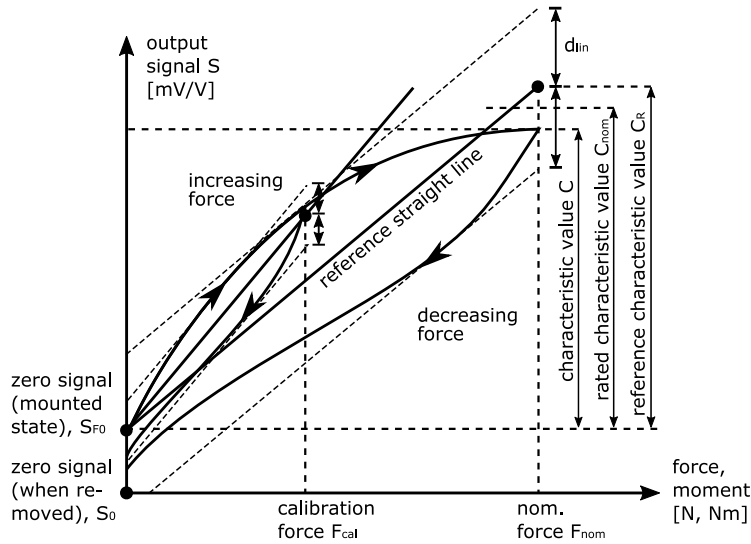
Figure 3.3: This figure, based on a graphic in VDI 2638[12, p.9], shows a schematic sensor characteristic, that would be obtained when plotting the sensor signal during applying an increasing force starting from zero up to nominal force F_{nom} and then back down to zero. The so-called reference straight line that will be used as characteristic curve represents a best fit of the curve obtained (It's exact derivation is described in DIN EN ISO 7500-1 [13]). The black curve represents the standard case when the sensor is calibrated for rated force F_{nom}, the second curve represents the special case when the sensor is calibrated for a different load scenario F_{cal}. C is the true signal measured at calibration force, C_R is the linear approximation evaluated at calibration force and C_{nom} is the value stated in the data-sheet or calibration certificate. Representation of uncertainties exaggerated and axes not drawn to scale for better visibility.

Another measurement uncertainty related to the zero signal is the rel. reversibility error or hysteresis μ, which describes the biggest difference between sensor output signal for an increasing and decreasing force from zero to rated force (Alternatively the hysteresis can also be given for specified forces such as 50% of the nominal force μ_{50} [12]). Figure 3.4-A shows that due to this the zero signal might change after one cycle (*german: Nullpunktrückkehrfehler*). The explanation are smallest in-elastic deformations of the casting compound that the sensor hull is filled with. To eliminate this change of zero

signal the sensor should be completely unloaded and set to zero after each cycle. This of course is not possible at the REPA test-rig which is why the error has to be taken into account at all times. Likewise, there is a temperature-related reversibility error that is equal to the difference in zero signal after one complete heating/cooling cycle. During test-rig operation the total hysteresis error might be bigger due to friction inside floating bearings.

Finally there is the rel. creep d_{cr}, which is represented in figure 3.4-C. Creep means the change in sensor output signal some time (usually 30 min) after loading or unloading a sensor. This means that d_{cr} does not apply if the sensor is loaded and then unloaded after a few seconds, as it is done during sensor calibration. At the REPA test-rig however, loading is continuous and lasting, d_{cr} therefore always applies and has to be added to the uncertainties stated in the calibration certificates.

Effects on Slope of Characteristic Curve

The rel. linearity error d_{lin} is defined as the maximum difference between actual sensor signal and reference straight line in 95% of the times a loading cycle is applied. d_{lin} and the rel. reversibility error μ are similar but not equal. As both describe the same phenomenon, resulting uncertainties may not be simply added. The same applies to the rel. repeatability error b_{rg} which describes the spread (2σ) of the output signal at nominal forces. Please compare figure 3.4-A. All these uncertainties are included in the uncertainties stated in the calibration certificates.
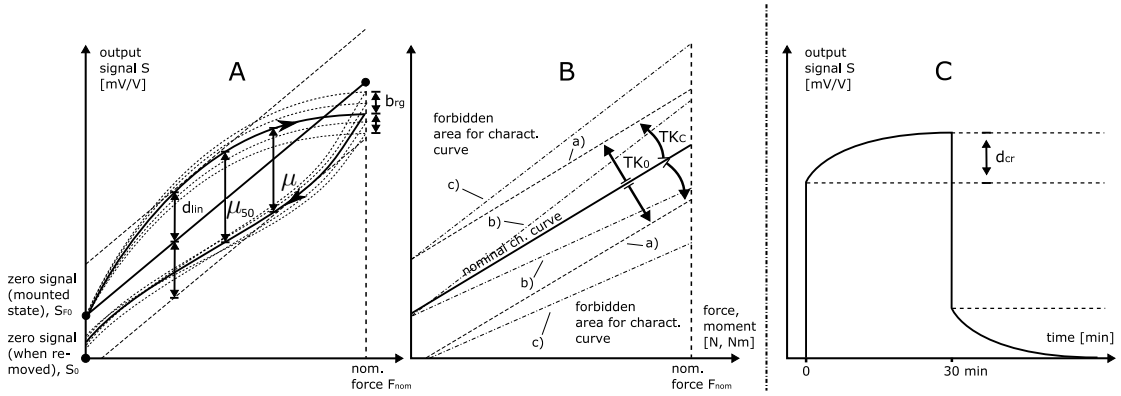
Figure 3.4: A schematic representation of most uncertainties affecting the dynamo-meter measurements. Values (95% confidence interval) are given in the data sheet [14]. Their possible effect is being evaluated in table A.4.2. A and B share the same axes: sensor output signal S vs. force F, C shows S vs. time. The uncertainties depicted are: A - rel. linearity error d_{lin}, rel. reversibility error μ, rel. repeatability error b_{rg}; B - temperature effect on zero signal TK_0, temperature effect on characteristic value TK_C; C - rel. creep d_{cr}. Please see the glossary for further information. Representation of uncertainties exaggerated and axes not drawn to scale for better visibility.

As most estimations for measurement uncertainties scale with the calibration loads (normally equal to the upper limit of the measurement range) and not with the actual

15

measurement value (compare the data sheet of the K6D175 dynamo-meter [14]) the relative uncertainty increases for smaller loads. This represents a first reason to have the sensor calibrated for the most representative load scenario possible. The second good reason is that the slope of the characteristic curve is dependent on the the calibration force F_{cal} as the comparison between the two curves in figure 3.3 indicates. This means that in order to keep calibration errors as small as possible, calibration loads should always be chosen in the range of the expected loads during operation. For all future sensor purchases for the three dynamo-meter positions that are still vacant, it is strongly recommended to buy the smallest sensor possible. This has advantages both accuracy and money-wise. Concerning safety, please keep in mind that for force transducers from ME-Messsysteme the failure load is 300% of the nominal load. Please also read the advice and information given in appendix A.5.

Temperature related Uncertainties

The nominal calibration curve is given for a specific calibration temperature, which is stated in the calibration certificate of the K6D175 [15] to be (21±1.5)°C. A sensor temperature that deviates from the calibration temperature leads to increasing measurement uncertainties. Figure 3.4-B shows that this is equivalent to a wider area the calibration curve possibly lies in and can be split up in two separate effects. First: The temperature effect on zero signal TK_0, which is equivalent to a possible parallel shift of the nominal calibration curve (lines a)). And second: The temperature effect on characteristic value TK_C, which is equivalent to a possible changing slope of the nominal calibration curve (lines b)). The total effect is the sum of both parts (lines c)).

The difference between TK_0 and TK_C is that there are two relatively easy ways to get rid of TK_0. The first possibility is to make sure that the sensor heats up before applying the first loads. That way, the change in zero signal can be neglected by simply offset compensation of the output (i.e. setting its value to zero which is equal to subtracting the initial value from every output) before starting the measurement. This however is not possible at the REPA test-rig, as the dynamo-meter and the piping system have a closed connection. However, it is possible to measure the TK_0 in un-mounted state (either completely free or with some parts connected) by putting the sensor in an oven and track both temperature and difference in zero signal due to increased sensor temperature $U_{0,\vartheta}$[2]. This will be referred to as *temperature test*. Under the assumption that conditions during temperature test and later operation are identical, this data can be used to mathematically exclude its effect from the dynamo-meter reading F_{dyn}:

$$F_{dyn}' = F_{dyn} - K \cdot U_{0,\vartheta} = K \cdot U - K \cdot U_{0,\vartheta} = K \cdot (U - U_{0,\vartheta}) \qquad (3.2)$$

The underlying assumptions are that there are no temperature and time gradients, meaning that the temperature distribution is always perfectly homogeneous and changes infinitesimally slow (steady state). Further more, we assume that $U_{0,\vartheta}$ is independent of

---

[2]Please note that the output signal has either the unit V or mV (symbol U) or the unit mV/V (symbol S). Compare appendix A.3 for explanations.

the loads applied and the mounting situation. In chapter 3.2 we will see that there is good reason to believe that both assumptions do not always hold. The change in zero signal after one complete heating/cooling cycle is $\Delta U_{0,20C}$.

3.2   Measurement Uncertainty Estimation

Normally all sensors are calibrated for nominal forces which more or less represent a reasonable upper limit for the expected loads: $F_{nom} = F_{calib} > \approx F$. At the REPA test-rig however, the dynamo-meter had been chosen in order to withstand the forces that would break a standard absorber tube support in a PTC power plant, multiplied by some security factor. The results were nominal forces in the range of 10-20 kN and 1-2 kN m, compared to best estimation of operating forces these make only approximately 10-20% of the forces and 50-70% of the moments. Please compare the appendix, table A.4.1 for calculations and exact values. The estimated load scenario will be the basis for all evaluations of uncertainty improvements.

When the first dynamo-meter was bought, a calibration was done for nominal forces and as it is good practice, the calibration was done for the whole measurement chain[3]. For the calibration, the dynamo-meter is clamped into a hydraulic press which then applies a set of known forces and moments. The output signal U is logged during approx. 80 distinct load stages, with three repetitions each. Between two loading cycles, the sensor is unloaded completely each time and offset compensated. Maximum load is applied for 30-40 seconds to account for transient oscillations. The results are then used to derive the 36 degrees of freedom of the 6x6 calibration matrix using a linear regression.

Calibration measurement data is also used to estimate the measurement uncertainties. These are calculated on the basis of twice the maximum difference within the three repetitions per load stage. Due to the fact that calibration measurements only last a few seconds and are done at ambient temperature, the found measurement uncertainties do neither include the relative creep d_{cr} nor any of the temperature related uncertainties. To be able to do that a re-calibration was done based on a load scenario estimated with data from first validation experiments (compare appendix A.8). The re-calibration included a temperature test which gives data for the temperature effect on zero signal TK_0, difference in zero signal due to increased sensor temperature $U_{0,\vartheta}$ and difference in zero signal after complete heating cycle $\Delta U_{0,20C}$.

When having to interpret measurement results, a single value for the measurement uncertainty comes in handy. In order to derive the measurement uncertainty of the REPA test-rig, individual values have been summed up in table A.4.2 of the appendix. There are three cases being compared: 1) the original state where calibration data was available for nominal loads only, 2) the current state after first re-calibration and the

---

[3]dynamo-meter (K6D175 10kN/1kNm, SN: 15401935) + amplifier (GSV-1A8USB K6D/M16, SN: 15156211.)

first temperature test and 3) an idealized future where temperature effect on zero signal TK_0 is perfectly known due to an advanced and repeated temperature test.

The total measurement uncertainty always depends on the calibration loads F_{cal}, the actual loads applied F and the dynamo-meter temperature ϑ_{dyn}, compare appendix A.3.2. In our comparison, all three parts of the table assume the worst case scenario of $\vartheta_{dyn} = 70\,°C$ and F being equal to the best estimation possible, derived in table A.4.1 in the appendix. What changes from case to case is the information about the behavior of the sensor.

This means that we can use the table to assess the improvements made and possible future improvements: Due to the re-calibration, the total non-temperature related uncertainties dropped by 56.6% in average. Together with the data from the first temperature test, total uncertainty estimates are now in average 67.8% lower than they were originally. Yet, there is still room for further improvement: If we assume that a repeated advanced temperature test yields perfect knowledge about the sensors behavior when heated, it is theoretically possible to simply subtract this behavior from the results and assume an uncertainty of zero. However, repeated test will most likely show that results spread a little, which is why the uncertainty in the end will be slightly greater than zero.

3.3   Implications of re-calibration and temperature test

In a perfect world there would be no difference between original and re-calibration matrices. Due to sensor aging however, and the circumstances shown in figure 3.3 we don't get the same values. This is supported by equation A.13 and table A.3.1 in the appendix.

As long as none of the forces and moments exceeds the re-calibration scenario, we can use the re-calibration matrix. In case any of the forces measured (absolute values!) exceeds the re-calibration scenario, both result and expected uncertainties (without temperature and aging effects) can be linearly interpolated according to equations A.17 and A.18 in the appendix.

For the temperature test by ME-Messsysteme, the free sensor has been put in an oven and heated up to $5\,K$ below its maximum operation temperature of $85\,°C$. The zero-signal has been continuously tracked. Exact temperature however has only been logged at the beginning, its peak and after reaching ambient temperature again. Figure 3.5 shows the results. the x-axis however does not represent temperature, as this has not been tracked. The only information we have that temperature steadily increases, then decreases, probably asymptotically and given enough time to even out temperature gradients. This lack of information significantly reduces our means to interpret the graphs.

Still we can make an interesting observation: In the cases of F_x, F_y and M_y the maximum error is reached shortly after the begin of either heating or cooling phase, in
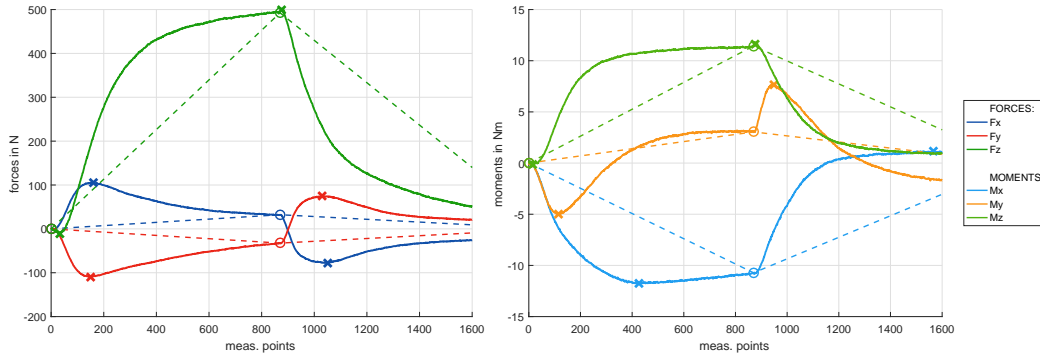
Figure 3.5: The results of the temperature test: the physically meaningless zero signals have been transformed to resolving forces and moments. Duration of test approximately 2 hours. Cross-markers for extreme values, circle markers for measurements for which temperatures are known. Dotted lines for eye guidance.

opposed directions. After that the value asymptotically converges to its final value at 80 °C, just like F_z, M_x and M_z do not show this behavior. We could suspect that the first group is more sensitive to temperature gradients (time or spacial) than the second.

The measurement data I obtained from ME-Messsysteme and which is plotted in figure 3.5 does not cover the end of the measurements. If they did, we would see that the forces and moments do not go back to zero, as it is stated in the calibration certificate. This behavior is called difference in zero signal after complete heating cycle $\Delta U_{0,20C}$ and part of the uncertainty estimation of table A.4.2 in the appendix. It can be interpreted as evidence for increased sensor aging after a few temperature and load cycles only (14 temperature validation experiments of a few hours each, compare chapter 6.1). Later during test-rig operation the sensor will eventually be loaded for thousands of cycles and months of time without being completely unloaded once. Severe aging and thus increases uncertainty could be an issue.

Sadly no standardized test procedure exists to evaluate and describe the long-term behavior of force transducers, which is why no respective parameters are given in neither data-sheet nor calibration protocol. I will therefore name two possibilities to deal with this issue: First, instead of one temperature test, many consecutive tests could help understand how $\Delta U_{0,20C}$ behaves over time. Second, Before mounting the sensor, some reproducible measurements with examination weights and levers should be performed, which could be repeated after a greater number of cycles to subsequently estimate the uncertainty from sensor aging.

Third, all measurements could be changed to relative measurements by regularly performing an offset compensation (setting all values to zero). In this sense, regularly could for example mean every time that the traverse begins a new cycle at $\varphi = 90°$ or every time the sensor reaches a certain temperature. The results would still be comparable, uncertainties would drop, but there would be no information about absolute forces onto the sensor.

4 Photogrammetry

The new REPA test-rig is meant to produce precise and accurate measurements of the stresses that lead to the deterioration of REPAs. Further more, the possibility to precisely measure the positions of both REPA connections allows intended misalignment of components in order to investigate its effect on REPA lifetime. In order to guarantee good functioning and reliable measurements, the test rig must conform with specified tolerances. During this thesis the exact geometry of the traverse piping system, treated in chapter 4.1, as well as correct orientation and alignment of all rotation axes, treated in chapter 4.2, were of special interest.

To verify these, a quick, efficient and accurate measurement of relative positions and distances between machine parts was required. After a first attempt with a tachymeter failed, a photogrammetric approach was chosen. Although more time and material expensive in the preparations, a photogrammetry has the advantage to be easily and very cost-effectively repeated, once the setup is put in place. The approach therefore offers the possibility to verify deformations due to mechanical stress and/or heating later during operation.

Close range photogrammetry (hereafter referred to as photogrammetry) is a computer-based measurement method that calculates 3D-positions of retro-reflecting targets from a set of photos taken from various perspectives. The photos can be taken by a normal SLR camera and a flash, the post-processing is done by specialized software, such as AICON 3D Studio in this case. A photogrammetry setup consists of coded and uncoded targets made from retro-reflective foil, scale bars and a coordinate cross. If a target appears on enough photos there is only one possible solution for their relative position in space, that can be iteratively found using a numerical approach. References sticks, that have a very precisely known length help to scale relative distances of points and increase the results accuracy. The coordinate cross serves to specify a first coordinate system for better orientation. For general information about close range photogrammetry please refer to [16], for information about the use of photogrammetry in CSP, please refer to [17].

The first step in a photogrammetry measurement is to put the targets onto the structure. The uncoded targets are put on every point of interest, as well as the background and other parts to give the setup more depth and create a more homogeneous point-cloud, which also improves measurement accuracy. If a measurement point itself is hidden, such as the center line of a pipe, an indirect measurement is needed: uncoded targets are put around the pipe circumference forming a circle, a so-called *sleeves*. The center is then later calculated by fitting a circle in the points on the pipe surface. In other cases adapters can help, e.g. bolts that exactly fit pockets which center needs to be measured, but stand out and can be equipped with targets.

The second step is then to make photos (about 200-300 per measurement) from various angles and from all around the structure, if needed with the help of a lifting
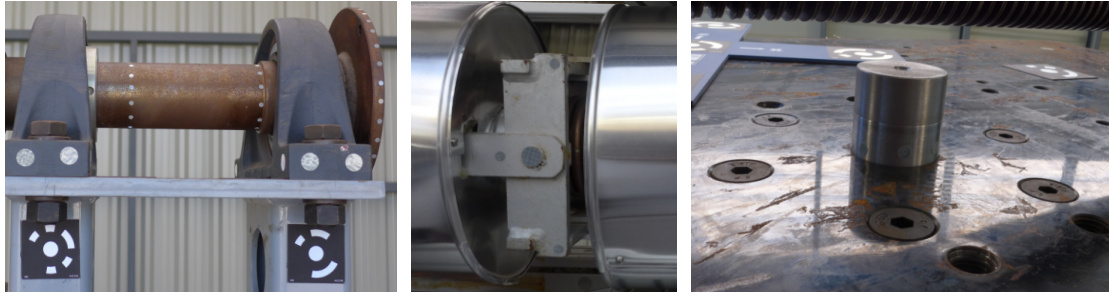
Figure 4.1: Indirect target placement: Left - axis sleeve: targets put around cylindrical object to get center; middle - compensator sleeve: rotation axis defined by two angle points; right - adapter (with sleeve) to find center of pocket

platform. The data is then fed into AICON 3D studio which gives back a list of 3D-coordinates as result. For best results, camera-positions have to form a homogeneous 'cloud' around the setup, compare figure 4.3c.

Finally the found points have to be named within AICON 3D studio as a preparation for automated post-processing, for example with MATLAB. The first time this has to be done manually, all following times this can be done automatically if relative point positions haven't changed more than a few millimeter. The desired coordinate system can be specified using coordinate transformation. For a detailed description of all necessary steps, please have a look Luhmann, 2006 [16] or other documentation[4].

4.1 Traverse: ideal pretension and model geometry

Objectives and Requirements

For most accurate model description (please compare chapter 5), as well as verification of correct pre-tensioning, the exact geometry of the piping system inside the traverse is needed. This comprises pipe segment length, coordinates of pipe segment connections and the bracing planes of the compensators. Ideally, the traverse piping system center line is only only two-dimensional. Deviations in the third dimension (here: x) are of special interest as they could be a possible explanation for the forces measured normal to the main axis.

Photogrammetry process

The seven pictures in figure 4.3 explain the seven steps necessary in order to obtain the exact traverse piping system geometry and change the ROHR2 model accordingly. The first step was to prepare the setup (a). To indirectly measure the center-line of the

---

[4]There is a REPA-specific Photogrammetry How To available on the DLR servers

piping system, as well as the angle points of the compensators, fourteen pipe sleeves and three compensator sleeves were used[5]. Their positions are depicted in figure 4.2. Then approximately 200 to 300 photos were taken (b) and fed into AICON 3D-software, which calculated camera and target positions (c).
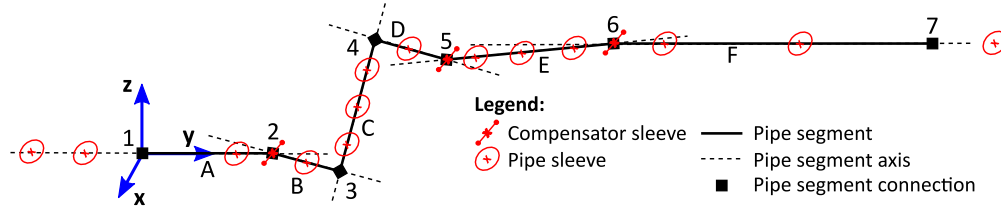
Figure 4.2: Traverse photogrammetry setup: pipe and compensator sleeve positions and segment names.

The post-processing was done by MATLAB which calculates sleeve centers by using a circle fit (d). The coordinate system was re-set, defining the fixed part of the dynamo-meter bearing as the origin and pipe axis A as parallel to the y-axis. Based on the center points found, pipe segment axes and connection points were derived as best fit through two or more pipe and compensator sleeve center points.

Finally the pipe section connection points were put into a 2D-geometric model in Inventor (f) in order to calculate and verify compensator angles in cold and hot state and in order to verify if pre-tentioning was done perfectly (compare chapter A.9). At last, the geometric representation and actual pretension of the traverse in the ROHR2-model was updated (g).

---

[5]Compensator sleeves refer to two targets placed on both sides of a compensator at which center the compensator angle point is assumed.

(a) Step 1: Preparations

(b) Step 2: Taking photos
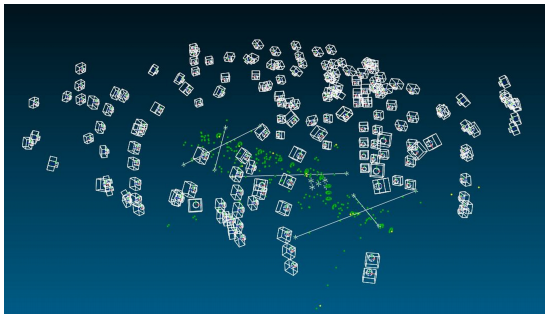
(c) Step 3: Running AICON 3D
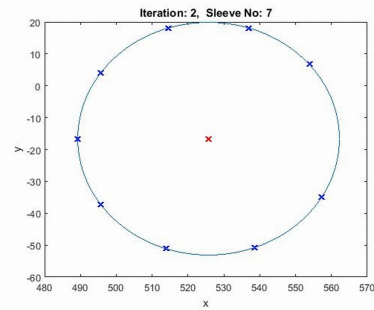
(d) Step 4: Make circle fit in MATLAB
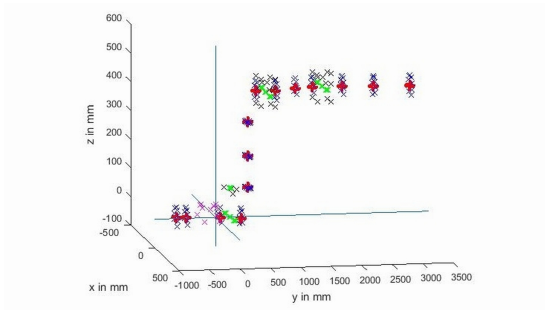
(e) Step 5: Plot pipe center points
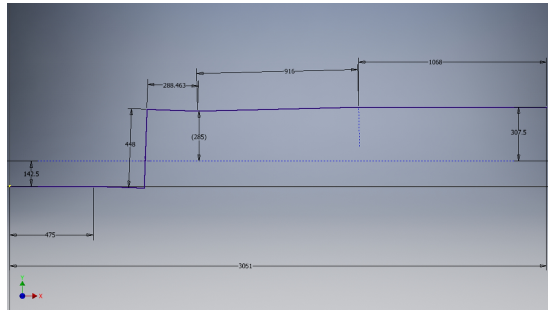
(f) Step 6: Geometric model as Inventor sketch
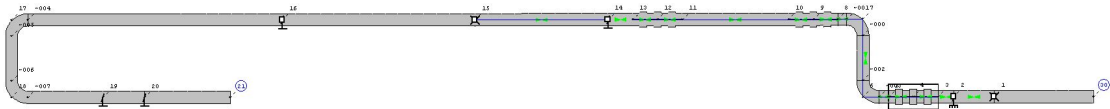
(g) Step 7: Update ROHR2-model

Figure 4.3: Workflow necessary in order to represent exact piping system geometry in ROHR2 model.

Results

Table 4.1 shows lengths of the piping systems segments and the coordinates of segment connection points as defined in figure 4.2. These constitute the result of the post-processing of the true dimensions of the piping system found by the photogrammetry. Ideally, the center line of the piping system does not have any extension in x-direction. Results show that this is not the case, as connection point 4 deviates from its ideal position by as much as 10.7 mm in x. During post-processing, this value has been calculated twice, column 'x' gives the mean of the two values found, column '$\delta_{x,calc.}$' gives the distance of this mean to each of the two solutions. This does not include the measurement uncertainty of the photogrammetric approach itself, which was sufficiently small to be ignored: the average measurement uncertainty, estimated by AICON 3D for each point individually, is only 0.04 mm. The maximum uncertainty is given to be 0.13 mm.

Based on the coordinates of the connections points, the pipe segment lengths can be calculated. When comparing these to lengths specified in the technical drawings of the traverse piping system, we can see that deviations are in the range of 5.7 mm. The true pipe lengths are then used in chapter 5.2 to derive ideal pretension.

Table 4.1: Photogrammetry results: traverse piping system geometry. All values in millimeters. The left part of the table shows coordinates of start and end points of pipe segments, as well as the uncertainty in the x-coordinate[6]. By definition the origin of the coordinate system is equal to point 1 (fix part of dynamo-meter bearing) and segment A is parallel to the y-axis. The right side of the table shows pipe segment lengths as planned and as built, as well as their difference.

Pipe segment connections					Pipe segments			
No.	x	y	z	$\delta_{x,calc.}$	Name	as planned	as built	Δl
1	0	0	0	0	A	470.5	475.5	5.0
2	0	477.1	-0.7	1.29	B	295.5	295.4	-0.1
3	-1	771.8	-9.7	4.55	C	450.0	451.5	1.5
4	-10.7	783.2	440.6	3.09	D	295.5	290.7	-4.8
5	-9.8	1073.2	430.7	0.88	E	915.0	915.8	0.8
6	1.2	1987.2	449.9	1.71	F	1075.5	1069.8	-5.7
7	9.5	3055.5	447.4	0				

.

---

[6]Only uncertainty stemming from axis fit only. Photogrammetry measurement uncertainty not included.

4.2 Test Rig: Alignment of rotation axes

Objectives and Requirements

The REPA test-rig is designed to perform rotational and translational motion. Figure 4.4 shows all axes that play a role in this motion. For the rotational motion five axes apply: the main axis defined by the drive pylon (a), the two axes of the two swivel drives (b) and the two axes of the swivel joints (c). For the translational motion eight axes apply: the two main axes defined by the drive pylon arm bearing (left and right) (A), the two axes of the drive pylon arm connections (B), and the four axes of the upper and lower bearing of the swivel drive arms (C) and (D).

These two groups of axes have to be aligned to prevent the test rig from suffering damage due to high stresses and deformation caused by the rotational or translational motion. Further more, it is desired to avoid possible effects on the force and torque measurements itself that could stem from any deformation of the traverse and or piping system. Badly aligned rotation axes may lead to high torsion of tables and bearings which may cause their destruction. Furthermore the greater the angle between one of the tables rotation axis and the drive pylon rotation axis, the greater the forces and the induced stresses which ultimately leads to greater deterioration of the REPA test-rig.
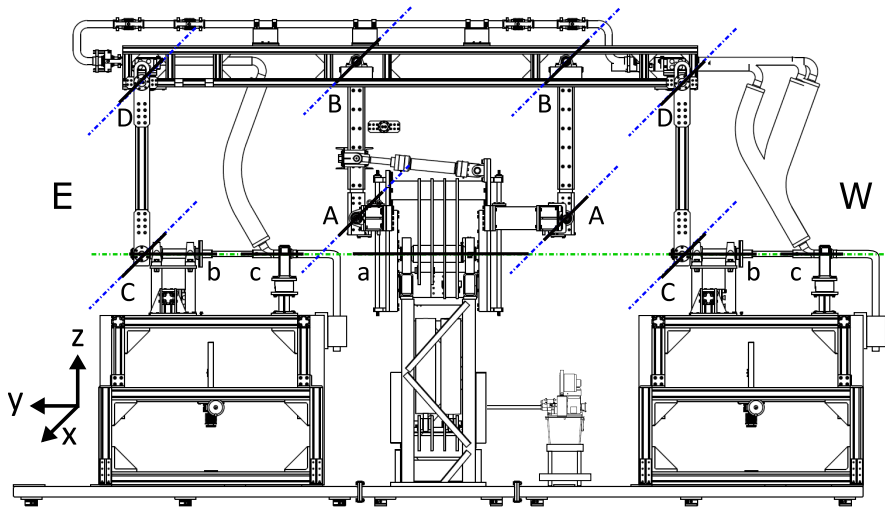
Figure 4.4: REPA rotation and translation axes. Rotation: a) drive pylon , b) swivel drives, c) swivel joints. Translation: A) drive pylon arm bearings, B) drive pylon arm connections, C) and D) - swivel drive arm bearing and traverse connections

During mounting, before adding end plates and arms to the main assembly, rotation axes a and b needed to be aligned. IW-Maschinenbau, the designer of the test-rig, states in their manual that translation axes A and B, as well as rotation axes a and b may not differ more than ±0.1 mm from each other [18]. As it is not feasible to even measure axes that are five meters apart with such high accuracy, tolerances were increased to ±1 mm,

meaning that each of the three rotation axes at the height of the ideal bearing positions may not have an offset greater than 1 mm from the main rotation axis, compare figure 4.5.

Senior Flexonics, the manufacturer of the first REPAs tested states that swivel joints axes and the main roation axes should not differ more than ± 2 mm [19] from each other. This, as well as the alignment of the translation axes will have to be verified, once the assembly of the test-rig is complete. In order to facilitate this, the method found and the code written for the post-processing should be easily adaptable. A photogrammetry was again chosen because it allows indirect measurements of the axes by using sleeves and adapters as well as quick repetition once the setup is put in place, while at the same time having a very low measurement uncertainty. The latter is important as all axes have to be measured multiple times while iteratively adjusting axis orientation[7].

Photogrammetry process

Figure 4.5: Main assembly photogrammetry setup: main rotation axis indicated in red. The three rotation axes of the two table bearings and the drive pylon have to be aligned. The allowed tolerance is defined as the maximum distance between the projections of the ideal bearing positions onto the main rotation axis 'X' and the respective rotation axis 'O'. This is represented for the left swivel joint bearing east only (exaggerated for better visibility).

The photogrammetry is carried out as previously described, using sleeves to find center lines of swivel drive bearing shafts and the drive pylon head rotation axis. Figure 4.5 shows two photos of the setup. The post-processing is done in MATLAB, which first calculates the centers of the sleeves via circle fits. The tree rotation axes are then found by linear regression. The result is shown in figure 4.6. Finally, the coordinate system is re-defined, setting the rotation axis of drive pylon as main rotation axis. The origin is set to be in the center of the drive pylon head.

---

[7]It turned out that using dial gauges and an adapted vice works best to move the heavy bearing structures. the effect of tightening screws has to be anticipated.

Results

The alignment process was successful and can easily be repeated. Several iterations were needed, adjusting table height and bearing orientation each time, in order to decrease horizontal offset and vertical offset below < 1 mm. Remaining offsets are shown in figure 4.7.
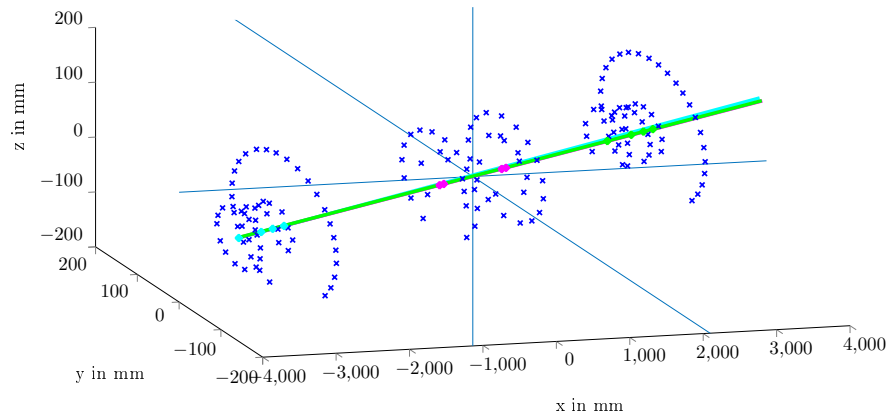
Figure 4.6: The plot shows all measured circle points (blue), their calculated center points (cyan, magenta and green) and the corresponding axes (colors as center points). Please note that y and z coordinates are not drawn to scale for better visibility. The coordinate system (solid blue lines) is rotated compared to the three axes, as could not be precisely defined before taking the photos.
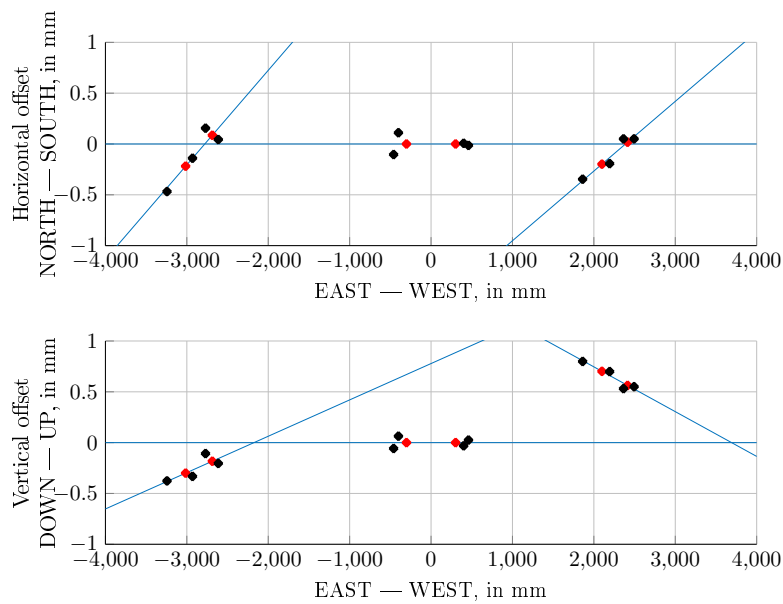
Figure 4.7: Rotation axes measured after last adjustment iteration: Blue lines indicate three rotation axes. Drive pylon head rotation axes defined to be main rotation axis. Black dots indicate measured centers of sleeves, red points indicate projections of the ideal bearing positions onto their respective rotation axis. Offsets are equal to the value of the y-axis of the plot.

5 The ROHR2 model

In complex piping systems it is not only necessary to assure that the static requirements are met. The combined influences of changing pressures and alternating fluid temperatures have to be considered also. ROHR2 is a simulation software of *Sigma Ingenieurgesellschaft* that predicts static behavior of complex piping systems. Usually ROHR2 models are used to perform strength calculations for industrial size piping systems. Bearing reactions are calculated to ensure safe operation. In chapter 3 we have seen that in the case of the REPA test-rig, we need to very accurately estimate comparably small residual bearing reactions that can not completely be eliminated by compensation of thermal expansion or other measures. This constitutes a very particular case. For this reason it is extremely important to describe the realized piping system as accurately as possible.

Here the ROHR2 model is needed to simulate forces and moments that the traverse piping system exerts onto the dynamo-meter at specific operational conditions, called Load Cases (LCs). LCs refer to the sum of HTF temperature, -pressure and the medium used. In ROHR2 the latter is defined by its density, which can be taken from the respective data-sheets given its temperature. The mass flow rate is not part of a LC as it can't be represented in ROHR2. The same is true for all time- and most spacial gradients of pressure and temperature. During a day a REPA moves through a number of very different LCs. These depend on the time of the year, the time of the day, the weather and the question which of the normally eight REPAs in a PCT power plant one is looking at. Please refer to chapter 2.1 for detailed information.

5.1 Model configurations

In his work, Andreas Plumpe created a model in ROHR2 that represents the piping system in between the two REPAs, called the traverse [8]. This chapter will describe how the model has been improved and modified to best represent the actual traverse piping system, before discussing its predictions.

In order to improve and adapt the model there are now four versions that have different specifications. The different versions serve as reference either during validation experiments or test-rig operation. The initial base model is called *Traverse_40*. In this model, pipe geometry, dimensions and pretensioning are represented as planned, later insulation thickness is realistically assumed. For better comparability during validation experiments, the insulation has been removed to create *Traverse_999*. To account for construction tolerances and changes to the initial design (missing compensators), this model has been improved and changed according to the final traverse as built, using a photogrammetric approach described in chapter 4.1. Two new base models have been created: *Traverse_100* without insulation to be compared with the validation experiments described in chapter 6 and *Traverse_200* with insulation for later test rig operation. A summary is shown in table 5.1.

Table 5.1: ROHR2 base models: main changes in the evolution of the base model.

Base model	Geometry	Insulation	Compensators	Purpose
Traverse_40	as planned	as planned	initial values	initial model
Traverse_999	as planned	none	initial values	ref. 'unchanged'
Traverse_100	photogr.	none	updated values	ref. 'validation exp.'
Traverse_200	photogr.	as built	updated values	ref. 'test-rig op.'

To introduce and investigate the effect of rotation, base model has been given a set of sub-models that represent the piping system at different rotation angles $\varphi = -120°, -110°, ..., 0°, 10°, ...90°$. Since it is not possible to define a rotation angle in ROHR2 or arbitrarily set the direction of gravity, which would have the same effect, each rotation angle means a new model (hereafter called sub-models).

Finally, LCs are defined in ROHR2. For good resolution up to 60 LCs have been created, each representing a static operation scenario covering the possible ranges of ϑ_{HTF} and p_{HTF}: five different pressures for each of the twelve different temperatures. More resolution or new fluids can easily be achieved by introducing more LCs to the models. Due to internal requirements of ROHR2, a so-called reference load case has to be defined. This represents a maximum stress scenario, i.e. contains the highest values for temperature, pressure and density of all LCs that are based upon this reference load case. The reference load case only serves for ROHR2-internal simulation purposes and has no value for interpretation.

The post-processing consists of calculating resulting forces onto the dynamo-meter using equation 2.3 and plotting the results. This is done in MATLAB. For automated plots and comparison, both the sub-model- and the LC-names have been coded. The sub-models' are named *Traverse_aaabccc*: three digits 'aaa' for the base model, one digit 'b' for the sign ('4' for '+' and '7' for '-') and three digits 'ccc' for the rotation angle φ in °, e.g.: *Traverse_1007080* is the base model *Traverse_100* rotated to $\varphi = -80°$. The LCs are named *TxxxPyy-Z*: three digits 'xxx' for the temperature in °C, two digits 'yy' for the pressure in bar and one digit 'Z' for the HTF used. Possible HTFs are Syltherm 800 (Z = S), HELISOL©(Z = H) and maybe more. During validation experiments the medium was air (Z = A). For Commissioning HELISOL©is used. To get results for any combination of operation variables, linear interpolation is used. Please refer to appendix A.6 for more information.

5.2 Model parameters

The traverse can be separated in two parts, east and west. The ROHR2 model follows this distinction. Figure 5.1 shows a graphic representation. As bearing 4 is assumed to be rigid enough to hinder any deformation or displacement, the two parts of the traverse piping system can be dealt with independently. In order to absorb pipe heat dilatation

and minimize the forces and moments that the traverse piping system exerts onto the dynamo-meter bearing, two single and one gimbal hinged angular expansion joints, called compensators, were installed in the western part.
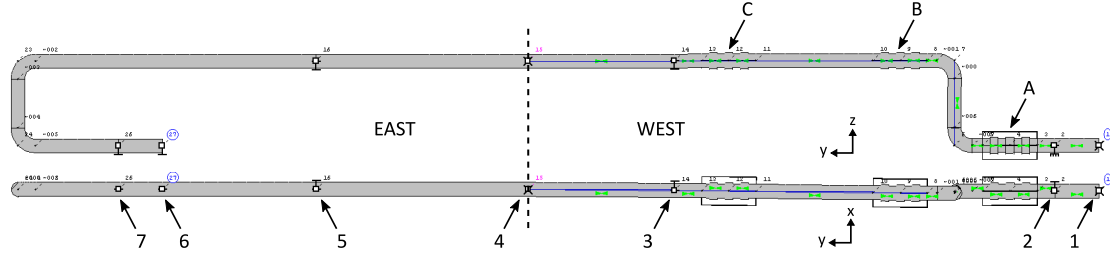
Figure 5.1: Top and side view of *Traverse_100* base model. A, B and C: compensators west-outer (gimbal hinged), west-center and west-inner (both single hinged). 1 and 4 are fix bearings. 2,3,5,6 and 7 are floating bearings.

As compensators work as springs that try to remain in un-deviated position, smallest deviation cycles also mean smallest moments that have to be applied to keep the compensators in deviated position and thus smallest bearing reactions. In order to have the resulting forces as small as possible, the three compensators are pre-tensioned, meaning that they are mounted slightly deflected at ambient temperature so that, reaching 350 °C the deflection is zero and the resulting forces are minimal. For a more detailed description and explanation of both compensation and pre-tensioning, please have a look at appendix A.9.

Table 5.2 shows resistance coefficients or spring constants as a function of HTF pressure p_{HTF} and compensator angle α as well as the torsion angle.

All values given in table 5.2 have to be applied with caution as the manufacturer states a tolerance of 30% for all values. In ROHR2 these constants can be set in the entry-mask belonging to each compensator. Strictly speaking these values only apply at ambient temperature. For higher temperatures a reducing factor K_c needs to added[20, p.42-43]. ROHR2 only considers reducing factors for pre-set compensators taken from the database. Custom-defined compensators as in this model do not allow reducing factors yet. This means that the ROHR2 model might not be the best choice of software for this task. This has to be kept in mind when assessing the model validation in chapter 6.

In order to address these limitations inherent to the used software the traverse piping system should be represented as accurate as possible. In order to account for all inevitable deviations of the final traverse piping system *as built* from the ideal geometry *as planned*, a photogrammetry measurement has been performed to find the true piping geometry. Please refer to chapter 4.1 for details. Photogrammetry results were also used to verify and improve pretensioning, please refer to appendix A.9 for detailed information.

Table 5.2: Compensator resistance coefficients and temperature dependent reducing factors. As defined by the help chapter of ROHR2: c_α is elastic angular bellow resistance, pressure-independent; c_r is pressure-dependent angular friction resistance; c_p is elastic angular bellow resistance, pressure-dependent; c_T is elastic bellow (german: 'Balg') resistance for torsion, values are big compared to others as compensators do not allow rotation around this axis; α is the compensator angle; $c_{i\vartheta} = K_c \cdot c_i$ are the operation temperature adjusted resistance coefficients[20, p.42]. Tolerance not included in values. In the model, regulating powers are increased by the tolerance, compare ROHR2-help chapter.

Comp.	Axes	Regulating powers at $20\,°\text{C}$				Max. allowed	
		c_α $\text{N\,m}/°$	c_r $\text{N\,m/bar}$	c_p $\text{N\,m}/(\text{bar}\,°)$	c_T $\text{N\,m}/°$	α_{max} $°$	moment $\text{N\,m}$
	x-axis	8.3	0.7	0.2	-	± 5.5	-
Single	z-axis	-	-	-	-	-	-
	y-axis (torsion)	-	-	-	6.6k	± 0,1	764
	x-axis	8.3	0.7	0.2	-	± 5.5	-
Gimbal	z-axis	8.3	0.7	0.2	-	± 5.5	-
	y-axis (torsion)	-	-	-	6.6k	± 0,1	764

Operation temperature	ϑ in $°\text{C}$	200	300	400	500	600	700	800	900
Reducing factor	K_c		0.93	0.90	0.86	0.83	0.80	0.75	0.71	0.67

5.3   Results and discussion

ROHR2 calculates displacements, rotations, forces, moments and relative stresses for every pipe segment and at every node. Expected dynamo-meter forces and moments are calculated as shown in figure 2.4 using the information of nodes one and two.

Looking at LC *T020P00-A* and *T350P00-A* at $\varphi = 0$, which are depicted in figure 5.2, we first find that in hot state ROHR2 estimates all compensators to be nearly undeviating, which means that pretension representation is done correctly.
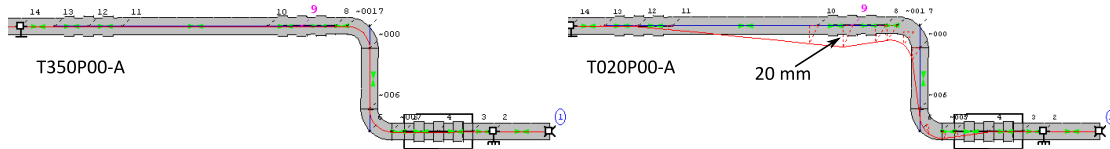
Figure 5.2: The displacement of the piping system (*Traverse_100*) open ($p = 0\,\text{bar}$) and air-filled. Left: LC *T020P00-A* at $\vartheta_{pipe} = 350\,°\text{C}$. Right: LC *T020P00-A* at ambient temperature.

The difference in height of the angle point of compensator B for this temperature change is $20\,\text{mm}$. The geometric model in Autodesk-Inventor[8] yields the same result. This value can easily be checked during experiments as vertical motion of the angle point of compensator B was continuously measured during validation experiments. The most comparable value obtained is $14.5\pm1\ mm$ resulting in a $6\,\text{mm}$ difference. An explanation

---

[8]3D-CAD-Software

could be a) that the average pipe temperature never reached 350 °C during experiments (max. average pipe temperature $\approx 320 - 340$ °C), b) huge temperature gradients in both axial and radial direction due to insufficient insulation and c) measurement error, both during the photogrammetry as well as when measuring the height of compensator B itself. Increasing the the compensator stiffness significantly was tried, but did not have an influence. Later during test-rig operation, compensator height measurements should be repeated.

In the following we will have a look at the traverse piping systems behavior if either rotation angle, HTF pressure or HTF temperature change, while the other parameters remain constant. We will call the respective change in dynamo-meter reading F_{dyn}: angle response F_{dyn}^{φ}, pressure response ΔF_{dyn}^{p} and temperature response $\Delta F_{dyn}^{\vartheta}$. Please note that F_{dyn}^{φ} is an absolute measure, while ΔF_{dyn}^{p} and $\Delta F_{dyn}^{\vartheta}$ are relative meaning they are decreased by the value for $p_{HTF} = 0$ bar or $\vartheta_{HTF} = 20$ °C.

Figure 5.3 shows representative model results predicted by all models, at the example of base model *Traverse_ 200*. The first observation is that all forces and moments are either symmetrical to the origin or to the y-axis. This is plausible, as the system itself is symmetrical if we neglect minor manufacturing tolerances. When rotating the system at constant temperature and pressure forces and moments will redistribute as the dynamo-meter rotates relative to gravity. Forces and moments itself do also change since the sum forces is not equal over all angles.
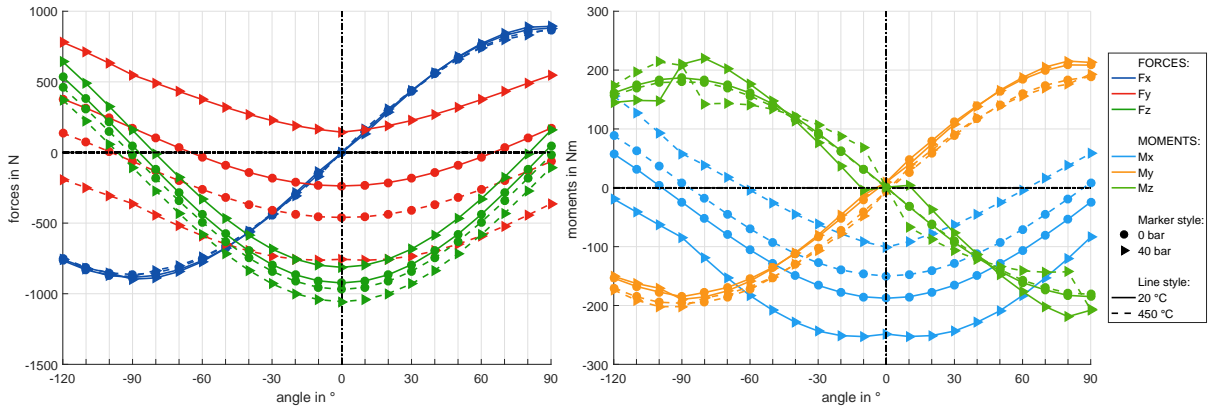
Figure 5.3: ROHR2 forces (left) and moments (right) over rotation angle φ for maximum and minimum HTF pressures p_{HTF} and HTF temperature ϑ_{HTF} each. The base model is *Traverse_ 200*. Please note, that for air, data only exists for $p_{HTF} = 0$ bar.

Second, it seems that the choice of fluid has very little effect on the results, which is why we will discuss results for the example of HELISOL only. This is plausible because the change of line mass with or without fluid is only 9.6%. Further, we can divide results in two groups: F_x, My and M_z, don't show temperature or pressure dependency, while F_y, F_z and M_x do. Theses temperature and pressure responses seem mostly independent of φ. In the following we will have a closer look at the second group.

Looking at forces and moments over HTF temperature ϑ_{HTF} at maximum pressure and for two different rotation angles, as shown in figure 5.4 we find that for HTF temperatures $\vartheta_{HTF} < 325\,^\circ\text{C}$ ROHR2 predicts a linear temperature response. For $p_{HTF} = 0\,\text{bar}$, the temperature response remains linear for higher temperatures, while for higher pressures, there is a swift step between $325\,^\circ\text{C}$ and $375\,^\circ\text{C}$ in some angle dependent cases: For $\varphi = 0°$ F_y, F_z, M_x and M_z show nonlinear behaviour, For $\varphi = 90°$ F_y, F_x, M_x and M_y show nonlinear behavior. An interesting observation is that F_x and F_z seem to have switched places after the 90° change depicted in figure 5.4. This might be plausible as in the first case gravity points in negative z, in the second case in negative x-direction. The described behavior is predicted by all four base-models, being significantly stronger for the models *Traverse_ 100* and *Traverse_ 200*, which have the updated, more complex geometry. The choice of fluid has a negligible effect on the results.
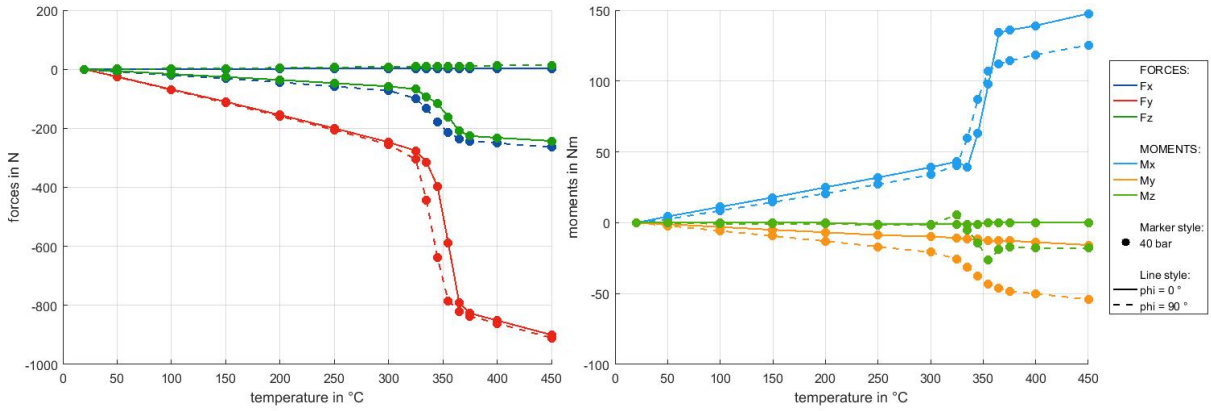
Figure 5.4: ROHR2 forces (left) and moments (right) over temperature. The model used is *Traverse_ 200* at maximum pressure and for two different rotation angles. Due to the nonlinear behavior between $320\,^\circ\text{C}$ and $370\,^\circ\text{C}$ the number of measurements has been increased around the non-linearity.

Finally, let's have a look at the predicted pressure response of the piping system: As figure 5.5 indicates, the change in dynamo-meter forces and moments is expected to linearly depend on HTF pressure p_{HTF} in all cases, except M_z. For all others the pressure response does not depend on the rotation angle, but strongly on the HTF temperature: Temperatures below $\approx 350 \pm 20\,^\circ\text{C}$ lead to a negative pressure response, while temperatures above $\approx 350 \pm 20\,^\circ\text{C}$ lead to a positive pressure response. Rising from ambient temperature to design temperature, the slope of the curve does not change steadily, but experiences the same swift step at about $350\,^\circ\text{C}$ that we have already seen for the temperature response. In the case of M_z, the temperature response does not depend on HTF temperature, but does depend on rotation angle, being symetrical aroung $\varphi = 0$. The described behavior is similar in all models: *Traverse_ 100* and *Traverse_ 200* show the same behavior, being slightly stronger than in *Traverse_ 999* and *Traverse_ 40*, meaning that the insulation has no effect on the pressure response.
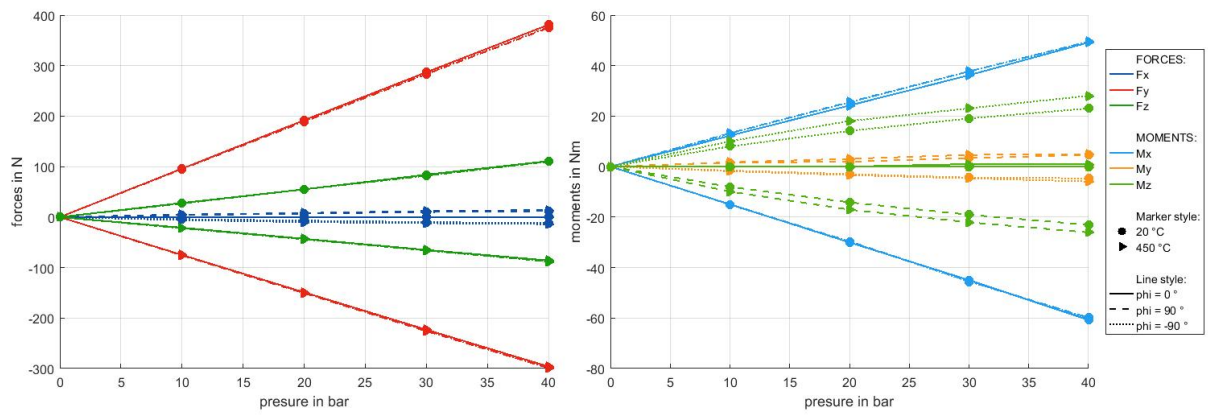
Figure 5.5: ROHR2 forces (left) and moments (right) over pressure. The model used is *Traverse_200* at maximum and minimum temperature and for three different rotation angles. The markers indicate at which points model results have been calculated.

6 Validation

The dynamo-meter that is mounted in the REPA test-rig always measures the sum of the effects from adjacent piping system and the REPA. Hence a ROHR2 model exists which is meant to estimate the effect of the traverse piping system onto the dynamo-meter reading F_{dyn} so that it can be subtracted. Please compare chapter 2.2 and equation 2.2. This chapter will present efforts undertaken to validate the model by comparing its results to those of an experiment.

The individual effects of rotation angle φ, HTF pressure p_{HTF} and HTF temperature ϑ_{HTF} onto the dynamo-meter reading F_{dyn} will be called (rotation) angle response, pressure response and temperature response (of the traverse). In order to be able to compare experiment and model results, both have to describe at least very similar circumstances. For this reason only temperature and angle response at ambient pressure and with air as medium can be used for validation. All other experiments require the traverse being mounted and the REPAs being connected to have oil circulating. This can not be represented in ROHR2. The effect of translation angle θ and HTF mass flow rate $\dot{m}_{HTF}$, called translation response and flow response (of the traverse) could not be investigated so far due to delayed test-rig commissioning.

Before entering the description of experiment setup, method and results, it has to be mentioned, that all experiments were conducted with a broken pin in the sensor-amplifier connection. This broken pin, that is visible in the photo in figure 6.1, has affected all experiments, but was discovered after the last experiment only. Consequently channel six of the dynamo-meter returned the constant value of $0\,\mathrm{V}$ in all measurements. However, the multiplication with the calibration matrix K still yields three forces and three moments. This is why it wasn't obvious that an error had occurred, falsifying all measurements to an extend that can not be estimated. Hence, all results obtained have to be dealt with caution. The pin is now repaired and the dynamo-meter produced results again.
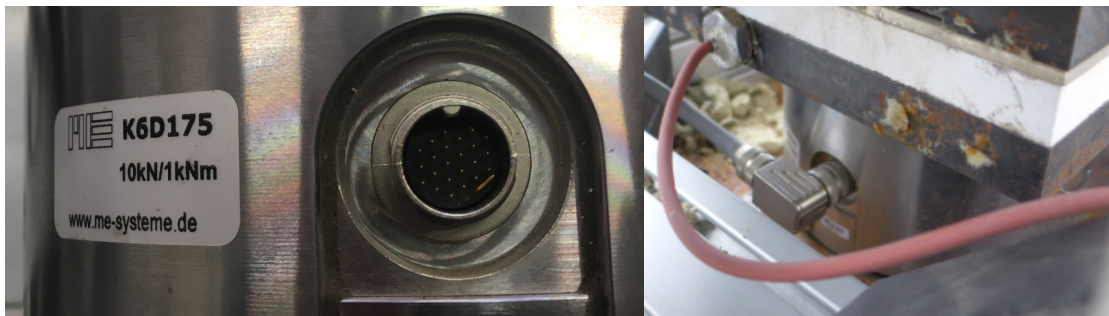
Figure 6.1: Left: The dynamo-meter with a broken pin. Right: The dynamo-meter-cable connection in the traverse. Fixing the union nut of the plug can be done with two fingertips only. Holding the plug straight at the same time is extremely difficult.

6.1 Temperature response

The temperature response is defined as the change in dynamo-meter reading $\Delta F_{dyn} = F_{dyn,\vartheta} - F_{dyn,amb.}$ that occurs when the mean traverse piping temperature ϑ_{pipe} ($\approx \vartheta_{HTF}$) changes, while all other parameters stay constant.

Experiment setup, method and uncertainties

The experiment setup is shown in figure 6.2. A compressor led air through an electric heating system and then further through the piping system inside the traverse, heating it up to $\approx 350\,^{\circ}\mathrm{C}$. The yellow compressor on the left is connected to the electric heater by a flexible green tube. The electric heater is 'flanged' to the traverse piping system, that is partially insulated. In order to experimentally measure the temperature response, the open traverse piping system was heated with hot air. The resulting forces and moments onto the dynamo-meter bearing were logged during both heating and cooling phase.

Figure 6.2: The experiment setup: Only the western part of the traverse piping system is of interest. The eastern part of the piping system, after the second fix bearing in the middle of the traverse, is left out as it should not have an influence. The second dynamo-meter bearing (east) has been left open as the heat dilatation of this part of the piping system is not compensated and would otherwise get destroyed.

In addition to the dynamo-meter, a total of twelve temperature sensors surveyed the temperature of pipe system, bearing and dynamo-meter. This is indicated in the photos in figure 6.3. Four PT100-temperature sensors were placed along the pipe: One just behind the floating bearing part of the dynamo-meter bearing, two just in front of compensator west-center and compensator west-inner, the last one just in front of the red steel bearing center (second fix bearing). Two type-K-thermocouples measured the temperatures of the air flowing in and out: one inside the open flange connection and the other at the outlet of the traverse. The dynamo-meter temperature was monitored by two PT1000-temperature sensors placed in the steel plate that connects bearing and dynamo-meter. As the steel plate heats up first, its temperature can be interpreted as an upper estimate of the dynamo-meter temperature ϑ_{dyn}.
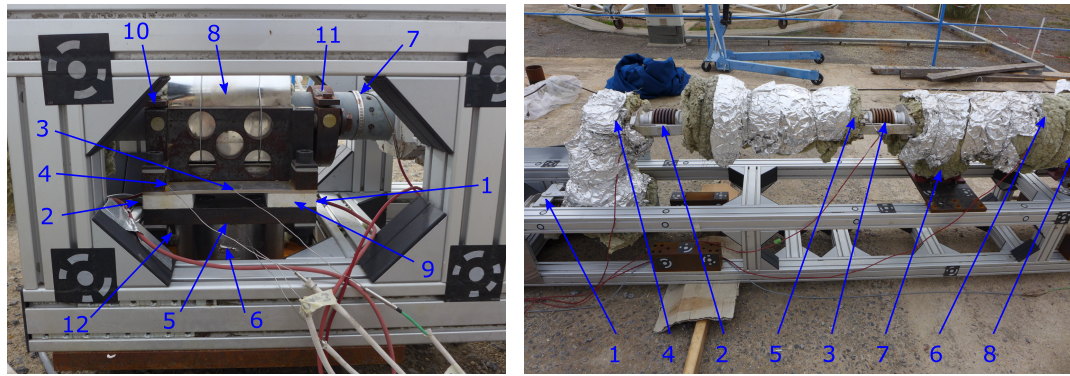
(a) temp. sensors: dynamo-meter bearing   **(b)** temp. sensors: traverse piping system

Figure 6.3: Temperature sensor wiring on dynamo-meter bearing (left) and traverse piping system (right). Left: 1 and 2: two PT1000 for sensor temperatures; 3, 4, 5 and 6: type K thermocouples for bearing temperatures; 7: PT100 for pipe temperature; 8: sensor insulation; 9: insulation plate (cut); 10: fix bearing; 11: floating bearing; 12: K6D175 output. Right: 1: Compensator west-outer; 2: Compensator west-center; 3: Compensator west-inner; 4, 5 and 6: PT100 for pipe temperature monitoring; 7: Red steel bearing west (sliding bearing); 8: red steel bearing center (fix bearing)

In order to investigate the individual effects of different parameters a total of fourteen experiments were executed. The first six experiments served to improve the setup. All following experiments create the basis for the model validation. An overview over all valid temperature experiments is given in table 6.1 which will be used as reference in the results and discussion section.

A typical experiment procedure consisted of a heating and a cooling phase. During heating, compressor and electrical heater were controlled manually in order to maintain the desired air temperature at the inlet as monitored by one of the thermocouples. The cooling phase begun after reaching the desired pipe temperatures or once the desired heating time had passed. During cooling the compressor was either left running for quick cooling or switched off to reduce temperature gradients.

During the experiments, changes to the original setup have been made. The results and discussion section of this chapter is therefore split in two parts. First, those results are discussed that motivated necessary improvements. Second, the temperature response of the traverse piping system will be investigated and compared to the respective results of the ROHR2-model.

Table 6.1: Overview over the eight validation experiments. The columns show from left to right: the experiment number; the rotation angle; four columns with information about sensor, pipe and bearing insulation as well as whether or not an exhaust pipe had been connected. Although insulation makes results more difficult to compare to model results, it was not possible to achieve higher pipe temperatures without. 1) wind shield; 2) sensor insulation as shown in figure 6.3a; the duration of the heating phase and some information about the 'flange' connection; the duration of the cooling phase and whether or not the compressor was left running; a column saying whether or not the dynamo-meter had been cooled actively; other commentaries. 3) stands for floating bearing opened, meaning that one side of the dynamo-meter bearing was opened when changing from heating to cooling. The graphic results of all other valid temperature response validation experiments (no. 7-14) are given in the appendix A.7.

No.	φ	Sens.	Pipe	Bear.	Exh.	Time	Flange	Time	Compr.	Vent.	Other
	°					hh:mm		hh:mm			
7	0	No	Yes	no	No	2:33	Open	1:26	Yes	No	
8	0	No	No	no	No	0:54	Open	0:29	Yes	No	
9	0	Yes	No	no	No	0:57	Open	0:35	Yes	No	
10	0	Yes	Yes	1)	No	2:45	Open	0:45	Yes	No	
11	-90	Yes	Yes	1)	No / Yes	1:28	Open	0:34	Yes	No	
12	-90	Yes	Yes	1)	Yes	4:00	Open	8:59	No	No	
13	0	Yes	Yes	2)	Yes	2:52	Open	6:02	No	No	
14	0	Yes	Yes	2)	Yes	3:07	Touching	6:01	No	Yes	3)

Insulation spans Sens./Pipe/Bear./Exh.; *Heating phase* spans Time/Flange; *Cooling phase* spans Time/Compr.; *Other* spans Vent./Other.

Results and discussion: Improvements and uncertainty

Within the first six experiments and still later, improvements to the experiment setup have been made. In order to rule out mayor sources of uncertainty and obtain trustworthy measurement results, seven changes to the original setup were needed:

1. open the flange connection between heater and piping system

2. remove insulation material from the compensators in order to free their movement

3. improve dynamo-meter insulation to reduce heat flow and install a ventilator in order to decrease measurement uncertainties

4. verify and improve pretensioning based on exact piping system dimensions obtained with a photogrammetric approach

5. re-calibrate the dynamo-meter based on a scenario that represents actual loads

6. install an exhaust pipe that prevents the ITEM-profile from heating and thus experiencing heat dilatation

7. apply grease to moving parts of floating bearings to decrease friction

For more information about the improvements and changes made to both sensor- and pipe insulation, the active cooling system as well as the pre-tensioning please compare to appendix A.9. For more information about dynamo-meter calibration, temperature dependence and uncertainties, please refer to chapter 3.

Figure 6.4 shows the results of Experiment no. 7 as an standard example. Main responses to actions taken can easily be detected: shortly after the beginning of the measurements, compressor and heater had been started, letting the air in temperature in (b) rise and settle at around 400 °C. Pipe temperatures follow increasing asymptotically to their steady state, at which further heating is made impossible by insufficient insulation. After $02 : 40\,h$ heating is turned off while the compressor remains working. The 'air in' temperature quickly drops to ambient temperature, effectively cooling the piping system from the inside.

During the first experiments the flange connection between heater and piping system had been closed to minimize air and thus heat losses. However, it quickly became apparent that to be able to observe the piping systems behavior in most isolated state, the flange connection had to be left open, leaving a small air gap in between both sides to prevent them from touching. All attempts to install a different kind of closed connection, that would prevent loosing hot air while at the same time ensure negligible parasitic forces, failed. As the pipes on both sides of the flange expanded with increasing temperature, the air gap had to be restored a few times during heating. This lead to a varying air gap and thus varying heat losses as well as short times in which both sides of the flange touched. Clearly observable peaks in the measurements were the consequence. In the discussion of the results, these peaks have not been taken into account, as long as they coincide with a *flange adjustment* in the experiment protocol. Flange adjustments are indicated as vertical black lines. A touching flange connection lowers the forces and moments measured by the dynamo-meter.

A first experiment without any insulation quickly showed that the naked piping system could not be heated up to 350 °C. Covering the whole system however significantly increased forces and moments onto the bearing. The insulation material around the compensators was therefore removed in order to free compensator movement. Measured forces decreased to $10-30\%$ of their original value. However, temperature gradients increased, which effect is difficult to quantify.

Another early result was that the dynamo-meter heated far more than expected. In the initial configuration sensor temperatures up to 60 to 70°C were reached after only one hour of operation and even though an insulation board had been installed. Higher sensor temperatures lead to greater measurement uncertainty, as chapter 3.1 explains. The sensor insulation has therefore been improved in between experiments 8 and 9.

Another interesting result is that with advanced cooling, dynamo-meter measurements do not go back to zero, please compare the right end of the graphs in figure 6.4a. Further more we can see in figure 6.4c, that when plotting forces and moments over the mean pipe temperature one finds that there seems to be a linear correlation between

(a) Forces and moments as $f(t)$

(b) Pipe temperatures as $f(t)$

(c) Forces as $f(\vartheta_{pipe})$

(d) Moments as $f(\vartheta_{pipe})$
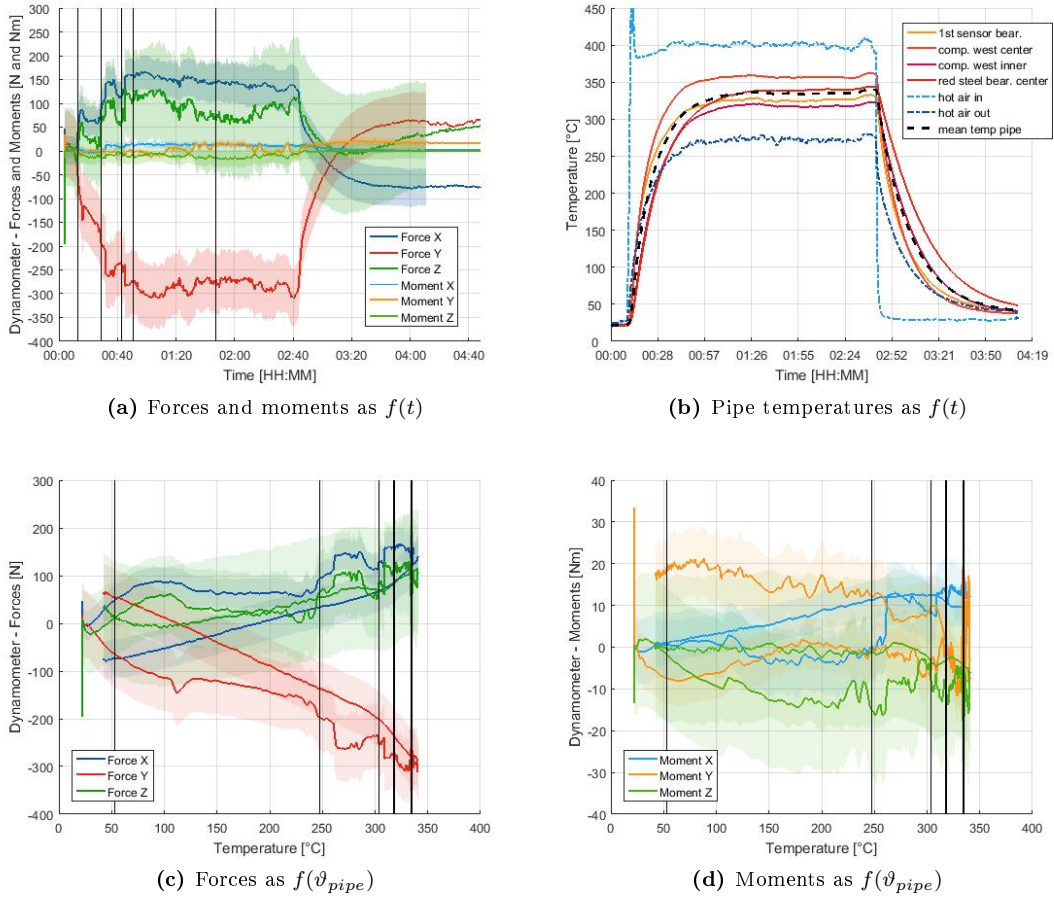
Figure 6.4: Results of Experiment No. 7: a) dynamo-meter reading during heating and cooling phase. b) Pipe and air temperatures: The rise and fall of 'hot air in' clearly shows when the heating had been turned on and off. The mean traverse piping temperature ϑ_{pipe} represented by the dotted line is calculated on the bases of the four pipe temperatures measured and serves as reference. c) and d) Forces and moments plotted over ϑ_{pipe}. Curves show hysteresis behavior. a), c) and d) The colored lines show the measured value, the colored areas show the respective uncertainty (95%-confidence interval, original calibration) of the measurement value as estimated on the basis of data sheet values and sensor temperature measured. Black vertical lines indicate when the flange-connection had been adjusted (correlation not perfect as adjustment itself took some time as well as short period of time between adjustment and notation).

temperature and dynamo-meter measurements with a superimposed hysteresis effect. Possible explanations for both *overshoot* and hysteresis are ITEM-profile temperature, dynamo-meter temperature, a change of zero signal after each temperature cycle and friction.

As the natural outlet of the piping system points inwards and none of the piping bearings is insulated (except the dynamo-meter bearings), parts of the aluminium-profile heat up to $\approx 60 - 70°$C. In order to decrease ITEM-profile heating a flexible exhaust pipe was added to the setup during the cooling phase of experiment 12 and in all tree

following experiments, leading the air away from the ITEM-profile. This also increased the flow resistance through the piping system, and therefore heat losses at the open flange connection increased. Comparing results, especially the overshoot during cooling phases does not reveal any systematic differences between the experiments before and after the exhaust pipe. The influence of the traverse ITEM-profile temperature ϑ_{trav} is therefore said to be not visible.

The most likely explanations for the overshoot remaining are therefore linked to the dynamo-meter temperature. Chapter 3.1 explained that both the temperature effect on zero signal as well as the difference in zero signal after complete heating cycle could be responsible.

Finally, we should have a look at friction. When changing the sensor insulation it was found that the floating bearing can not be moved by hand, once the screws of the lid are tightened, even at cold state. Further more, the plain bearing bushing (german: *Gleithülse*) had suffered plastic deformation in one of the experiments or during mounting. In hot state, the friction is even higher: The plain bearing bushing is made out of brass (german: *Messing*) which has a higher linear heat dilatation coefficient than the steel of the surrounding bearing (brass: $18.4\,\mu\mathrm{m}/(\mathrm{m\,K})$ and steel: $13.5\,\mu\mathrm{m}/(\mathrm{m\,K})$). Before opening the floating bearing in hot state, loosening tension by softly hammering against bearings and piping system. The effect was very small. The conclusion is that brass as material is not appropriate for both its heat dilatation and softness.

To see if high friction between plain bearing bushing (brass) and the floating bearing was responsible for at least some of the forces and moments measured, the floating part of the fix-floating sensor-bearing was opened, when changing from heating to cooling in experiment 14. The result was a drop in F_x ans F_z by about 30% and a drop (rise towards zero) of F_y by about 10% of the measurement value, even though high temperature grease was applied to ensure low friction. This effect however seems implausible because both, fix bearing and floating bearing are connected to the dynamo-meter, compare figure 2.4. Therefore tension between these two should not affect the measurements.

The ROHR2 model assumes homogeneous temperature distribution along the pipe and through the pipe wall. However temperature measurements show that this is not the case during the experiments. As temperature gradients generally lead to stress and deformation, this may be a plausible explanation for the differences between model and experiment. An observation which could be presented as evidence for this hypothesis is that the piping system immediately responds to switching off the electric heating. It seems implausible that this fast reaction stems from homogeneous cooling of the piping system, but more plausible that in this short of time only the inner pipe wall has experienced a change in temperature. Later during test-rig operation, temperature gradients will be smaller because of better insulation, the heat capacity of the HTF and more steady operational conditions.

Results and discussion: Model validation

For validation purposes experiments were grouped by the rotation angle. For each group, forces and moments of all experiments were plotted over the mean pipe temperature, omitting extreme values[9]. Then, the linear regression of the experiment results is made and compared to the results obtained from base model *Traverse_100* and for air as fluid. A graphical comparison is shown in figure A.7.2, a statistical comparison is shown in table 6.2.

(a)

(b)

(c)

(d)
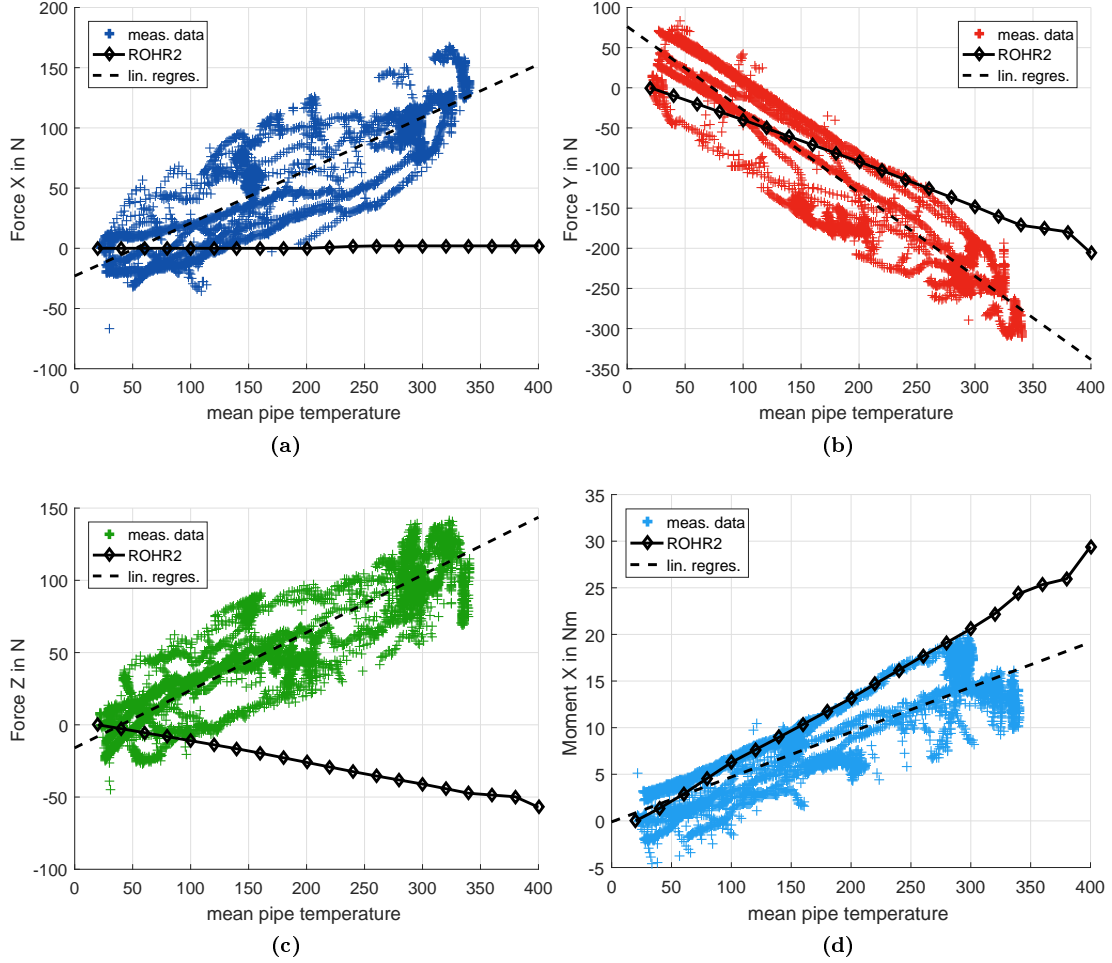
Figure 6.5: Temperature response experiment results: measurement data, linear regression and ROHR2 results (*Traverse_100*) of all experiments that have been conducted at rotation angle $\varphi = 0°$. All measurement results for both for $\varphi = 0°$ and $\varphi = 0°$ can be found in appendix A.7.

To evaluate the model prediction, we use the standardized Roots-Mean-Squared-Error (std. RMSE), which is a measure for the goodness of fit between a predictive model

---

[9]A value is said to be extreme if its difference to the (first) regression is more than twice the standard deviation σ of all differences.

Table 6.2: Temperature response experiment results and assessment of model predictions: The first two columns show slope and intercept of the linear regression of all temperature response experiments at rotation angle $\varphi = 0°$. Results show that rotation angle φ did not have a significant effect on dynamometer reading. The right half of the table presents values that help assessing the goodness of prediction both absolute and relative: the total uncertainty of the measurements that has been estimated in chapter 3.2 and which is presented in the appendix in table A.4.2; The Root-Mean-Square-Error (RMSE) is calculated as the square root of the variance of the prediction error[21]. Lower values mean a better fit [22]; The standardized RMSE finally is a relative measure that helps inter-comparing different models: 0 means a perfect prediction, while 1 means the opposite.

	Regression		Assessment of model predictions		
F_i	$F_{dyn,i}^{regres} = a \cdot \vartheta_{pipe} + b$ a	b	*experiment* U	*model: Traverse_100* RMSE	std. RMSE
	in N/K	in N/K	in N	in N	-
F_x	0.46	-28.15	116	70	0.97
F_y	-1.03	69.55	117	68	0.28
F_z	0.38	-13.33	508	91	0.99
	in Nm/K	in Nm/K	in Nm	in Nm	-
M_x	0.05	-0.30	19	4	0.19
M_y	-0.01	5.52	16	13	0.80
M_z	-0.01	0.40	28	5	0.85

and an experiment: the value 0 zero means that the prediction is perfect, the value 1 means that the model has no predictive value. Here, the presented results can only be explained in the cases of F_y and M_x. The model does not seem to have any explanatory power in any of the other cases.

High values for relative measurement uncertainty make the interpretation of the results difficult. Throughout all experiments, minimum relative measurement uncertainty was as high as 358% in the case of F_z (other values: 66% for F_x, 38% for F_x, 93% for M_x, 80% for M_y and 139% for M_z, compare table A.4.2 in the appendix). Absolute values for the uncertainty U are given in table 6.2.

The measurement uncertainty U is greater than the RMSE in all six cases, which means that it is theoretically possible to explain the differences between experiment and model with the measurement uncertainty. This, of course, does not mean that the model is therefore validated. On the contrary, the only valid statement that can be made is that it is reasonably possible that repeated validation results might produce this outcome. Before doing that however, it is utterly important to address the uncertainty issues. Against this background this work passes a detailed discussion of the differences in the predictions of the different base models (compare chapter 5) which should be done, once the uncertainty and measurement issues have been addressed.

So far we have been looking at the temperature responses of the traverse for $\varphi = 0°$ only. The two experiments at $\varphi = -90°$ yield similar results. The temperature response is

not dependent of the rotation angle, a result, that we have already found when discussing the model results in chapter 5.3. Even though all experiment results might be false to some extend because of the broken pin, this statement can be made, ass both groups of experiments would be affected equally.

6.2 Rotation angle response

The rotation angle response is defined as the dynamo-meter reading F_{dyn} that occurs when the traverse is rotated around its main axis at constant temperature and pressure. As the dynamo-meter rotates with the traverse the re-partition of forces onto the six dynamo-meter channels changes even though the total force might be the same.

Experiment setup, method and uncertainties

To estimate the effect of rotation onto the dynamo-meter reading the traverse has been rotated 180° ([−90°,90°]) at ambient temperature with the use of a crane and long wooden levers. While doing so the dynamo-meter reading has been logged for every 10° of rotation. Figure 6.6 shows a photo of the setup. At that time the traverse still hadn't been mounted on the KU, the traverse was empty and there were no REPAs and no insulation to be taken into account. Therefore results obtained by the ROHR2-model and the experiment can directly compared. However, a few differences and possible sources of uncertainty have to be considered:

Figure 6.6: The photo shows the experiment setup to investigate the pressure response of the traverse piping system under ambient temperature and pressure.

1. There has been a flange connection welded to the end of the pipe of the traverse which couldn't be represented in the model, but which weight of ca. 5 Kg contributes to the experiment result.

2. During rotation the traverse has been hanging from to ropes attached to the ITEM-profile while still be partly resting on some pieces of wood with its lower edge. As crane movements led to observable dynamo-meter reading instability, traverse bending and torsion may be an issue. In the model, the ITEM-profile is not represented and therefore it's bending isn't either.

3. The unsertainty of the rotation angle measurement is in the range of 3°.

Results and discussion

Figure 6.7 shows the results of the first experiment. The two plots compare the measurement data with the results of the adequate ROHR2 model: In most cases (all forces and moments except F_z and M_y) the model results predict the range of measurement data quite well. However it seems that the the curves for F_y and M_x are shifted along the x-Axis. At this point it should be noted that the measurement results show some unexpected behavior as some curves have their minimum at approximately $-60°$ (F_y and M_x) and $30°$ (F_z), instead of at $0°$ as the model predicts and as it would be plausible for symmetry reasons. The biggest deviations between model and experiment results can be observed for F_z and M_y.
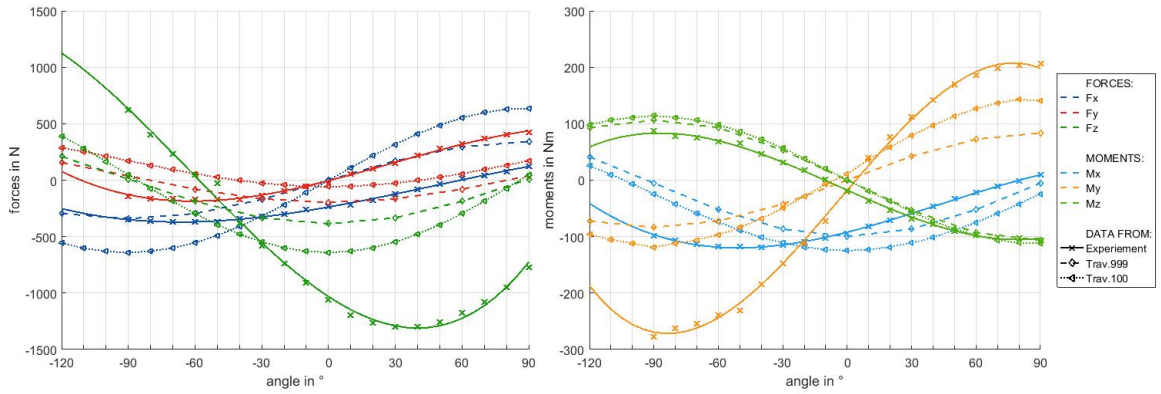
Figure 6.7: Absolute (not offset compensated) forces (left) and moments (right) measured with dynamometer top-west while rotating the system at ambient temperature with no REPAs connected and no insulation. Cross-markers: measurement data (from rotation angle $\varphi = -90°$ to $\varphi = +90°$), solid lines: cubic fit of measurement data, diamond-markers: ROHR2 results of base model *Traverse_999* (with insulation, geometry as planned), triangle-markers: ROHR2 results of base model *Traverse_100* (no insulation, geometry as measured by photogrammetry)

The assessment of the predictive power of the ROHR2 model is again done in an objective manner. Table 6.3 shows absolute and standardized RMSE for both models and each of three forces and three moments measured. The total uncertainty of the dynamo-meter measurements is also given. Comparing these values to each other we find that the predictions of the more sophisticated base model 'Traverse_100', which includes photogrammetrically measured piping system dimensions, over the original model 'Traverse_999'. Referring to the standardized RMSE, predictions are better in 4 out of 6 cases and in average.

Again, we compare the means squared unexplained measurements, the RMSE, with the total measurement uncertainty U, in order to see whether the first can be explained by the second. This time, other than when assessing the temperature response experiments, the RMSE can not be explained by the measurement uncertainty. This means that the

three named sources of systematic uncertainty, as well as the problem of the broken pin remain to explain the differences.

Table 6.3: Angle response experiment results and assessment of model predictions: values that help assessing the goodness of prediction both absolute and relative are presented for two base models: the total uncertainty of the measurements that has been estimated in chapter 3.2 and which is presented in the appendix in table A.4.2; The Root-Mean-Square-Error (RMSE) is calculated as the square root of the variance of the prediction error. Lower values mean a better fit [22]; The standardized RMSE finally is a relative measure that helps inter-comparing different models: 0 means a perfect prediction, while 1 means the opposite.

		Assessment of model predictions			
	experiment	*model: Traverse_999*		*model: Traverse_100*	
F_i	U	$RMSE$	*std. RMSE*	$RMSE$	*std. RMSE*
	in N	in N	-	in N	-
F_x	16	214	0.43	361	0.50
F_y	35	261	0.75	212	0.69
F_z	56	710	0.61	608	0.45
	in Nm	in Nm	-	in Nm	-
M_x	5	45	0.29	45	0.25
M_y	4	122	0.51	94	0.34
M_z	8	17	0.11	20	0.13

Given these results, it appears necessary to repeat validation experiments under different circumstances and with improved dynamo-meter measurement uncertainty. Chapters 7 and 8 provide more information.

7 Conclusion

Rotation and Expansion Performing Assemblies (REPAs) are an important part in parabolic through collector power plants. Their correct and safe operation is crucial from a economical, ecological and safety perspective. The REPA test-rig at the PSA in Tabernas is now nearly ready to contribute investigating and improving this simple yet complex part. Between June and December 2016, essential elements of the REPA test-rig have been mounted and prepared for commissioning. As one can see comparing the two photos in figure 7.1, the progress was significant.

Figure 7.1: Top: REPA test-rig in June 2016, bottom: January 2017

This thesis described the efforts undertaken to guarantee correct functioning of the REPA test-rig and to validate the force-measurement principle and simulation model. Additionally, measurement uncertainties have been estimated and decreased by applying a number of improvements to test-rig, sensor and simulation model. The main improvement tasks carried out and described in this thesis and the correlations between these tasks are shown in figure 7.2.

In order to verify that both traverse and main assembly comply with the allowed tolerances, a photogrammetric setup has been installed and adapted to the specific requirements: Pipe sleeves and adapters have been placed, allowing indirect measurements
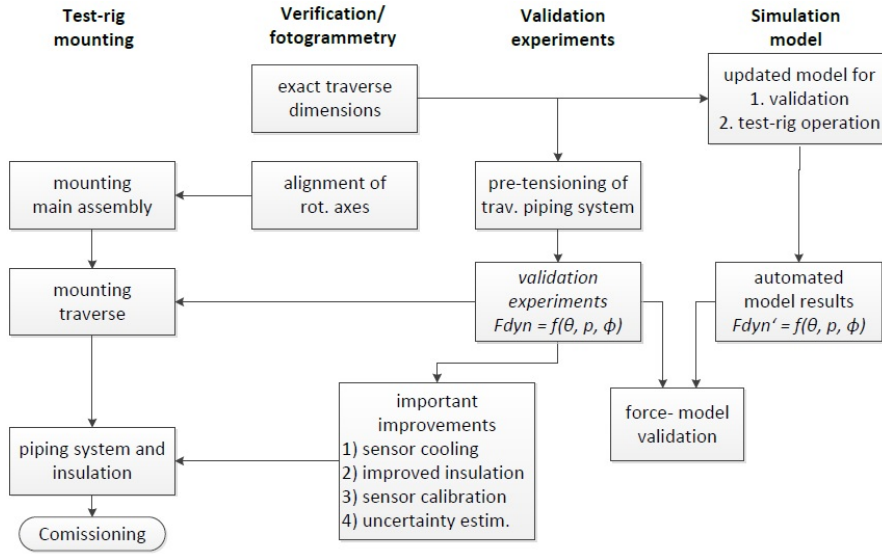
Figure 7.2: Main tasks that were carried out during this thesis in order to improve the performance of the REPA test-rig. These can be subdivided in four groups: test-rig mounting, verification, validation and simulation model. Lines indicate which tasks are required to complete before another task.

of the center lines of pipes and the exact positions of axes hidden inside a structure. Results could be obtained with measurement uncertainties below 0.1 mm. Three important tasks could be successfully accomplished: rotation axes alignment, model adaptation and improvement of pre-tensioning.

Well aligned rotation axes help to prevent the test rig from suffering damage due to high stresses and deformations. Further more, possible effects on the force and torque measurements can be ruled out. After several iterations of photogrammetric measurements and small adaptations of the bearing positions and orientations, all rotation axes have been aligned with the main rotation axis with a tolerance of less than 1 mm. The setup and the code can also be used for the alignment of the translation axes and to verify the alignment of the rotation axes after some extended test-rig operation. It can also be used in order to investigate temperature driven deformation of some parts of the test-rig and spot problems before damage occurs.

The second result of the photogrammetry were the exact dimensions of the traverse piping system. These were used improve and adapt the ROHR2-model, which is an important element behind the measurement principle of the REPA test-rig. After adapting the model to the traverse piping system as built, temperature- and rotation angle responses of the model were compared to the results of several validation experiments.

This comparison between model and experiment results showed that the model is not yet able to explain all the forces and moments measured. With the help of the Roots Mean Squared Error (RMSE) as quantitative statistic measure, it could be shown that the reliable prediction with the ROHR2 model so far is limited to two out of six target

variables during temperature response experiments and three out of six target variables during the angle response experiments. However, measurement uncertainties were huge, especially during the temperature response experiments, where their lower boundary was 146% of the measurement values in average.

These results have two main implications. First, the model validation experiments will have to be repeated, as a broken pin in the sensor-amplifier connection was discovered after the last experiment. it is believed to be the main reason for the unexplained differences between model and experiment and for the implausibilities within the experiment results. Its effect on the results however can not be quantified. A part of the information is lost and all six measured forces and moments are affected. Please compare the introduction of chapter 3 and equation A.6 in the appendix.

Second, the REPA test-rig requires further improvements to the measurement accuracy in order to yield valid force-measurements. This is especially true for all uncertainties caused by an increased dynamo-meter temperature. Improvements can be accomplished in three manners: a) Sensor heating can be reduced by improving sensor insulation and/or by installing an active cooling system. b) The effect of increased dynamo-meter temperature can be measured in isolated state in a number of extended temperature tests and then be subtracted from later measurements. If the effect is precisely known, it doesn't have to be considered in the total uncertainty anymore. c) All measurements can be changed to relative measurements, performing an offset compensation after each temperature- (and/ or load-) cycle. Doing this, experiment results would loose their information about absolute forces and moments onto the REPAs, but statements about the relative difference between two cycles would be more accurate.

In the course of this thesis, uncertainties have already been decreases significantly by the above mentioned measures a) and b). Next to the dynamo-meter measurements, the fourteen temperature response experiments have also been used to investigate the heating behavior of the dynamo-meter. It was found that the insulation board alone, that was placed between pipe bearing and dynamo-meter is not enough to maintain the dynamo-meter at a temperature below the maximum allowed temperature. Next to the potential danger to the dynamo-meter itself, increased temperatures also influence the measurement uncertainty. Two measures have therefore been installed: First, the insulation has been improved by adding insulation washers that reduces the thermal connection between bearing and sensor through the four bolts. Second, a ventilator has been installed. The effect was a drastic decrease in dynamo-meter heating. Please refer to appendix A.9 for detailed information.

Further more, model results were used to get a better estimation of the forces and moments the dynamo-meter will most likely measure during operation. Using this information, the sensor has been re-calibrated, clearly improving measurement accuracy. At the same time a first temperature test of the sensor has been made. The combined effect was a reduction of the total uncertainty by as much as 68% in average. As the relative measurement uncertainty depends on the actual value measured. A smaller absolute measurement leads to greater relative uncertainty. This is why especially measurements

of isolated effects such as the temperature response during validation experiments require further reductions of the measurement uncertainty.

Other than agreed, ME-Messsysteme did not provide the exact dynamo-meter temperatures during the temperature-test they performed, but only provided three measurement signal - temperature combinations. This means that the uncertainty stemming from temperature effect on zero signal can only be estimated. Further more, the test indicates a change in zero signal after the temperature test was complete. It could be that this change increases with every temperature cycle. To get a better understanding, an advanced temperature test should therefore be repeated, including multiple temperature cycles.

The commissioning of the REPA test-rig is a work in progress. Being a complex prototype, it is difficult to accurately schedule dates of important milestones. At the time this master's thesis started, the mounting and commissioning process was expected to be even more advanced than it is today. The original idea of this thesis has therefore been adapted to the given circumstances. In doing so, this work has provided important support and introduced interesting new aspects to the continued REPA test-rig project.

8   Outlook

Using the information and experience obtained during this thesis we can map out the steps that need to be taken in order to continue and finish the commissioning of the REPA test-rig. The principal steps are presented in the flowchart in figure 8.1.
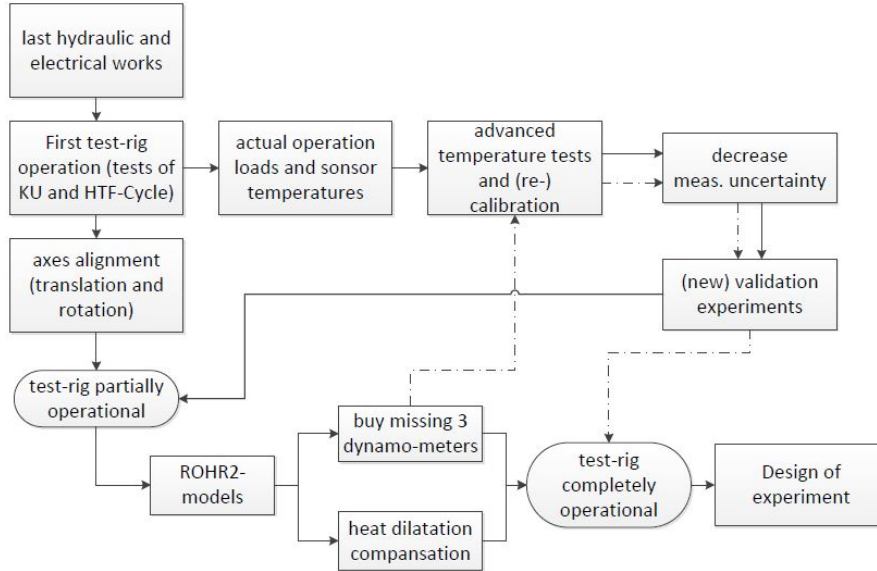
Figure 8.1: Future steps required to complete the commissioning of the REPA test-rig. Dotted lines indicate the path of the next three dynamo-meters that will be bought.

First we need further decrease dynamo-meter temperature. Insulation has already been improved and an active cooling system has been added. When commissioning the HTF-Cycle, attention has to be paid to the question whether these measures are sufficient to keep the sensor temperature below 50-60 °C. Under all circumstances the sensor-temperature has to be held below 80 °C to prevent the sensor from taking damage.

Once we know the temperature range in which the dynamo-meter will be working during test-rig operation, better temperature-tests should be designed. These tests can either be performed at the PSA or by ME-Messsysteme. Temperature tests must be as close to actual working conditions as possible. To guarantee that, it might be useful to perform the oven test with the bearing and connection plate being mounted onto the sensor and maybe with some constant load on the sensor.

Before performing any experiments, it is important to add a routine check to the post-processing that automatically gives out an alert, in case one of the channels stops producing reasonable output. It would thereby be ensured that no other problem in the hardware, like the broken pin, affects the measurements for such a long time without being discovered.

Before the validation experiments test-rig commissioning has to be completed. Next, the hydraulic unit and all the cylinders and perform first rotational and translational motion. During that, special interest should be paid to the question if the hydraulic unit is able to produce the swift rotational steps that occur in real PTC power plants due to breakaway torques. Afterwards nitrogen cycle (pressure), pump (mass-flow) and band heaters (temperature) have to be tested, before all sub-units are ready and first real experiments can be made.

Once the measurement uncertainty is in a reasonable range, validation experiments will have to be repeated to some extend. Rotation angle, and pressure experiments could be performed without disconnecting the traverse from the kinematic unit. But one of the REPAs will have to be disconnected. To do that, the oil has to be discharged, the REPA has to be cut off and the two open ends have to be blanked off with a metal plate that is able to withstand pressures up to 40 bar. Then oil has to be filled in again, allowing the combined test of both rotation angle and HTF pressure without the effect of the REPAs. If these experiments yield good results, it might not be necessary to also perform temperature response experiments.

During the commissioning of the HTF-Cycle great attention has to be paid to the dynamo-meter temperature. This involves both the position that is already equipped with an dynamo-meter as well as all three positions that are currently not filled with a dynamo-meter and only contain a dummy. Every upper connection plate has slots for two PT1000 temperature sensors and every information about realistic dynamo-meter temperatures during operation is of great value when designing temperature tests for sensor calibration. Further more a photogrammetry should be performed after some hours of HTF-Cycle operation to check for unwanted deformation of traverse and tables in order to spot problems before they cause damage.

As soon as validation was successful for the upper-west dynamo-meter position and the measurement principle is successfully tested, the last three dynamo-meter positions can be equipped. Any other position can be equipped a ROHR2-model needs to be created for the respective adjacent piping systems. For further advice, please have a look at appendix A.5. The first use of this will be to estimate whether the heat dilatation of the short piping sections adjacent to the lower dynamo-meters, between swivel-joints and feed-in / feed-out will damage the dynamo-meters if not compensated. Before equipping the upper-east dynamo-meter position, the eastern part of the traverse-piping system has to be equipped with three angular compensators, just like the western part is. Until this is done the fix bearing at the eastern end of the traverse may not be closed to prevent the bearing from taking damage.

Reaching this point, the test-rig is finally ready for complete REPA lifetime tests as designed. As last preparation, test have to be designed which wear REPAs in accelerated manner and at the same time reproduce authentic REPA operation conditions.

References
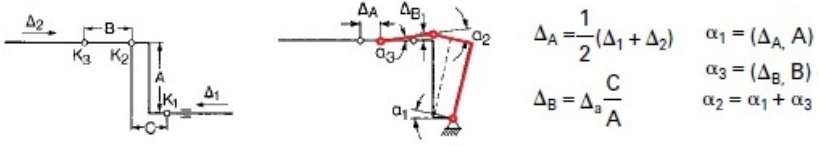
[1] European comission. Key elements of the paris agreement. website, January 2017. available at `http://ec.europa.eu/clima/policies/international/negotiations/paris_en`, downloaded: 13/01/2017.

[2] Christoph Hilgert, Christoph Happich, Timo Effertz, and Nicole Janotte. Repa teststand, 2015. available at `http://www.dlr.de/sf/Portaldata/73/Resources/dokumente/soko/soko2015/poster/Hilgert_-_REPA_Test_Rig_-_DLR_2015.pdf`, 2016-11-03.

[3] International Renewable Engery Agency (IRENA). Renewable engery technologies: cost analysis series, 2012. Volume 1: Power Sector, Issue 2/5.

[4] iNTERURBE.com. Incendio en la planta andasol. Video - Youtube, December 2009. available at `https://www.youtube.com/watch?v=aGyvicfgZm0`,2016-11-15.

[5] Lourdes A. Barcia, Rogelio Peón Menéndez, Juan Á. Martínez Esteban, Miguel A. José Prieto, Juan A. Martín Ramos, F. Javier de Cos Juez, and Antonio Nevado Reviriego. Dynamic modeling of the solar field in parabolic trough solar power plants. *Energies*, 8(12):12373, 2015.

[6] Senior Flexonics. Kurzpräsentation einbausituation, dlr-teststand, rotationflex® -system, konfiguration eurothrough, October 2015.

[7] Christoph Happich, Christoph Hilgert, Andreas Plumpe, Niels Algner, Wolfgang Reinalter, and Nicole Janotte. Teststand für flexible rohrverbindungen (repa), 2016. available at `http://www.dlr.de/sf/Portaldata/73/Resources/dokumente/soko/soko2016/poster/DLR-Sonnenkolloquium2016_Poster_Happich_DLR_Teststand_f_flex_Rohrverbindungen.pdf`, 2016-11-03.

[8] Andreas Plumpe. Design of a test rig and its testing methods for rotation and expansion performing assemblies in parabolic trough collector power plants. *Master's Thesis - RWTH - University, Aachen, Germany*, 2016.

[9] Tobias Hilbel. Design of the motion control for a test rig analyzing rotation and expansion performing assemblies in parabolic through collector power plant applications. *Bachelor's Thesis - Hochschule Mannheim, Mannheim, Germany*, 2016.

[10] ME-Messsysteme GmbH. Faq: Skalierung des ausgangssignals. Technical report, ME-Messsysteme GmbH, 23.05.2015. available at `https://www.me-systeme.de/docs/de/basics/pdf/kb-display.pdf`, 2016-11-07.

[11] M. E.-Messsysteme GmbH. Inbetriebnahme von sensoren. available at `https://www.me-systeme.de/docs/de/basics/kb-measure.pdf`,2016-11-23.

[12] Fachbereich Fertigungsmesstechnik. Vdi/vde/dkd 2638 - german: Kenngrößen für kraftaufnehmer - begriffe, english: Characteristics of force transducers - terms and definitions. Technical report, VDI/VDE-Gesellschaft Mess- und Automatisierungstechnik, 2008-10.

[13] DIN Deutsches Institut für Normung e. V. Din en iso 7500-1: Metallische werk- stoffe – prüfung von statischen einachsigen prüfmaschinen – teil 1: Zug- und druck- prüfmaschinen – prüfung und kalibrierung der kraftmesseinrichtung (iso/dis 7500- 1:2014); deutsche fassung pren iso 7500-1:2014. Technical report, DIN Deutsches Institut für Normung e. V., 2014.

[14] ME-Messsysteme GmbH. Data sheet for k6d175 10kn/1knm. Technical report, ME-Messsysteme GmbH, Stand: 29.06.2015.

[15] Tommy Künstner. Werkszertifikat 20543306, prüfbericht kalibrierung mehrkomponenten-sensor:, typ k6d175 10kn/1knm s/n: 15401935. Technical report, ME-Messsysteme GmbH, 15.10.15.

[16] Thomas Luhmann, Stuart Robson, Stephen Kyle, and Ian Harley. *Close range photogrammetry: Principles, Techniques and Applications*. Whittles Publishing, 2006.

[17] Klaus Pottler, Eckhard Lüpfert, Glen HG Johnston, and Mark R Shortis. Pho- togrammetry: A powerful tool for geometric analysis of solar concentrators and their components. In *ASME 2004 International Solar Energy Conference*, pages 719–726. American Society of Mechanical Engineers, 2004.

[18] iw Maschinenbau GmbH. Betriebsanleitung repa-testrig 2014149. Manual, 2015.

[19] Mirko Saur. Senior flexonics. email, October 2016.

[20] Witzenmann GmbH. Handbuch der kompensatoren. Technical report, Witzenmann GmbH, Nov 2012.

[21] JCGM. *Evaluation of measurement data — Guide to the expression of uncertainty in measurement, GUM 1995 with minor corrections*. JCGM, first edition edition, 2008.

[22] Karen. Assessing the fit of regression models. http://www.theanalysisfactor.com/, January 2017. available at http://www.theanalysisfactor.com/ assessing-the-fit-of-regression-models/,2017-01-15.

[23] Tommy Künstner. Werkszertifikat 20547788, prüfbericht kalibrierung mehrkomponenten-sensor:, typ k6d175 10kn/1knm s/n: 15401935. Technical report, ME-Messsysteme GmbH, 2016.

Abbreviations

Term	Description
BJA	Ball Joint Assembly
CIEMAT	Centro de Investigaciones Energéticas, Medioambientales y Tecnológicas
CSP	Concentrated Solar Power
DLR	German Aerospace Center
GUI	Graphical User Interface
HTF	Heat Transfer Fluid
KU	Kinematic Unit
LC	Load Case
LV	LabVIEW
OPC-Server	Open Platforms Communications Server
PLC	Programmable Logic Controller
PSA	Plataforma Solar de Almería
PTC	Parabolic Trough Collector
REPA	Rotation and Expansion Performing Assembly
RFHA	Rotary Flex Hose Assembly
SCA	Solar Collector Assembly
SCADA	Supervisory Control and Data Acquisition
SCE	Solar Collector Element
STC	Solar Tower Collector

Glossary: Test-Rig Operation

Symbol	Unit	Description
θ	°	**Translation angle** *Translationswinkel* The angle between the drive pylon arms and the plane perpendicular to the rotation axis. The design specifications state that θ lies within the range of $[0°, 45°]$.
α	°	**Compensator angle** *Kompensatorenwinkel* The angle of deflection of one of the thee angular expansion joints: α_1, α_2 and α_3 counting from east to west. Please not that because of their geometrical connection $\alpha_2 = \alpha_1 + \alpha_3$. In order to have α_i as small as possible during operation, the piping system is pre-tensioned such that $\alpha_i \approx 0°$ for $\vartheta_{HTF} = 350\,°C$. (Source graphic: [20, p.63])

$$\Delta_A = \frac{1}{2}(\Delta_1 + \Delta_2) \qquad \alpha_1 = (\Delta_A, A)$$
$$\alpha_3 = (\Delta_B, B)$$
$$\Delta_B = \Delta_a \frac{C}{A} \qquad \alpha_2 = \alpha_1 + \alpha_3$$

Symbol	Unit	Description
φ	°	**Rotation angle** *Rotationswinkel* The angle inside a plane perpendicular to the rotation axis, measured between traverse and a vertical line seen from the rotation axis. Around the vertical position, $\varphi = 0°$, which is called rest position, the range of φ is $[-120°, 90°]$. The lowest position, $\varphi = -120°$, is called 'stow position', $\varphi = 90°$ is called 'end position'.
$\bar{\alpha}$	µm/(m K)	**Average linear heat dilatation coefficient** *Mittlerer Wärmeausdehnungskoeffizient* The piping system is made of 13CrMo4-5 (Material-No. 1.7335). The data-sheet states the linear dilatation coefficient of thermal expansion between $20\,°C$ and $300\,°C$ to be $12.9\,µm/(m\,K)$, between $20\,°C$ and $400\,°C$ to be $13.5\,µm/(m\,K)$ and between $20\,°C$ and $500\,°C$ to be $13.9\,µm/(m\,K)$. the value for $400\,°C$ applies.
ϱ_{HTF}	g/cm^3	**HTF density** *HTF Dichte* The density of the HTF used, normaly dependent of HTF temperature ϑ_{HTF}, compare respective data sheets. Typical HTFs used in commercial parabolic trough collector power plants are: Diphenyl-Diphenyl oxides such as *Therminol*©VP-1 and DOWNTHERM A, Silicone oils such as *Syltherm 800* and HELISOL©5A, Molten salts such as *Solar Salt*, *Hitec*©and *Hitec*©XL and steam/water [8].
$\dot{m}_{HTF}$	l/s	**HTF mass flow rate** *HTF Massenstrom* Flow rate of HTF in HTF-Cycle. Due to latest (not final!) version of specification sheet to be set between $1.7\,l/s$ and $17\,l/s$

Symbol	Unit	Description
p_{HTF}	bar	**HTF pressure** *HTF Druck* The pressure of the HTF inside the piping system. The maximum pressure allowed is defined by data sheet of the HTF used and the HTF temperature set. The maximum design pressure is 40 bar
ϑ_{HTF}	°C	**HTF temperature** *HTF Temperatur* The temperature of the HTF inside the piping system. Load Cases are defined according typical situations in parabolic trough power plants. Temperature at Inlet of trough $T_{HTF} = 300$ °C, temperature at Inlet of trough $T_{HTF} = 400$ °C. The highest temperature the REPA test rig has been designed for is $T_{HTF} = 450$ °C[8]. Due to latest (not final!) version of specification sheet to be set between 40 °C and 450 °C, taking into consideration the specifications for the HTF used and adjust the HTF pressure accordingly.
ϑ_{amb}	°C	**Ambient temperature** *Umgebungstemperatur* If not individually measured, the ambient temperature is given the value 20 °C.
$\vartheta_{abs.tube,avg.}$	°C	**Average absorber tube temperature** *Durchschnittliche Temperatur der Absorberröhre* We assume that absorber-tube temperatures in a real-life PTC power-plant are equal to the HTF temperature in the tube in every section, and that these rise linearly from start to end. That way $\vartheta_{abs.tube,avg.} = (\vartheta_{HTF,start} + \vartheta_{HTF,end})/2$. For a REPA situated at an inlet, the important pipe section is from inlet to the drive pylon in the middle, for a REPA situated at an outlet, the important pipe section is from the drive pylon to the outlet (please compare figure 1.2). The average absorber tube temperatures important for the translation angles for the LCs are therefore: 'LC Inlet': $\vartheta_{abs.tube,avg.} = 325$ °C and 'LC Outlet': $\vartheta_{abs.tube,avg.} = 375$ °C.
ϑ_{pipe}	°C	**Mean traverse piping temperature** *durchschn. Rohrtemperatur* Average temperature of traverse piping. In temperature-response validation experiments calculated as the mean of the four pipe temperature measurement values taken during the validation experiments. ϑ_{pipe} is used for all plots in which 'pipe temperature' is one of the axes. Be aware that maximum and minimum pipe temperature might deviate from the mean value by up to 50 K. During later test-rig operation estimated to equal the HTF temperature.

Glossary: Dynamo-Meter Theory

Symbol	Unit	Description
U_D	mV	**bridge voltage of the Wheatstone bridge** *Brückenspannung der Wheatstone'schen Brücke* The output voltage of the dynamo-meter is equal to the bridge voltage of the Wheatstone bridge and scales with the supply voltage U_s. The output signal u_S is therefore given per V supply voltage U_s.
K	N/V	**Calibration matrix** *Kalibriermatrix* The calibration matrix K contains the combined effects of both slope of sensor calibration curve c_S and slope of amplifier calibration curve c_A. It's unit can either be N/V, then $F_{dyn} = K \cdot U$; or N/(mV V), then $F_{dyn} = K' \cdot S$. $K' = K \cdot \frac{5V}{2mV/V} = K \cdot 2.5 \frac{V}{mV/V}$
F_{dyn}	N,Nm	**Dynamo-meter reading** *Dynamometer Messwert* The vector of three forces and three moments that are obtained after multiplying the amplifier output voltage with the calibration matrix. This is equal to the output of GSV-multi.
S	mV	**Sensor output signal** *Sensor-Ausgangsspannung* The absolute output voltage of the dynamo-meter. $S = U_D \cdot U_S$.
U_s	V	**Supply voltage** *Speisespannung* The output signal of the dynamo-meter scales with the supply voltage from the measurement amplifier. Sensor signals are therefore given in mV/V. For the K6D175 the supply voltage is 5 V.
c_A	V/(mV V)	**Slope of amplifier calibration curve** *Steigung der Messwertverstaerkerkennlinie* The slope of the amplifier calibration curve is the output voltage of the amplifier per input given in relation to the supply voltage and therefore in the unit mV/V. It is equal to the amplifying factor.
c_S	mV/(V N)	**Slope of sensor calibration curve** *Steigung der Sensorkennlinie* The slope of the sensor calibration curve is the output voltage of the sensor per input per N of the force (or Nm of the moment) applied.
U_A	mV/V	**Input sensitivity** *Eingangsempfindlichkeit des Verstaerkers* The input sensitivity is equal to the highest signal at the input of the amplifier which is produced if the dynamo-meter is loaded with nominal forces and moments.
U_A	V	**Upper limit of measuring range** *Messbereichsendwert des Verstaerkers* The upper limit of the measurement range is equal to the amplifier output voltage at nominal forces.
U	V	**Amplifier output voltage** *Verstaerker-Ausgangsspannung* The amplifier output voltage that is multiplied with calibration matrix K to obtain the dynamo-meter reading F_{dyn}.

Symbol	Unit	Description
u_S	mV	**sensor output signal per V supply voltage** *Sensor-Ausgangsspannung pro V Speisespannung*, see bridge voltage of the Wheatstone bridge U_D.

Glossary: Dynamo-Meter Uncertainty

Symbol	Unit	Description
C	mV/V	**Characteristic Value** *Kennwert* Output signal at rated force F_{nom}, decreased by the zero signal when mounted S_{F0}[12].
F_{cal}	N,Nm	**Calibration force** *Kalibrierkraft* The forces and moments the dynamo-meter is calibrated for.
d_{cr}	%FS	**Relative creep** *Relatives Kriechen* By creep the time-dependent variation (in 30 min)of the out-put signal of the force transducer after force variation is understood. A distinction is to be made be-tween: creep under load and creep when load is relieved[12].
F_{nom}	N	**Rated force** *Nennkraft* Greatest force for which the transducer is nominally designed, i. e. up to which the manufacturer's metrological specifications are complied with[12].
F	N	**Force** *(Wirk-)Kraft* Vectorial physical quantity with point of application, direction of action and amount ($1\,\mathrm{N} = 1\,\mathrm{kg\,m^{-1}\,s^{-2}}$[12].
b_{rg}	%FS	**Relative repeatability error (in un-changed mounting position)** *Relative Spannweite (in unveraenderter Einbaustellung)* Maximum difference of the output signals at equal force, determined from several series of measurements without the mounting position being changed, in relation to the mean output signal decreased by the zero signal in the mounted state. The rel. repeatability error is a measure of the repeatability[12].
d_{lin}	%FS	**Relative linearity error** *Relative Linearitaetsabweichung* Maximum deviation of a characteristic curve of a force transducer, determined at increasing force, from the reference straight line, in relation to the upper limit of the measurement range used[12].
μ	%FS	**Relative reversibility error** *Relative Umkehrspanne* Difference of the output signals of an increasing and decreasing series at equal force F, in relation to the output signal at increasing force, decreased by the zero signal when mounted S_{F0}[12].
F_{dyn}^{φ}	N,Nm	**Angle angle response** *Rotationswinkelantwort* Absolute dynamo-meter reading F_{dyn} for changing rotation angle φ at constant HTF temperature ϑ_{HTF}, HTF pressure p_{HTF} and translation angle θ. The angle response is a absolute value.

Symbol	Unit	Description
ΔF_{dyn}^{p}	N,Nm	**Pressure response** *Druckantwort* Change in the dynamo-meter reading F_{dyn} for changing HTF pressure p_{HTF} at constant HTF temperature ϑ_{HTF}, rotation angle φ and translation angle θ. The pressure response is a relative value as ΔF_{dyn}^{p} is set to zero for $p_{HTF} = 0\,\mathrm{bar}$.
$\Delta F_{dyn}^{\vartheta}$	N,Nm	**Temperature response** *Temperaturantwort* Change in the dynamo-meter reading F_{dyn} for changing HTF temperature ϑ_{HTF} at constant HTF pressure p_{HTF}, rotation angle φ and translation angle θ. The temperature response is a relative value as $\Delta F_{dyn}^{\vartheta}$ is set to zero for $\vartheta_{HTF} = 20\,^{\circ}\mathrm{C}$.
TK_0	%FS/K	**Temperature effect on zero signal** *Temperatureinfluss auf das Nullsignal* Variation of the zero signal of the force transducer, in relation to the rated characteristic value, due to variation of the dynamo-meter temperature ϑ_{dyn} by 10 K, within a defined temperature range after steady states free of gradients have been adjusted[12]. (Value adjusted to change for 1K)
TK_C	%RD/K	**Temperature effect on characteristic value** *Temperatureinfluss auf den Kennwert* Relative variation of the characteristic value of the force transducer due to variation of the dynamo-meter temperature ϑ_{dyn} by 10 K, within a defined temperature range after steady states free of gradients have been adjusted[12]. (Value adjusted to change for 1K)
ϑ_{dyn}		**Dynamo-meter temperature** *Dynamometertemperatur* The effective internal temperature of one of the four dynamo-meters. Influences measurement uncertainty via temperature effect on zero signal and temperature effect on characteristic value. The sensor temperature is measured by two PT1000-temperature sensors placed in the steel plate that connects bearing and dynamo-meter. As the steel plate heats up first, their measurement value is used as an (upper) estimate of the sensor temperature. Having two PT1000 placed in the dynamo-meter by the manufacturer would have been possible on request but was unfortunately forgotten when purchasing the dynamo-meter. The maximum operation temperature for the K6D175 is $70\,^{\circ}\mathrm{C}$, the maximum allowed temperature is $85\,^{\circ}\mathrm{C}$. A greater temperature will do harm to the sensor (change the zero-signal).

Symbol	Unit	Description
$U_{0,\vartheta}$	V	**Difference in zero signal due to increased sensor temperature** *Drift des Sensor-Nullsignals bei Temperaturerhöhung* When a dynamo-meter is heated, it's zero signal changes in relation to it's internal temperature. This effect is measured in a so-called temperature test. The data obtained is then used to subtract the effect from the actual measurements. During the temperature test, the sensor is either completely unloaded and unmounted, or loaded with a constant force. It is assumed, but not necessarily true, that the then measured behavior will be the same during test-rig operation. Another problem are temperature gradients. Their effect as well as the gradients itself are difficult to measure. The first temperature test however indicates that the effect of the gradients might even be greater than the effect of a higher but constant temperature. This might be, because the six strain gauges inside the sensor are temperature compensated, which only works if all six strain gauges experience the same temperature.
$\Delta U_{0,20C}$	V	**Difference in zero signal after complete heating cycle** *Nullpunktrückkehrfehler nach Temperaturzyklus* The first temperature test showed that the zero signal at ambient temperature had changed after heating up to $80\,°C$ once. A change in zero signal is equal to an undesired offset in the measurement results. Please compare appendix A.3.2 for values. This behavior could be a major problem, if this effect is found to increase (accumulate) with repeated cycles. An advanced temperature test should do a series of temperature cycles to investigate this.
S_0	mV/V	**Zero signal when removed** *Nullsignal im ausgebauten Zustand* Output signal of the unloaded force transducer, without mounting parts in the unit milli volt per volt supply voltage. $S_0 = U_0 \cdot (5\,\text{V}/2\,\text{mV/V}) = U_0 \cdot 2.5V/(mV/V)$[12]
S_{F0}	mV/V	**Zero signal when mounted** *Nullsignal im eingebauten Zustand* Output signal of the force transducer when not mechanically loaded, with mounting parts, at the beginning of a loading cycle[12].
U_0	V	**Zero signal when removed** *Nullsignal im ausgebauten Zustand* Output signal of the unloaded force transducer, without mounting parts in the unit volt. $U_0 = S_0 \cdot (2\,\text{mV/V})/5\,\text{V} = S_0 \cdot 0.4(mV/V)/V$.

Appendices

A   Additional Information

A.1   Test-rig specifications and problems

Rotational motion

Geometric calculations, shown in figure A.1.1 give reason to believe that the cylinder stroke of 700 mm is not sufficient to perform the whole rotation margin specified. The stroke needed to geometrically perform the whole range of φ is 648.4 mm (east) and 686.8 mm (west), however as in the lowest position, the cylinders are already pushed out a little: 84.3 mm (east and west), the effective stroke is only 667 mm (east) and 629 mm (west). The possible angle φ with the effective cylinder stroke is then ca. $[-90°, 80°]$. Elongating the rotation cylinders may be considered.
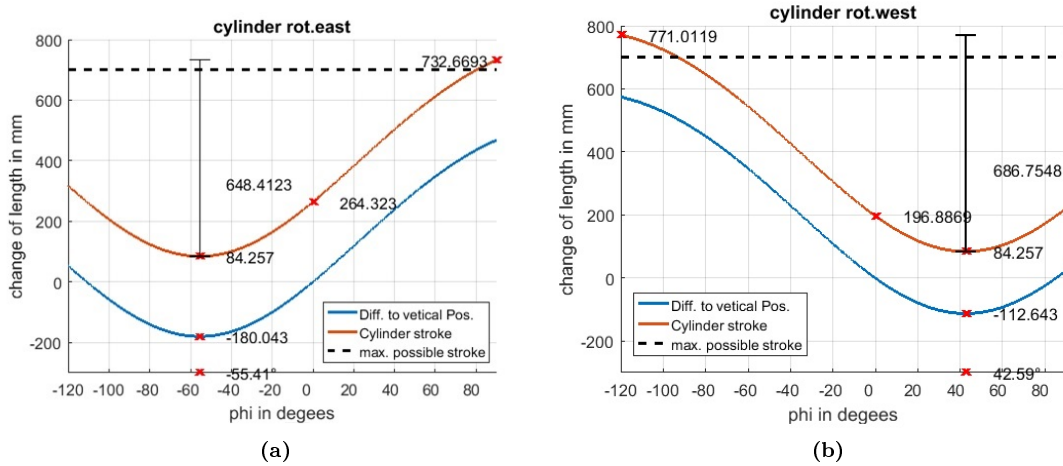
Figure A.1.1: Rotation cylinder stroke east (left) and west (right). The blue lines indicate the difference in stroke compared to the vertical position: $\varphi = 0°$. The red line indicates the actual cylinder stroke. Geometric calculations show that the cylinder is not long enough to perform the full rotation, as its shortest position is already too far out.

Translational motion

In real-life trough collectors the translational motion of the REPAs due to heat dilatation can be described as a function of the HTF-temperature ϑ_{HTF}. If we assume that absorber-tube temperatures in a real-life PTC power-plants are equal to the HTF temperature in the tube in every section, and that these rise linearly from inlet to outlet and

62

finally that the dilatation is small compared to the focal length so that the small angle approximation applies, we can express the translation angle θ as a linear function of the average absorber tube temperature. Using this relation, translational motion cycles for different REPA-positions in the loop can be designed.

Necessary translation angles needed to reproduce typical values were first calculated by Senior Flexonics (SF), on the basis of which (compare App. A.10) the test-rig geometry has been designed. They define the corresponding ϑ_{HTF} at $\theta = 0°$ to be $\vartheta_{HTF,\theta=0,ap} = 342.0\,°\mathrm{C}$. Here the index 'ap' stands for 'as planned'. Due to deviations from the original plan during construction (compare section 4) this temperature has to be redefined 'as built': $\vartheta_{HTF,\theta=0,ab} = 331.8\,°\mathrm{C}$.

Knowing this, three different relations for $\theta = f(\vartheta_{HTF})$ can be found using a linear fit: 1) approximation on basis of angles and corresponding temperatures given by SF: $\theta = -0.0524\,°/\mathrm{K}\cdot(\vartheta_{HTF}-\vartheta_{HTF,\theta=0})$; 2) approximation on basis of translational positions and corresponding temperatures given by SF: $\theta = -0.0418\,°/\mathrm{K}\cdot(\vartheta_{HTF}-\vartheta_{HTF,\theta=0})$; or using small angle approximation: 3) calculation on basis of linear heat dilatation model: $\theta = -\frac{\bar{\alpha}\cdot l_{abs}}{f}\cdot\frac{360}{2\pi}[°/K]\cdot(\vartheta_{HTF}-\vartheta_{HTF,\theta=0}) = -0.0424\,°/\mathrm{K}\cdot(\vartheta_{HTF}-\vartheta_{HTF,\theta=0})$, with average linear heat dilatation coefficient $\bar{\alpha} = 1.8\,\mu\mathrm{m}/(\mathrm{m\,K})$, absorber length $l = 75\,\mathrm{m}$ (typical for EuroTrough) and focal length $f = 1.825\,\mathrm{m}$.

In this thesis approach 1) is used, as is was introduced first and the question whether to use another one is still pending. That way the translation angle equivalent to standard operation temperatures $\vartheta_{HTF} = [400\,°\mathrm{C}, 18\,°\mathrm{C}]$ is $\theta = [-3°, 17°]$ and the translation angle equivalent to design temperatures $\vartheta_{HTF} = [450\,°\mathrm{C}, 18\,°\mathrm{C}]$ is $\theta = [-5.65°, 17°]$.

With the stroke of the translation cylinder of 450 mm a range of $\theta = [-19°, 28°]$ is theoretically possible. What range will also be mechanically possible (i.e. without any parts of the test-rig touching) will have to be tested. Special positions: $\theta = 17°$ is called 'maximum cold position' and is equivalent to ambient temperature, $\theta = 12°$ is called 'maximum cold position in operation' and is equivalent to their position at $110\,°\mathrm{C}$ in a commercial power plant and finally $\theta = -3°$ is called 'maximum hot position in operation' and is equivalent to their position at $400\,°\mathrm{C}$ in a commercial power plant.

HTF pressure

The highest pressure allowed at higher temperatures is defined by the data sheets of the HTF used, but may never exceed the design pressure of 40 bar. At cold ambient temperature a pressure test up to 75 bar was successfully passed. Appendix A.10 states that the maximum operational conditions of the REPAs currently used are: 40 bar at $400\,°\mathrm{C}$ for a short period of time and static conditions and 35 bar at $400\,°\mathrm{C}$ as maximum operation conditions. The maximum operation conditions of the Witzenmann compensators used is 40 bar at $450\,°\mathrm{C}$ for all three.

Table A.1.1: The table shows parameters as planned and as built and compares them to other typical values found. It also states the measurement accuracy for the respective parameter in the test-rig. Subscripts: 1) range possibly smaller due to mechanical obstacles, see glossary; 2) ambient temperature ϑ_{amb} defined as 20 °C, see glossary; 3)possibility when testing new silicone based oils; 4) calculated for HELISOL©at LCs 'Inlet' and 'Outlet' as typical REPA test-rig working conditions; 5) complete stroke can't be used, as cylinder is already pushed out a little in lowest position, see glossary. Sources: AP - Andreas Plumpe, master's thesis, [8]; CH - Christoph Hilgert, Hydraulic_Torque_and_Forces_CHa.xlsx; GG - Gines Garcia, Instrumentations department PSA, verbal information, no written documentation; SF - Senior Flexonics, Manufacturer for flex hose REPAs; SI - Sigma Ingenieurgesellschaft, technical drawings of REPA test-rig as planned; TH - Tobias Hilbel, bachelor's thesis, [9].

Variable	Unit	As planned	Source	As built	Source	Compare to	Source
rotation angle φ							
full range	°	-120...90	AP	-90...80[5]	A.1	-124...91	SF
day cycle range	°	-120...90	AP	[5]	A.1	-124...91	SF
stow position	°	-120	AP	[5]	A.1	-124	SF
end position	°	90	AP	[5]	A.1	91	SF
measurement accuracy	°	$\pm(0.014 + 0.004\%)$ of meas. val.	TH			0.1	TH, GG
rotational motion							
max speed rot.	°/s	1.4	TH			0.6	TH, GG
max. speed cylinder	m/s					0.1	data sheet
max. cylinder stroke	mm	700	CH	total: 700[5]	data sheet		
step interval	s					20...40; > 3	AP; TH, GG
pos. precision	°	0.1	TH (excl. uncert. of meas.)			0.1	GG
step size	°	≤ 0.25	TH				
tolerance axis orientation	mm	1; 2	SI; SF (email)		Photogr., sec 4		
translation angle θ							
design range (poss. w. cyl. stroke))	°	0...45	AP	-19...28[1]	SF, A.1		
operation range	°	-5.65...17	see below	-4.94...13.03; -5.01...13.22	SF, A.1	-3...17	calc. based on SF
max. hor. dist. REPA at $\theta = 0$	mm	600	SF		Photogr., sec 4		
temp. at $\theta = 0$	°C	342	SF, A.1	331.8	SF, A.1		
slope lin. rel. $\theta = f(\vartheta_{HTF})$	°/K	-0.0524	A.1	-0.0418; -0.0424	see glossary		
max. cold (20°C)	°	17	SF	13.03; 13.22	calc.		
max. cold in op. (110°C)	°	12	SF	9.27; 9.40	calc.		
max. hot in op. (400°C)	°	-3	SF	-2..85; -2.89	calc.		
design max. hot (450°C)	°	-5.65	A.1	-4.94; -5.01	calc.		
measurement accuracy	°						
translational motion							
max speed transl.	°/s						
max speed cylinder	m/s	0.03	CH				
max cylinder stroke	mm	450	CH	450	data sheet		
tolerance axis orientation	mm	1; 2	SI; SF (email)		Photogr., sec 4		
HTF temperature ϑ_{HTF}							
operation range	°C	20[2]...450[3]				20[2]...400	SF
day cycle range	°C						
inlet	°C	300	AP			293	SF
outlet	°C	400	AP			393	SF
design (max.)	°C	500	AP				
HTF pressure p_{HTF}							
operation range	bar	0...40	AP			0...35	SF (max. val.)
typical range	bar	20...30	AP				
inlet	bar	30	AP				
outlet	bar	20	AP				
design	bar	45	AP				
HTF mass flow rate $\dot{m}_{HTF}$							
design range	m³/h	6...60	AP				
... with HELISOL HTF	kg/s	0.9...11[4]	calc. based on AP				
operation range	kg/s					6...7.3	SF
General operation							
cycles per day	1/d	ca. 400	AP			336	calc.
focal length	m	1.825	SI		Photogr., sec 4		

A.2   Definition of terms

1. Overview: Main Assembly + HTF Cycle

2. Main Assembly

3. HTF Cycle

4. Sensors part 1/3

5. Sensors part 2/3

6. Sensors part 3/3

7. List of sensor details

Overview: Main Assembly + HTF Cycle

Compensator
(one of six)

REPA East

Transl. Cylinders
(north and south)

Traverse

Drive Pylon Arms
(east and west)

REPA West
for three main transl. positions

Table Arm
East

Base Frame

Table Arm Bearing

Table
East

Swivel Joint

S

Dynamo-meter
here: West-bottom

Drive Pylon
Head

Positions of six
band heaters

Rot. Cylinders
(east and west)

Direction
of flow

Pump

Drive Pylon
Frame

N

Table
West

Feed Line Out (In)

W

E

Main Assembly

Main Parts

A. Traverse
B. Drive Pylon
C. Table East
D. Table West
E. Hydraulic System

HTF-Cycle

1. Dynamo-meter (two per REPA: bottom and top)
2. Swivel Joint
3. Torsion Sword
4. Torsion Sword Flange
5. REPA West (depicted for three typical transl. angles)
6. Sensor Bearing (fix bearing, including dynamo-meter top position)
7. Compensator West-Outer (gimbal hinged angular expansion joint)
8. Compensator West-Center (single hinged angular expansion joint)
9. Compensator West-Inner (single hinged angular expansion joint)
10. Red Steel Bearing West (sliding bearing)
11. Red Steel Bearing Center (fix bearing)
12. Red Steel Bearing East (sliding bearing)
13. Compensator East-Inner (single hinged angular expansion joint)
14. Compensator East-Center (single hinged angular expansion joint)
15. Compensator East-Outer (hinged angular expansion joint)
16. REPA East (only one transl. angle)
17. Swivel Joint Bearing
18. ITEM-Profile
19. Intermediate Pipe Knee
20. Table Pipe Bearing (fix bearing, east and west)

Kinematic

21. Base Frame
22. Drive Pylon Base Frame
23. Drive Head Assembly
24. Drive Pylon Arm
25. Drive Pylon Arm Bearing
26. Drive Pylon Arm Support Bracket
27. Drive Pylon Arm Support Intake
28. Drive Pylon Arm Connection
29. Translation Cylinder (north and south)
30. Translation Cylinder End Plate Bearing
31. Translation Cylinder Arm Bearing
32. Translation Cylinder Traverse Connection
33. Drive Pylon Head Lever
34. Spindle Drive
35. End Plate (east and west)
36. End Plate Frame
37. Rotation Cylinders (east and west)
38. Swivel Drive Arm
39. Swivel Drive Arm Traverse Connection
40. Swivel Drive
41. Swivel Drive Support
42. Swivel Drive Support for small REPAs (currently not used)

Hydraulic System:

43. Hydraulic Unit
44. Hydraulic Tubing
45. Hydraulic Unit Support
46. Hydraulic Unit Oil Tray

Instrumentation

1. HTF Pump
2. PT Pump discharge / Vent valve discharge
3. Shut-off Pump discharge
4. Drain valve discharge
5. Bypass shut off valve
6. Band heaters
7. Volume flow orifice
8. Feed Line – In Flexible Hose
9. Feed Line – Out Flexible Hose
10. PT Kinematic out / Vent Valve Kinematic - Out
11. Drain Valve (Check Valve)
12. Check Valve
13. Shut-off Expansion Vessel In
14. Shut-off Expansion Vessel Bypass
15. Shut-off Expansion Vessel Out
16. Strainer
17. Shut-off Pump suction
18. PT Pump suction / Vent valve suction
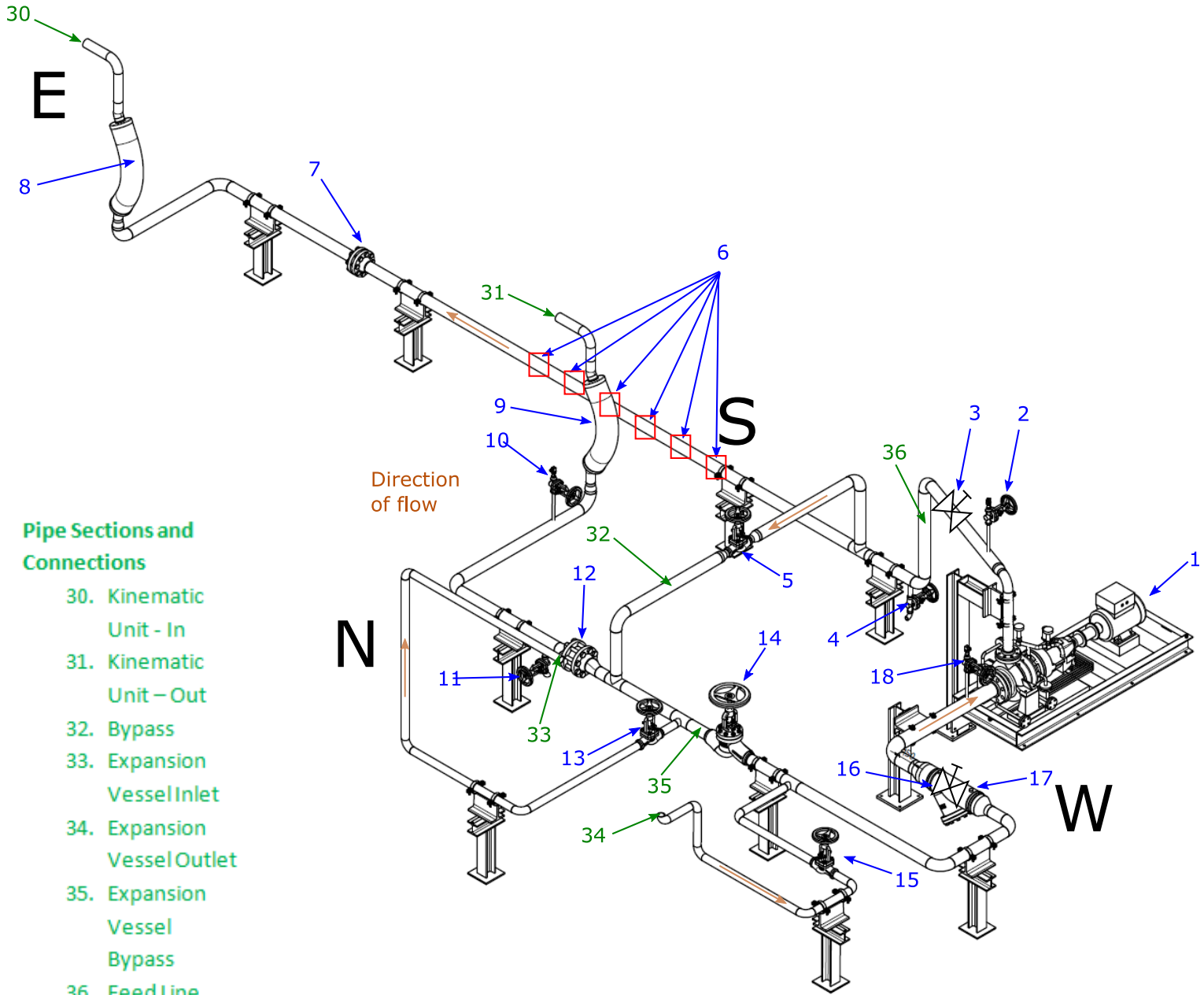
Pipe Sections and Connections

30. Kinematic Unit - In
31. Kinematic Unit – Out
32. Bypass
33. Expansion Vessel Inlet
34. Expansion Vessel Outlet
35. Expansion Vessel Bypass
36. Feed Line

Direction of flow

HTF-Cycle without expansion vessel and piping inside kinematic unit

E

S

N

W

E

N

S

W

19

6

7
8
9
10
11
12

20

2

1

46

3

4

5

Sensors (part 2)

25
26
27
28
future

21

23

123
124
125
126
future

44

43
45

41

40
42

E

22

W

24

119
120
121
122
future

47
64-69
EVs

48

127
128
129
130
future

117
118

61

62

M1 servo
control
controller

63

table design
changed

table design
changed

150 5000 5000 5000 600

3064

3050

810 600 995

2589

2000

3850

4690

9340

3050

3850

1100

1100

30
31 future

29

500

5000 5000 5000 600
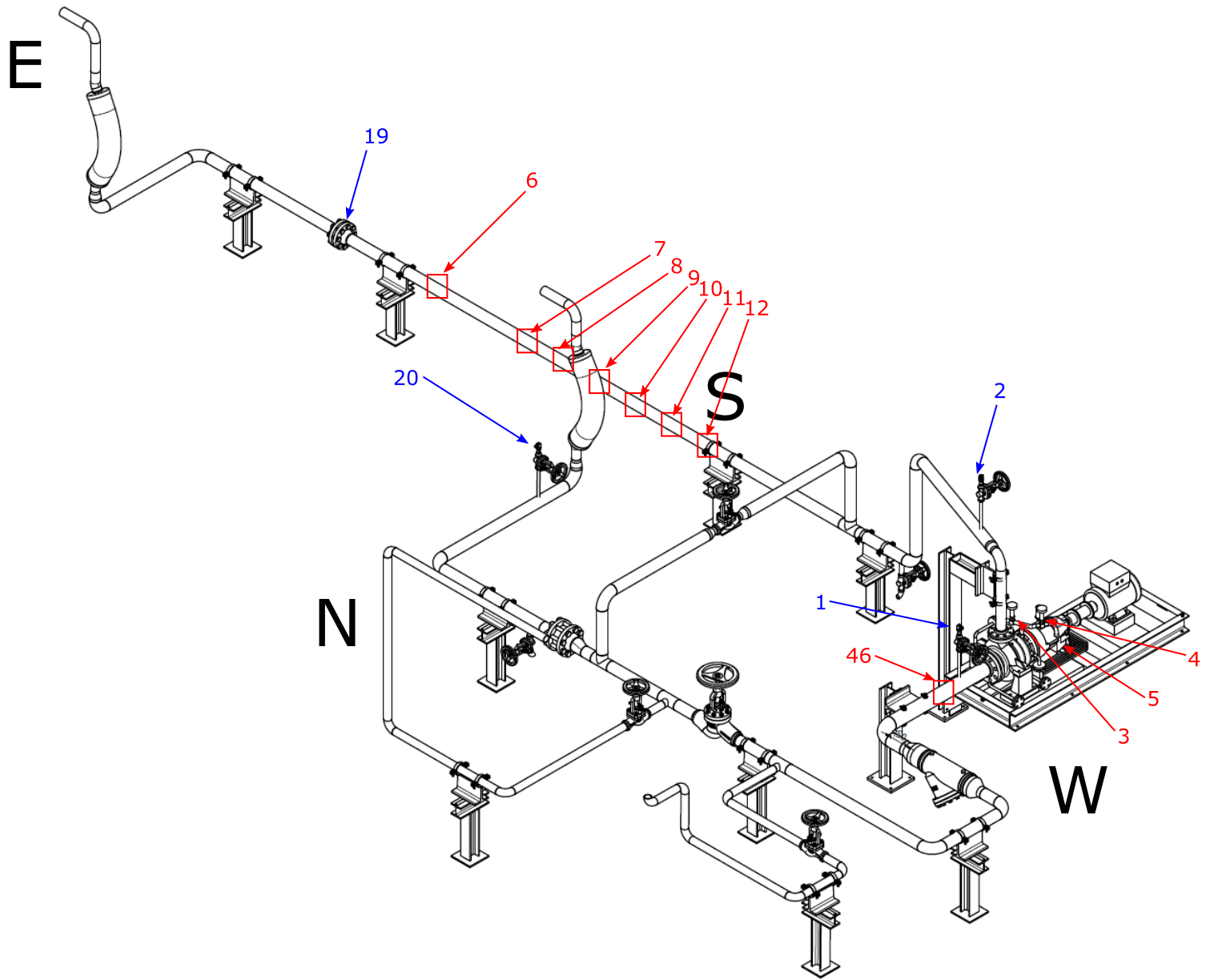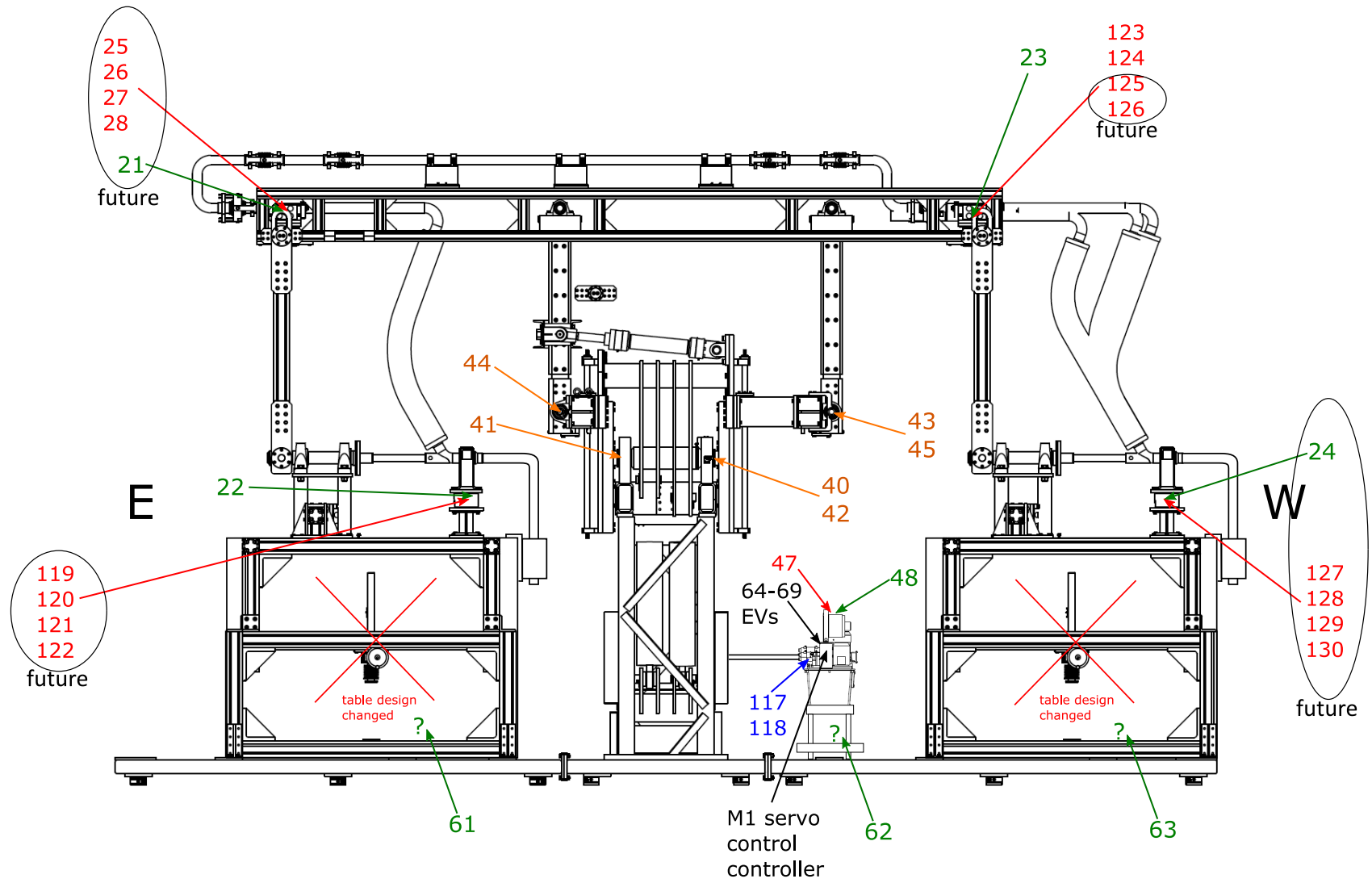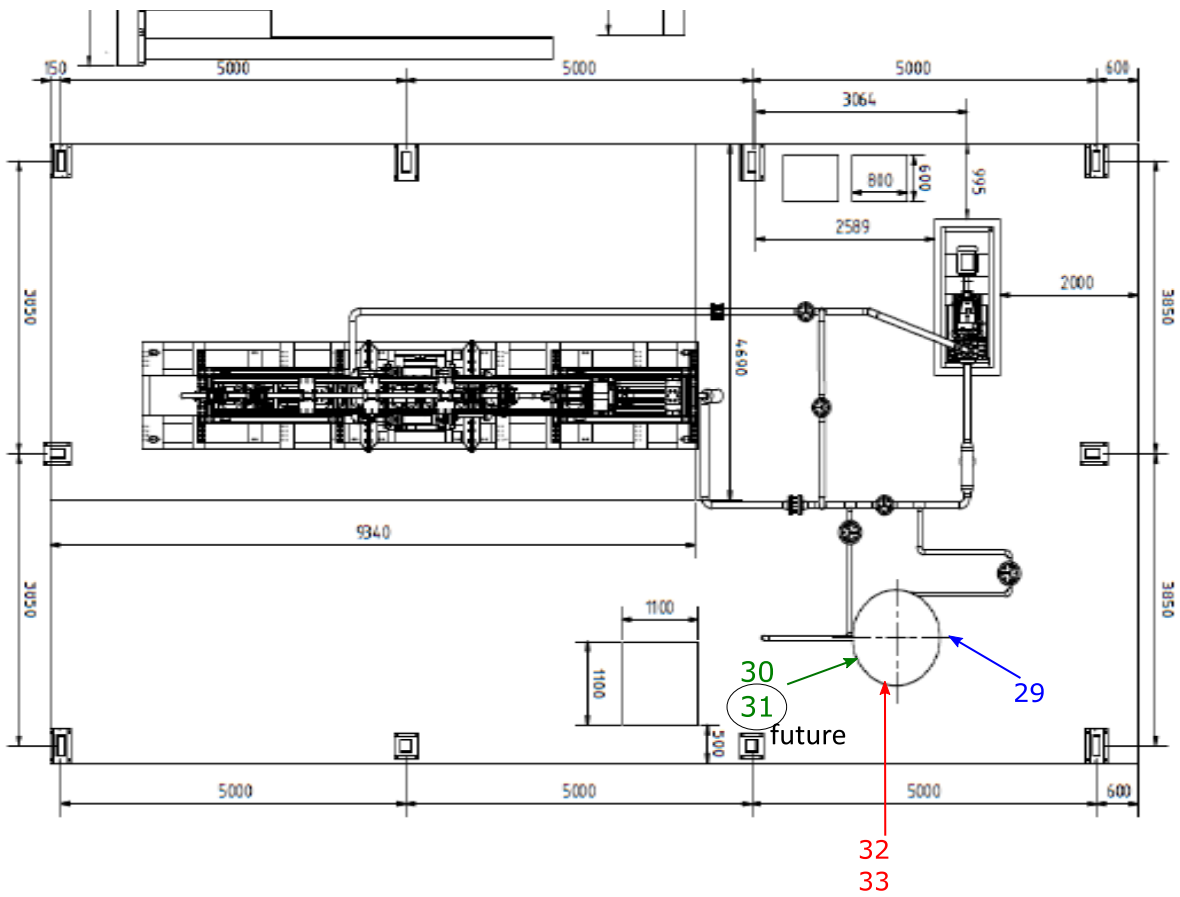
32
33

Table A.2.1: Sensor descriptions: taken from signal list (02. Dec 2016)

No.	Ch.-Type	Description	Sensor-Type	PSA-nom.
1	absolute pressure	suction side absolute	S-20	PE-HTF-01-W
2	absolute pressure	pressure side absolute	S-20	PE-HTF-02-W
3	temperature	motor, HTF pump	Pt100_T1, 4 wire	TT-HTF-01-W
4	temperature	Bearing, HTF pump	Pt100_T2, 4 wire	TT-HTF-02-W
5	temperature	lubricating oil, HTF pump	Pt100_T3, 4 wire	TT-HTF-03-W
6	temperature	fluid temp. heater outlet	Thermocouple Type K TC-15	TT-HTF-04-W
7	temperature	tube surface temp. heater 1	Thermocouple Type K	TT-HTF-05-W
8	temperature	tube surface temp. heater 2	Thermocouple Type K	TT-HTF-06-W
9	temperature	tube surface temp. heater 3	Thermocouple Type K	TT-HTF-07-W
10	temperature	tube surface temp. heater 4	Thermocouple Type K	TT-HTF-08-W
11	temperature	tube surface temp. heater 5	Thermocouple Type K	TT-HTF-09-W
12	temperature	tube surface temp. heater 6	Thermocouple Type K	TT-HTF-10-W
19	differential pressure	orifice plate differential pressure	DTP-10	PE-HTF-03-W
20	absolute pressure	absolute pressure test facility outlet	S-20	PE-HTF-04-W
21	multi axis load cell	force/torque REPA No. 1 east top	K6D175	
22	multi axis load cell	force/torque REPA No. 2 est bottom	K6D175	
23	multi axis load cell	force/torque REPA No. 3 west top	K6D175	
24	multi axis load cell	force/torque REPA No. 4 west bottom	K6D175	
25	temperature	temperature multi force east top 1.1	Pt1000	
26	temperature	temperature multi force east top 1.2	Pt1000	
27	temperature	temperature multi force east top 1.3	Pt1000	
28	temperature	temperature multi force east top 1.4	Pt1000	
29	absolute pressure	absolute pressure, N2 tubing	S-20	PE-HTF-05-W
30	level switch	level switch expansion vessel (top)	2 x SPDT	FA-HTF-01-W
31	level switch	level switch expansion vessel (bottom)	2 x SPDT	FA-HTF-03-W
32	temperature	temperature expansion vessel 1 (liquid)	Thermocouple Type K TC-10	TT-HTF-15-W
33	temperature	temperature expansion vessel 2 (gas)	Thermocouple Type K TC-10	TT-HTF-16-W

No.	Ch.-Type	Description	Sensor-Type	PSA-nom.
40	limit switch	inductive sensor rotation negative	Balluf BES M12MI-POC40B-S04G	ZS-CI-01-W
41	limit switch	inductive sensor rotation positive	Balluf BES M12MI-POC40B-S04G	ZS-CI-02-W
42	inclination	magnetic tape sensor rotation	ASM PMIS3-50-50-20Khz-HTL-21-7M-S	ZT-CI-11-W
43	limit switch	inductive sensor translation negative	Balluf BES M12MI-POC40B-S04G	ZS-CI-04-W
44	limit switch	inductive sensor translation positive	Balluf BES M12MI-POC40B-S04G	ZS-CI-05-W
45	rotary encoder	rotary encoder -translation	MH64-1023MU multiturn FSG	ZS-CI-06-W
46	temperature	HTF temperature pump inlet	Thermocouple Type K TC-15	TT-HTF-17-W
47	temperature	hydraulic oil temperature	SSM.1.B4.150.54.S1 level switch with PT100	TT-CI-13-W
48	level switch	hydraulic oil level	SSM.1.B4.150.54.S1 level switch with PT100	LA-CI-03-W
61	leakage sensor	leakage / swim sensor		FA-HTF-02-W
62	leakage sensor	conrad leakage sensor		FA-HTF-02-W
63	leakage sensor	conrad leakage sensor		FA-HTF-02-W
117	relative preasure	pressure transmitter hydraulic unit rotation (150)	MODS-250-G1/4-A-M12	PE-CI-01-W
118	relative preasure	pressure transmitter hydraulic unit translation (151)	MODS-250-G1/4-A-M12	PE-CI-02-W
119	temperature	temperature multi force east bottom 2.1	Pt1000	
120	temperature	temperature multi force east bottom 2.2	Pt1000	
121	temperature	temperature multi force east bottom 2.3	Pt1000	
122	temperature	temperature multi force east bottom 2.4	Pt1000	
123	temperature	temperature multi force west top 3.1	Pt1000	TT-HTF-11-W
124	temperature	temperature multi force west top 3.2	Pt1000	TT-HTF-12-W
125	temperature	temperature multi force west top 3.3	Pt1000	TT-HTF-13-W
126	temperature	temperature multi force west top 3.4	Pt1000	TT-HTF-14-W
127	temperature	temperature multi force west bottom 4.1	Pt1000	
128	temperature	temperature multi force west bottom 4.2	Pt1000	
129	temperature	temperature multi force west bottom 4.3	Pt1000	
130	temperature	temperature multi force west bottom 4.4	Pt1000	

64-69   EVs
M1   servo control controller

A.3   Dynamo-meter algebra

A.3.1   Theory

The dynamo-meter that is used transforms forces and moments into six output voltages with the magnitude of a few mV. These output voltages are equal to the bridge voltages of the Wheatstone bridges U_D which form the core of every dynamo-meter that is based on resistance strain gauges. For further information, please have a look at the FAQ and documentation section of www.me-systeme.de. This chapter is based on the content provided there, if not indicated else.

The bridge voltage U_D is proportional to the supply voltage U_s, that is provided by the measuring amplifier, the output signal u_S is usually given in relation to the supply voltage. In this sense, the actual signal S equals u_S if the supply voltage was set to 1 V. As linear behavior is assumed, the output signal u_S can be described as a function dependent on only one parameter, that is the slope of the calibration curve of the sensor c_S in [mV/VN]. c_S is derived as the fraction of the characteristic value C, i.e. the signal obtained when the dynamo-meter is exposed to nominal force F_{nom} and the nominal force itself. Please note that C is given in [mV/V], i.e. per V of supply voltage. In doing so, characteristic values of different dynamo-meters and other force measurement devices can be compared to one another. For the value of C the data sheet states a value of ca. 0.5 mV/V [14], however it's exact value is never derived but contributes to the calibration matrix K, provided by the manufacturer on demand.

$$u_S = \frac{U_D}{U_S} = c_S \cdot F = \frac{C}{F_{nom}} \cdot F \tag{A.1}$$

The sensor output u_S becomes the amplifier input. It's behavior is also assumed to be linear which is equivalent to a constant amplification factor c_A independent of the input voltage. The amplifier output voltage U then is the product of amplification factor c_A and measurement voltage signal u_S. The amplification factor is the quotient of the upper limit of the measurement range U_A in [V] and the input sensitivity U_A in [mV/V] and therefore has the unit [V/mV/V]. The input sensitivity can be interpreted as the maximum measurement signal the amplifier can process per V of supply voltage.

$$U = c_A \cdot u_S = \frac{U_A}{u_E} \cdot u_S \tag{A.2}$$

To describe the behavior of the whole measurement chain, both characteristic curves, equations A.1 and A.2 can be combined to a single function describing the amplified output voltage U as a function of the forces (and moments) induced: equation A.3. The inverse function, eqaution A.4, can be written using K, the calibration matrix.

$$U = c_A \cdot c_S \cdot F = \frac{U_A}{u_E} \cdot \frac{C}{F_{nom}} \cdot F \tag{A.3}$$

$$F_{dyn} = F = K \cdot U \tag{A.4}$$

The Calibration matrix K is a 6x6 matrix given in the calibration certificates (original calibration [15] and re-calibration [23]. It's unit is N or Nm per V output signal of the amplifier.

Please note that the matrix loaded into GSV multi, the configuration and logging software provided by the manufacturer in a .mat-file, K', has the unit N and Nm per mV/V sensor output:

$$K' = K \cdot \frac{U_S}{u_E} = \frac{F_{nom}}{C} \cdot \frac{U_S}{U_A} K' = K \cdot \frac{5V}{2mV/V} = K \cdot 2.5 \frac{V}{mV/V} \tag{A.5}$$

A.3.2 Some actual values

Calibration Matrices

Equation A.6 and A.8 show the calibration matrices before and after re-calibration. As K is fully occupied, a force along one axis or a moment around another will always affect all six output voltages U.

$$K_{orig} = \begin{bmatrix} -4.94 & 1987.29 & -1942.62 & 1.02 & 1952.86 & -2044.15 \\ -2186.25 & 1160.60 & 1140.62 & -2339.92 & 1139.83 & 1171.18 \\ -3164.33 & -3057.03 & -3225.61 & -3162.95 & -3207.57 & -3154.80 \\ -114.53 & -103.25 & -112.21 & -122.35 & 238.17 & 235.81 \\ -194.06 & -200.09 & 206.67 & 196.83 & -0.58 & 11.69 \\ 125.94 & -137.18 & 140.15 & -130.11 & 128.32 & -143.87 \end{bmatrix} \begin{matrix} in \ N/V \\ or \ Nm/V \end{matrix} \tag{A.6}$$

$$U_{CC}^{orig} = \pm(30N, \ 70N, \ 80N, \ 8Nm, \ 6Nm, \ 16Nm) \tag{A.7}$$

$$K_{recal} = \begin{bmatrix} 6.10 & 1988.56 & -1971.82 & 8.49 & 1954.07 & -2055.73 \\ -2161.41 & 1223.06 & 1196.94 & -2338.29 & 1204.39 & 1231.05 \\ -3175.05 & -3057.37 & -3257.57 & -3212.59 & -3216.90 & -3174.84 \\ -115.66 & -115.22 & -123.88 & -124.54 & 226.16 & 222.88 \\ -194.49 & -193.88 & 200.39 & 199.22 & 5.30 & 8.36 \\ 128.81 & -136.12 & 131.60 & -137.26 & 131.52 & -138.73 \end{bmatrix} \begin{array}{l} in \ N/V \\ or \ Nm/V \end{array}$$

$$\text{(A.8)}$$

$$U_{CC}^{recal} = \pm(6N, \ 12N, \ 40N, \ 3.0Nm, \ 1.5Nm, \ 2.0Nm) \tag{A.9}$$

Zero signal

Both calibration certificates state zero signal when removed U_0.

$$u_{0,orig} = \left(\ 0.0047, \ 0.0050, \ 0.0022, \ 0.0114, \ 0.0047, \ -0.0003 \ \right) \ mV/V$$
$$u_{0,recal} = \left(\ 0.0075, \ 0.0160, \ 0.0146, \ 0.0037, \ 0.0141, \ -0.0063 \ \right) \ mV/V \ ; \tag{A.10}$$

As we can see, these values are given in mV/V. S_0 in V can be calculated similar to equation A.5:

$$U_0 = S_0 \cdot \frac{5V}{2mV/V} = S_0 \cdot 2.5 \frac{V}{mV/V} \tag{A.11}$$

Using both equations A.10 and A.11 we can calculate the dynamo-meter reading that the dynamo-meter displays if it is not offset compensated:

$$F_{dyn,0}^{absolute} = K \cdot U_0 = K \cdot S_0 \cdot 2.5 \frac{V}{mV/V}$$

$$F_{dyn,0,orig}^{absolute} = \left(\ 38.61, \ -59.08, \ -218.60, \ -4.12, \ 1.95, \ -1.56 \ \right) \begin{array}{l} in \ N \\ or \ Nm \end{array} \tag{A.12}$$

$$F_{dyn,0,recal}^{absolute} = \left(\ 109.02, \ 53.52, \ -393.84, \ -7.99, \ -2.19, \ 7.33 \ \right) \begin{array}{l} in \ N \\ or \ Nm \end{array}$$

These results explain why it is utterly important to make an offset compensation of the dynamo-meter before each measurement starts. Otherwise the results contain an zero-error as high as the values shown. Due to the expected offset compensation, neither S_0, U_0 nor F_0 are part of equation A.4.

Evaluating the change from one calibration to another

Due to the re-calibration, we now have two calibration matrices we could possibly apply to any measured output voltage U. The result will not be the same, as figure 3.3 indicates. The difference can be calculated with equation A.13. Please keep in mind, that this calculation is very sensitive to the signs of the six values of F.

$$\Delta F_{dyn} = F_{dyn,re-calib} - F_{dyn,orig} = K_{re-calib} \cdot U - K_{orig} \cdot U$$
$$\text{with } U = K_{orig}^{-1} \cdot F$$
$$\Delta F_{dyn} = K_{re-calib} \cdot K_{orig}^{-1} \cdot F - K_{orig} \cdot K_{orig}^{-1} \cdot F \qquad (A.13)$$
$$= (K_{re-calib} \cdot K_{orig}^{-1} - I) \cdot F$$

Table A.3.1: Change in dynamo-meter reading due to re-calibration: Rows 1 and 2 show the min. and max. value of the best estimate of future dynamo-meter forces according to table A.4.1. Rows 3 and 4 show the min. and max. result of equation A.13 that have occured testing a subset of the countless combinations there are for the three forces and three moments within their margin.

Name		Fx	Fy	Fz	Mx	My	Mz	Unit
F_{estim}	Min	-1,457	-224	-2,310	464	-521	-1,062	N, Nm
	Max	1,555	849	126	675	575	895	N, Nm
ΔF_{dyn}	Min	-56	-89	-73	-5	-18	-33	N, Nm
	Max	30	48	86	15	11	8	N, Nm

Change in zero signal due to temperature test

estimation of the relative temperature reversibility error due to the change in zero signal after the temperature test $\Delta S_{0,\vartheta}$, stated in the calibration certificate of the re-calibration [23].

$$U_{\Delta U0,20\,°C} = K \cdot \Delta U_{0,20\,°C} = K \cdot \Delta S_{0,20\,°C} \cdot 2.5 \frac{V}{mV/V} \qquad (A.14)$$

$$\Delta S_{0,20\,°C} = \Big(\ -0.0001, \ -0.0012, \ 0.0003, \ -0.0036, \ -0.0021, \ 0.0013 \ \Big) \ mV/V$$

$$U_{\Delta U0,20\,°C}^{orig} = \Big(\ -24.32, \ 16.80, \ 42.59, \ 0.87, \ -0.93, \ 0.51 \ \Big) \ \begin{matrix} in \ N \\ or \ Nm \end{matrix}$$

$$U_{\Delta U0,20\,°C}^{recal} = \Big(\ -24.46, \ 16.49, \ 43.01, \ 0.94, \ -1.01, \ 0.57 \ \Big) \ \begin{matrix} in \ N \\ or \ Nm \end{matrix}$$

$$(A.15)$$

Uncertainties

The total uncertainty of the dynamo-meter measurements of the REPA test-rig U can be calculated as the square root of the sum of the squared parts[21] stemming from calibration certificate (CC), temperature effect on zero signal TK_0, temperature effect on characteristic value TK_C, rel. creep d_{cr} and difference in zero signal after complete heating cycle $\Delta U_{0,20C}$. This technique has been derived with and approved by Mr. Kabelitz from ME-Messsysteme, the manufacturer of the K6D175 dynamo-meter. Conditions are that none of the forces and moments exceeds the nominal value too much and that sensor temperatures stay below $70\,°\text{C}$.

$$U = \sqrt{U_i^2} = \sqrt{U_{CC}^2 + U_{TK0}^2 + U_{TKC}^2 + U_{dcr}^2 + U_{\Delta U0,20\,°\text{C}}^2} \qquad (\text{A.16})$$

If any of the six forces and moments of the dynamo-meter reading $F_{dyn,i}$ exceeds the re-calibration scenario, uncertainties and resulting forces and moments can be linearly interpolated between the results of the two calibration scenarios using equations A.17 and A.18

$$U_{CC} = \begin{cases} U_{CC}^{recal} & \text{if } F_{dyn,i} \leq F_{cal,i}^{recal} \quad \forall \quad i = 1 \dots 6 \\ U_{CC}^{recal} + k \cdot (U_{CC}^{orig} - U_{CC}^{recal}) & \text{else} \end{cases} \qquad (\text{A.17})$$

$$F_{dyn} = \begin{cases} K_{recal} \cdot U & \text{if } F_{dyn,i} \leq F_{cal,i}^{recal} \quad \forall \quad i = 1 \dots 6 \\ K_{recal} \cdot U + k \cdot (K_{orig} - K_{recal}) \cdot U & \text{else} \end{cases}$$
$$(\text{A.18})$$

$$k = \max_i \left(\frac{F_{dyn,i} - F_{cal,i}^{recal}}{F_{cal,i}^{orig} - F_{cal,i}^{recal}} \right) \qquad (\text{A.19})$$

The effect of TK_0 has been derived in chapter 3.1. The effect of TK_C and d_{cr} is derived according to the data-sheet value, the best load estimation F_{estim} from table A.4.1, the re-calibration scenario F_{cal}^{recal} and the difference between dynamo-meter temperature ϑ_{dyn} and ambient temperature ϑ_{amb}.

$$U_{TKC} = 0.05\,\%\text{FS/K} \cdot F_{estim} \cdot (\vartheta_{dyn} - \vartheta_{amb})$$
$$U_{cr} = 0.1\,\%\text{FS} \cdot F_{cal}^{recal} \qquad (\text{A.20})$$

The effect of $\Delta U_{0,20C}$ has been derived above.

A.4 Calibration and data sheet values

Table A.4.1: **Content:** This table compares 'Nominal loads', 'Estimated Loads', 'Measured Loads' and 'Calibration Loads'. Nominal loads are loads the sensor has been designed for. Estimated loads are loads that the dynamo-meter will probably measure during operation and should therefore be calibrated for. 'Measured Loads' are loads that have actually been measured during temperature response experimetns. Calibration Loads are the loads the sensor has actually been calibrated for. **Sources:** DS - data sheet of the K6D175 [14], compare appendix B; R2 - ROHR2 simulation based on *Traverse_200* base model for 40 bar, 350 °C and the complete range of rotation angle φ; AP - Andreas Plumpe, master's thesis, [8]; MF - Data from REPA manufacturer for operation at 20 and 30 bars, ambient temperature, without mass flow, for ± 120° rotation and the upper side of the REPA; CC - calibration certificates for original calibration [15] and re-calibration [23]. **Explanations:** Loads are estimated as the sum of forces from the traverse (ROHR2 simulations), the calculated effect from mass flow and estimated loads for the REPA. Sensor calibration is done for specified loads, both positive and negative (exception: F_z only negative). Best calibration loads are therefore calculated as $\pm mean(abs(min), abs(max))$ (min value for F_z). The re-calibration loads, compare appendix A.8, had been calculated on the base of faulty measurement results (dead channel) and have to be used with caution.

Dynamometer K6D175 - Loads estimation

Name		Fx in N	Fy in N	Fz in N	Mx in Nm	My in Nm	Mz in Nm	Source
Nominal Loads								
nominal load / calibration load, F_{nom}		10,000	10,000	20,000	1,000	1,000	2,000	DS
working load (allowed load), F_{work}		15,000	15,000	30,000	1,500	1,500	3,000	DS
failure load, F_{fail}		30,000	30,000	60,000	3,000	3,000	6,000	DS
Estimated Loads during test-rig operation								
ROHR2 (40 bar,350 °C)	Min	-882	-714	-1,045	-109	-201	-207	R2
	Max	880	-141	386	149	195	215	
max. mass flow		0	-110	110	-66	0	0	AP
estim. REPA (40 bar)	Min	-575	600	-1,375	639	-320	-855	MF
	Max	675	1,100	-370	592	380	680	
sum	Min	-1,457	-224	-2,310	464	-521	-1,062	
	Max	1,555	849	126	675	575	895	
max. % of nominal load		16	8	12	67	58	53	
Measured loads during temperature response experiments								
measured forces $F_{temp.\ response}$	Min	-67	-311	-45	-5	-19	-17	
	Max	176	83	142	20	23	11	
max. % of nominal load		2	3	1	2	2	1	
Measured loads during angle response experiments								
measured forces $F_{angle.\ response}$	Min	-371	-171	-1,296	-119	-278	-107	
	Max	121	427	620	9	207	87	
max. % of nominal load		4	4	6	12	28	5	
Calibration Loads								
original calibration loads, F_{cal}^{orig}		±10000	±10000	-20,000	±1000	±1000	±1000	CC
re-calibration loads, F_{cal}^{recal}		±2350	±800	-2,050	±400	±400	±300	CC
best calibration loads, F_{estim}		±1506	±537	-2,310	±569	±548	±978	

Table A.4.2: **Content:** This table shows estimations for total measurement uncertainties for the original, the current and a possible future state. All calculations use the best load estimation from A.4.1 as load scenario and assume the worst case for the sensor temperature. Some results are also compared to max. results of validation experiments. **Sources:** DS - data sheet of the K6D175 [14], compare appendix B; CC - calibration certificates for original calibration [15] and re-calibration [23] IMPORTANT: values only true for whole system composed of dynamo-meter K6D175 (serial number: 15401935) and measurement amplifier GSV-1A16USB K6D/M16 (serial number: 15156211/15356132), compare appendix B; TT - Calculated on basis of temperature test; TT2 - Calculated on basis of ideal future temperature test. **Explanations:** Some uncertainties scale with the nominal loads the sensor is designed for (FS = full scale) and some scale with the actual load of the sensor (RD = reading). For the original calibration temperature effects on zero signal and sensitivity were not part of the calibration and have been estimated using values given in the data sheet. Together with the re-calibration, a temperature test has been performed, compare chapter 3.3.

Dynamometer K6D175 - Uncertainties estimation

Name	Param	Fx	Fy	Fz	Mx	My	Mz	Unit	Source
1) Original state: (original calibration, $\vartheta_{dyn} = 70\,°$C)									
measurement uncertainty, U_{CC}		30	70	80	8	6	16	N, Nm	CC, eqn. A.7
rel. creep, U_{cr}	0.1 % FS	10	10	20	1	1	2	N, Nm	DS, eqn. A.20
sum. uncertainty, U (without temperature effects)		32	71	82	8	6	16	N, Nm	eqn. A.16
min % of F_{estim}		*2*	*13*	*4*	*1*	*1*	*2*	*%*	
temp. effect on zero signal, U_{TK0}	0.1 % FS / K	490	490	980	49	49	98	N, Nm	DS
temp. effect on sensitivity, U_{TKC}	0.05 % RD / K	37	13	57	14	13	24	N, Nm	DS, eqn. A.20
rel. temperature reserv. error, $U_{\Delta U0}$		25	17	43	1	1	1	N, Nm	TT, eqn. A.14
sum. uncertainty, U		493	496	986	52	51	102	N, Nm	eqn. A.16
min % of F_{estim}		*33*	*92*	*43*	*9*	*9*	*10*	*%*	
2) Current state: (First re-calibration, $\vartheta_{dyn} = 70\,°$C)									
measurement uncertainty, U_{CC}		16	35	56	5	4	8	N, Nm	CC, eqn. A.9
rel. creep, U_{cr}	0.1 % FS	3	1	3	1	1	1	N, Nm	DS, eqn. A.20
sum. uncertainty, U (without temperature effects)		16	35	56	5	4	8	N, Nm	eqn. A.16
min % of F_{estim}		*1*	*7*	*2*	*1*	*1*	*1*	*%*	
min % of $F_{angle.\,response}$		*4*	*8*	*4*	*4*	*1*	*7*	*%*	
temp. effect on zero signal, U_{TK0}		106	110	500	11	8	12	N, Nm	TT, eqn. A.18
temp. effect on sensitivity, U_{TKC}	0.05 % RD / K	37	13	57	14	13	24	N, Nm	DS, eqn. A.20
rel. temperature reserv. error, $U_{\Delta U0}$		25	17	44	1	1	1	N, Nm	TT, eqn. A.14
sum. uncertainty, U		116	117	508	19	16	28	N, Nm	eqn. A.16
min % of F_{estim}		8	22	22	3	3	3	%	
min % of $F_{temp.\,response}$		66	38	358	93	70	254	%	
3) Ideal future state: (Improved temperature test, $\vartheta_{dyn} = 70\,°$C)									
measurement uncertainty, U_{CC}		16	35	56	5	4	8	N, Nm	CC, eqn. A.9
rel. creep, U_{cr}	0.1 % FS	3	1	3	1	1	1	N, Nm	DS, eqn. A.20
temp. effect on zero signal, U_{TK0}		0*	0*	0*	0*	0*	0*	N, Nm	TT2
temp. effect on sensitivity, U_{TKC}	0.05 % RD / K	37	13	57	14	13	24	N, Nm	DS, eqn. A.20
rel. temperature reserv. error, $U_{\Delta U0}$		25	17	44	1	1	1	N, Nm	TT, eqn. A.14
sum. uncertainty, U		47	41	91	15	14	25	N, Nm	eqn. A.16
min % of F_{estim}		3	8	4	3	3	3	%	

A.5   Important information for future sensor purchases

Before it makes sense to think about what sensors to buy to equip the last three dynamo-meter positions, the test-rig has to be functional enough to perform authentic operations for at least a short period of time. These have to be used to further understand the sensors behavior and well estimate authentic load and temperature scenarios. Buying new dynamo-meters only makes sense if their later usage is exactly known. Calibration and temperature-tests have to be performed for scenarios as close to the real ones as possible. To do that, it makes sense to also send in the connection plate and the bearing to perform these tests in mounted state. In any case the measurement amplifier, which has already been bought for all four positions, has to be send back for calibration, as this is always done for the whole system.

At the current state of knowledge, the K6D175 is to 'big' for its application. Please keep in mind that allowed forces are 300% of the nominal forces, best accuracy is normally reached at 70% - 100% of nominal forces (= calibration forces). Yet the best available load scenario estimates forces of only 15% of the nominal forces and moments of at least 60% of the nominal moments. A 'smaller' sensor would therefore be more suitable. In case this 'smaller' sensor is also physically smaller, adapters have to be made to fit the new sensor in the spaces provided. Maybe ME-Messsysteme can help here and build customized sensors with lower nominal forces but the same dimensions.

At the same time it is very important to ask for two PT1000 placed inside the dynamo-meter by the manufacturer at the exact place where increased temperatures act upon the sensor signal. Further more, it might be considered to ask for a more durable cable connection. To decrease the difference in zero signal after complete heating cycle $\Delta U_{0,20C}$, it might make sense to do without potting the inside of the sensor. The polymer used might suffer smallest plastic deformations when heated. Its normal purpose is to protect the sensor from high humidity. In the desert of Tabernas, this might not be an issue. In principle, ME-Messsysteme is able to build their sensors according to their clients needs. It is therefore advised to make the decision in close collaboration with them. Even non-linear calibration is an option.

Once the new sensors are bought, they need to be mounted and commissioned. It is utterly important that no new sensor is mounted before it has been confirmed that its adjacent piping system will not exert to high forces stemming from heat dilatation, which might damage the sensor. The top-east position may not be equipped under any circumstances until the last three compensators have been added to the eastern part of the traverse.

A.6 ROHR2 - MATLAB post-processing

When adding new LCs make sure to proceed as follows: first add LCs to the base model, best saving it under a new name and following the nomenclature. Then proceed iteratively: rotate the model (select all, edit-rotate around y-axis and node 1), save it under new name, run the simulation, export results as .csv to the default folder *R2DOC* (documentation - exports results in csv format, only relevant load cases), save again, repeat. The same procedure has to be chosen, if model parameters, e.g.: insulation thickness, are altered. It's quite boring work, I know;)

Evaluating the model results is done using a MATLAB script. Running *ROHR2_ReadIn.m* creates and saves a four-dimensional array *FMall_Z*. There is two variations of FMall, for two different fluids, HELISOL©(H) and air (A), with the difference that the pressure dimension of FMall_A only contains one pressure: $0\,\mathrm{bar}$. containing all six dynamometer forces and moments predicted by the model for the different HTF temperatures, HTF pressures and rotation angles using linear interpolation[10]. Evaluation for all possible combinations of ϑ_{HTF}, p_{HTF} and φ can now easily be done using N-dimensional interpolation:

```
load('27-12-16_17-53_Traverse_100.mat')

tq        = 345;           % in degC, range [20,450]
pq        = 10:5:35;       % in bar,  range [0,40]
phiq      = -63.5;         % in deg,  range [-120,90]
axq       = 2;             % 1 = Fx; 2 = Fy ... 6 = Mz
f = interpn(tH,pH,axH,alphaH,FMall_H,tq,pq,axq,phiq,'linear')
```

Automated plots can be made using *ROHR2_PlotResults.m*, here comparing models *Traverse_100* and *Traverse_200*, for two fluids and plotting forces and moments over HTF temperature as x-axis:

```
models     = [2,3]            % index of modelno. in [40,100,200,999]
fluids_str = {'H','A'}        % 'H' for Helisol, 'A' for Air
xaxis_str  = 'temperature'    % also possible: 'pressure','angle'
ROHR2_PlotResults(tq,pq,axq,phiq,models,fluids_str,xaxis_str)
```

---

[10]'linear' is the default option of interpn, other options, such as 'spline' may be chosen.

A.7 All temperature response validation experiment results

Figure A.7.1: Temperature response experiment results: measurement data, linear regression and ROHR2 results (*Traverse_100*) of all experiments that have been conducted at rotation angle $\varphi = 0°$.
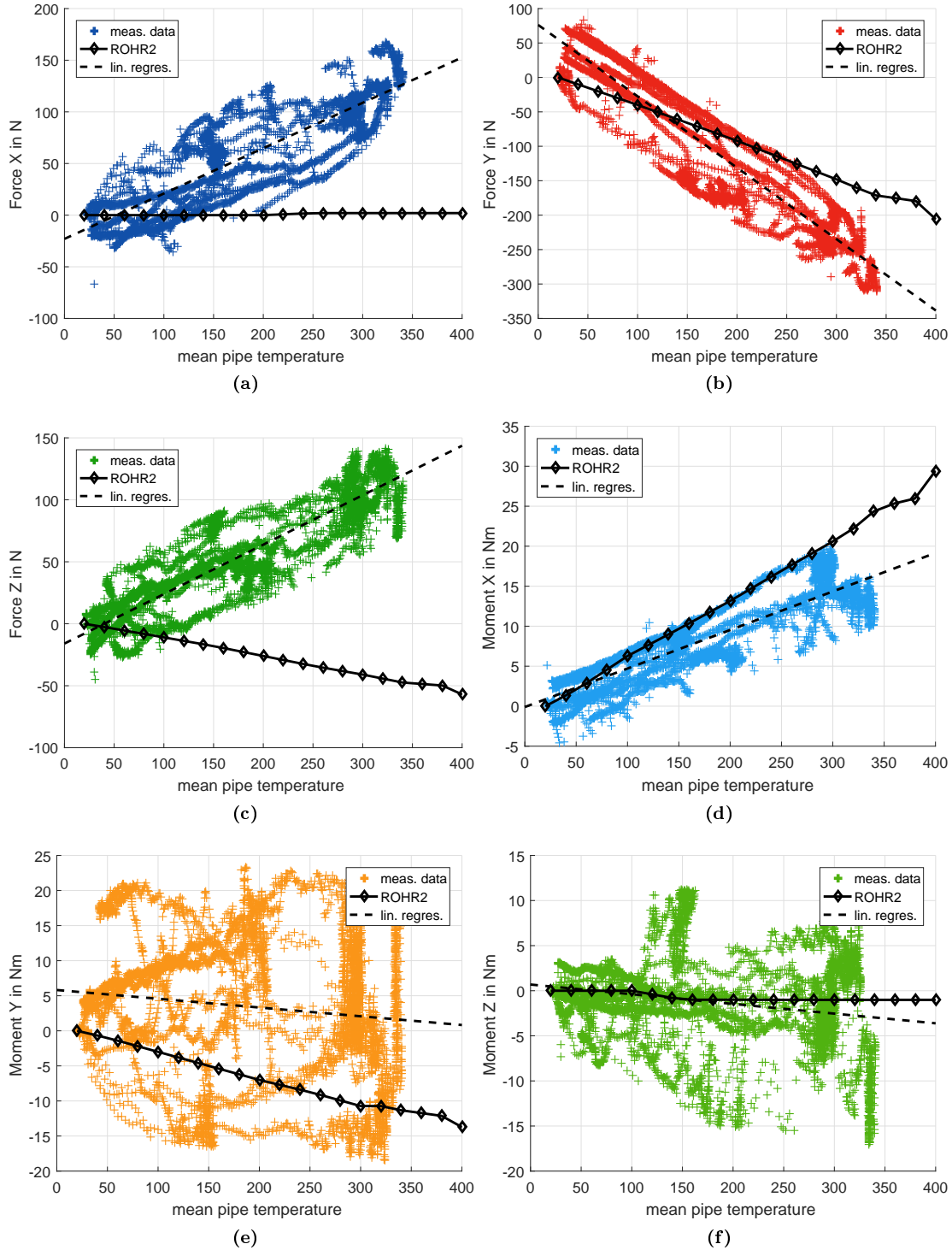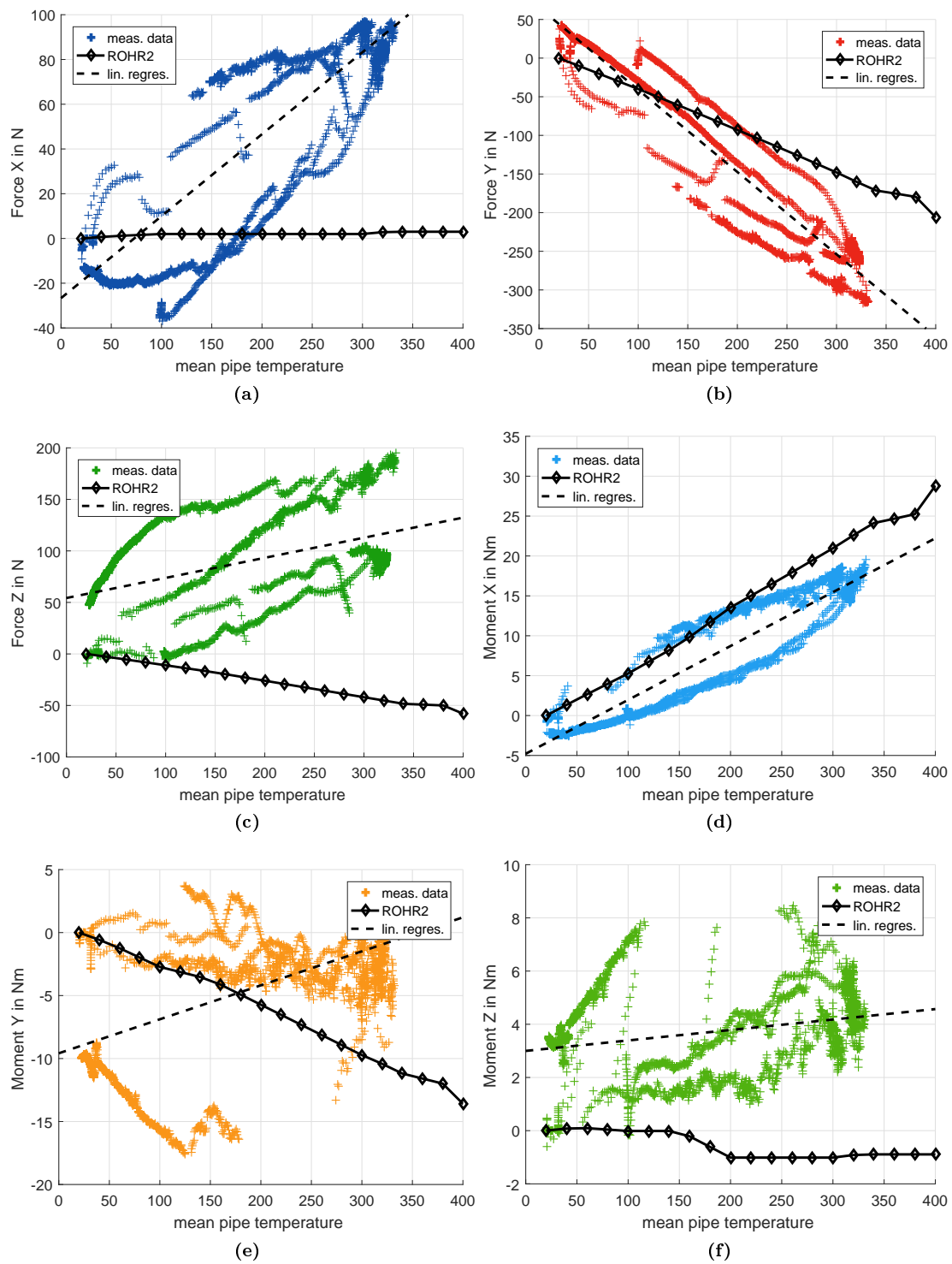
Figure A.7.2: Temperature response experiment results: measurement data, linear regression and ROHR2 results (*Traverse_100*) of all experiments that have been conducted at rotation angle $\varphi = -90°$.
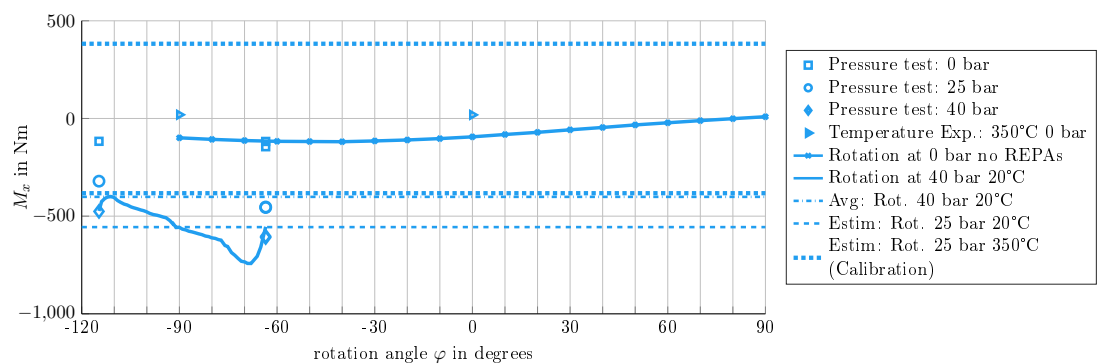
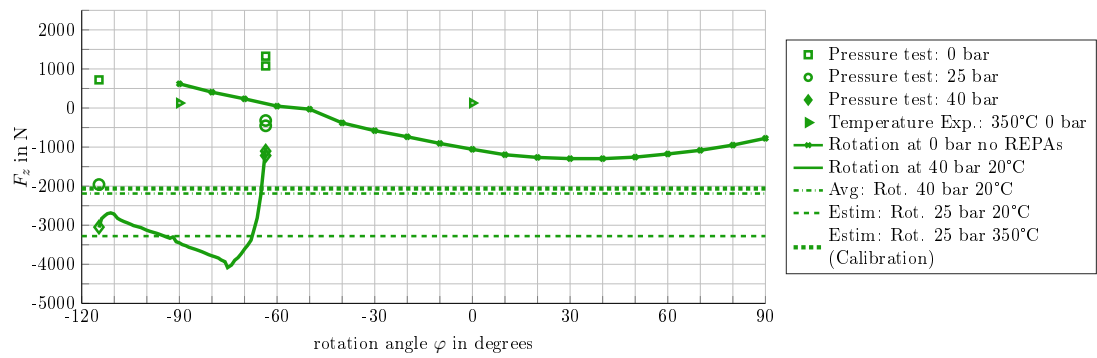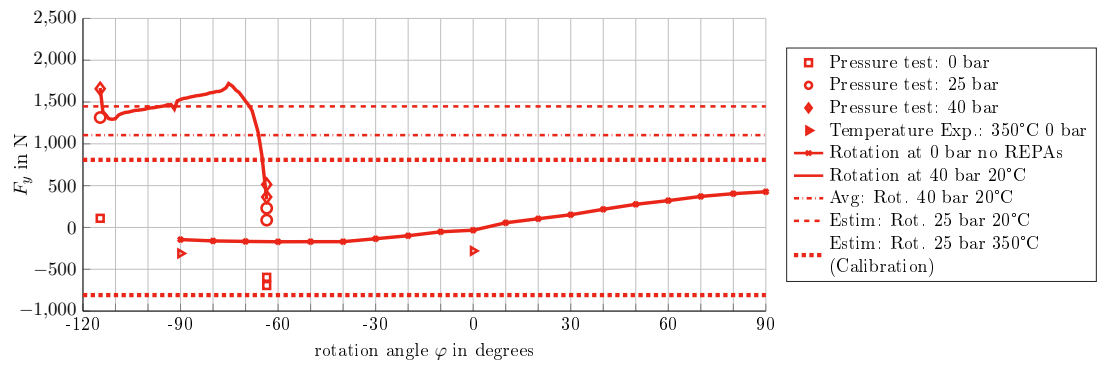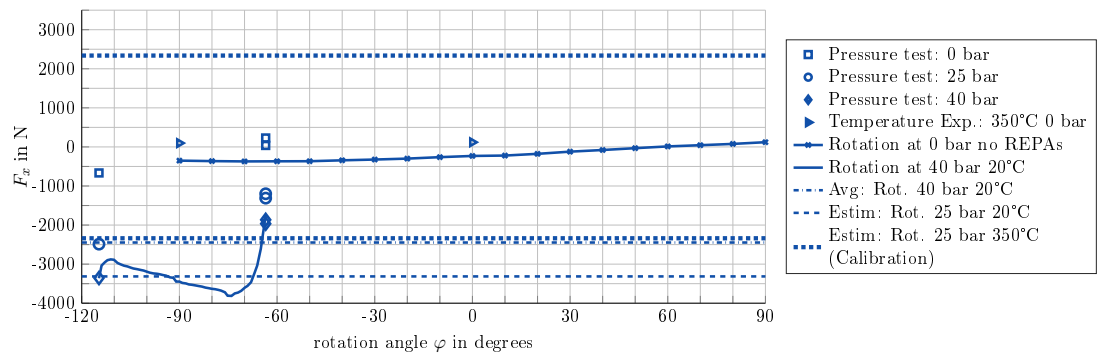## A.8 Operation loads estimation from experiment results

In order to re-calibrate the dynamo-meter for a more appropriate load scenario, operation loads had to be estimated. At the time the re-calibration could best be performed, no complete traverse rotation at average operational conditions (25 bar and 350 °C) had yet been possible. The best data available was that taken during the rotation of the traverse at design pressure 40 bar and ambient temperature (a small range of φ only). To account for the difference in pressure and temperature the calibration scenario was calculated as follows:

$$avg_{20\,°C}^{40\,bar} = mean(abs('Rotation\ at\ 40\ bar'))$$
$$estim_{20\,°C}^{25\,bar} = avg_{20\,°C}^{40\,bar} + load_{\varphi=114.7°,\ 20\,°C}^{25\,bar} - load_{\varphi=114.7°,\ 20\,°C}^{40\,bar} \quad (A.21)$$
$$calibration = estim_{350\,°C}^{25\,bar} = estim_{20\,°C}^{25\,bar} + load_{350\,°C}^{0\,bar}$$

The data (experiment results) used in equation A.21 and the results are shown in table A.8.1 and figure A.8.1.

Table A.8.1: Re-calibration scenario

Channel:	F_x	F_y	F_z	M_x	M_y	M_z
value:	2350 N	800 N	2050 N	400 Nm	400 Nm	300 Nm

F_x in N

rotation angle φ in degrees

Pressure test: 0 bar
Pressure test: 25 bar
Pressure test: 40 bar
Temperature Exp.: 350°C 0 bar
Rotation at 0 bar no REPAs
Rotation at 40 bar 20°C
Avg: Rot. 40 bar 20°C
Estim: Rot. 25 bar 20°C
Estim: Rot. 25 bar 350°C
(Calibration)

F_y in N

rotation angle φ in degrees

Pressure test: 0 bar
Pressure test: 25 bar
Pressure test: 40 bar
Temperature Exp.: 350°C 0 bar
Rotation at 0 bar no REPAs
Rotation at 40 bar 20°C
Avg: Rot. 40 bar 20°C
Estim: Rot. 25 bar 20°C
Estim: Rot. 25 bar 350°C
(Calibration)

F_z in N

rotation angle φ in degrees

Pressure test: 0 bar
Pressure test: 25 bar
Pressure test: 40 bar
Temperature Exp.: 350°C 0 bar
Rotation at 0 bar no REPAs
Rotation at 40 bar 20°C
Avg: Rot. 40 bar 20°C
Estim: Rot. 25 bar 20°C
Estim: Rot. 25 bar 350°C
(Calibration)

M_x in Nm

rotation angle φ in degrees

Pressure test: 0 bar
Pressure test: 25 bar
Pressure test: 40 bar
Temperature Exp.: 350°C 0 bar
Rotation at 0 bar no REPAs
Rotation at 40 bar 20°C
Avg: Rot. 40 bar 20°C
Estim: Rot. 25 bar 20°C
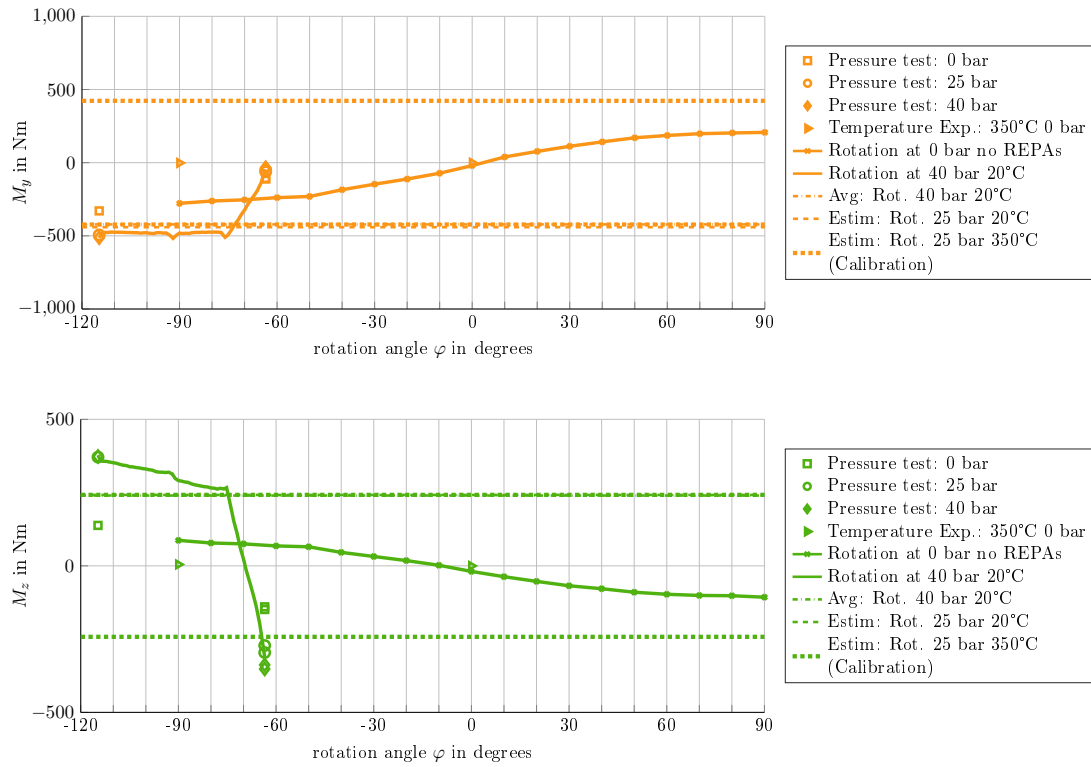Estim: Rot. 25 bar 350°C
(Calibration)

Figure A.8.1: The six plots above show all experiment results, i.e. pressure, temperature and rotation angle response, in one plot per force or moment. Data showing the effect of pressurizing the system was taken during the official pressure tests and is available for two rotation angle φ. For better readability, the plots only contain values for the pressurized state 0 bar, the average operation pressure 25 bar and the design pressure 40 bar. Data showing the effect of additional support forces due to heating up to 350 °C was taken in several experiments without REPAs and for two angles only. Please compare chapter 6.1. Data showing the effect of rotating the traverse was taken once for the empty traverse without any REPA's connected and once built in at 40 bar. Please compare chapter 6.2. The horizontal line *Avg: Rot. 40 bar* 20 °C shows the average value of the curve *Rotation at 40 bar* 20 °C. On the basis of this value the horizontal lines 'Estim: Rot. 25 bar 20 °C' and 'Estim: Rot. 25 bar 350 °C' have been calculated. The latter is used as re-calibration scenario (positive and negative value, as calibration is done for both, except F_z: calibration only for negative value. Please compare chapter A.3).

A.9 Improvements

Pretension

If the maximum compensator angle stays below $\alpha_{max} = 5.5°$ and if operating pressure and temperature do not exceed $40\,$bar and $450\,°$C the thee Witzenmann compensators of the western part of the traverse piping system withstand at least 10.000 angular deviation cycles.

The total magnitude of compensator angle would be smaller if all compensators reached $\alpha = 0°$ at $(450\,°C - 20\,°C)/2 = 215\,°C$[8, p.81] (Andreas Plumpe's thesis states $235\,°$C, which should be a typo.) This estimation however is based on a very simple model and should be verified using a real geometric model, e.g. in Inventor.

However, REPA testing will mainly be performed within $300\,°$C and $400\,°$C. Compensators therefore live longest, if their average angular deviation is smallest. This is equivalent to $\alpha = 0$ at $350\,°$C[8, p.81].

Having all compensators un-deviated at design temperature means that all compensators have to be built in slightly deviated. This deviation can be realized by pulling the piping system out of the traverse by a few millimeters, here called *pretensioning*. To verify correct pretensioning, a geometric model was created in Inventor based on the correct pipe geometry derived by a photogrammetric approach[11], compare chapter 4.1.
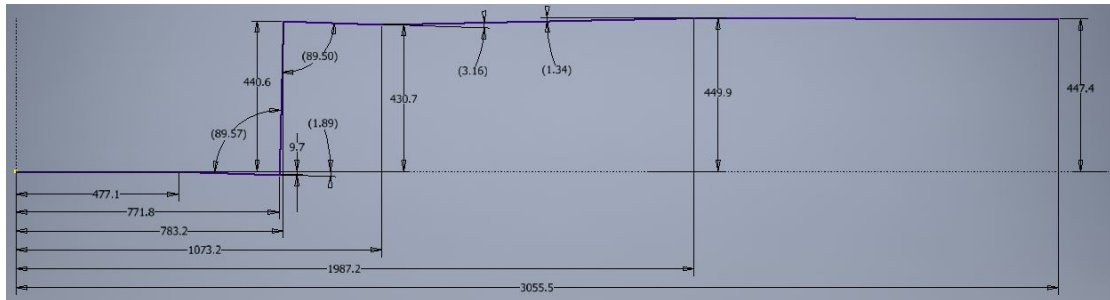

Figure A.9.1: Geometric model of piping system and compensator angles (center line) at ambient temperature with dimensions found by photogrammetric approach.

The geometric model in figure A.9.1 shows how the center line of the piping system looks like at ambient temperature. To verify that compensator angles are close to zero at average operation temperature of $350\,°$C, we first allow pipe segments movement by freeing lower and upper "knee" of the S-shape middle part and also replace all pipe segment intersection dimensionings by pipe length dimensionings. Node 1 and 15 (compare ROHR2-model nodes), start and end of our piping system, stay fix. That way, the compensators are now able too move when we enlongate each pipe segment according to

---

[11]This approach had already been used to design perfect pretensioning and is here repeated for validation.

formula A.22, just like the real system would. Here ΔL_ϑ is the change in pipe length, L is the length of the pipe section, $\bar{\alpha}$ is the average linear heat dilatation coefficient and $\Delta\vartheta$ is the change in pipe temperature.

$$\Delta L_\vartheta = L \cdot \bar{\alpha} \cdot \Delta\vartheta ; \quad \bar{\alpha} = 13.5\,\mu\text{m}/(\text{m K}) \tag{A.22}$$

Figure A.9.2 now shows the piping system and compensator angles at validation temperature. We see that angles are already small compared to the cold system: $\alpha_1 = 0.2°$, $\alpha_2 = 0.16°$ and $\alpha_3 = 0.09°$, as the angle point of compensator 2 (West-Center) raised by $450.7\,\text{mm} - 430.7\,\text{mm} = 20\,\text{mm}$.
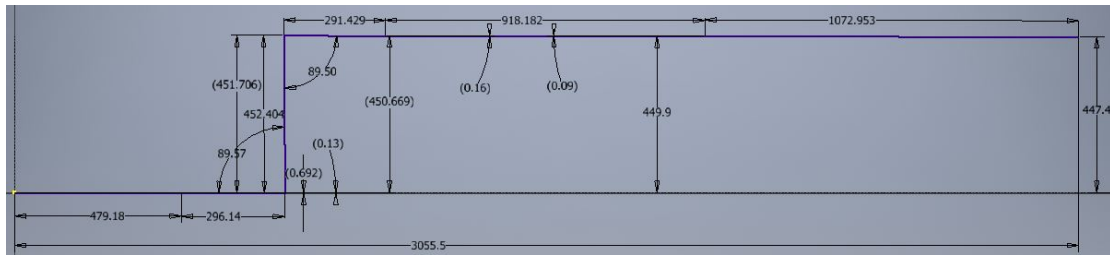

Figure A.9.2: Geometric model of piping system and compensator angles (center line) at 350 °C.

We can thus conclude that pretensioning was done correctly. To determine what change is needed to establish perfect pretension, we can free the length of the first pipe section and fix the deviation angle of compensator 2 to be 0°. The result is most perfect pretension with the given geometry: $\alpha_1 = 0.04°$, $\alpha_2 = 0°$ and $\alpha_3 = 0.02°$, shown in figure A.9.3. If we wanted to change the traverse piping system accordingly, we had to change the length of the first pipe segment by pushing it into the ITEM-profile by $479.9\,\text{mm} - 479.2\,\text{mm} = 0.7\,\text{mm}$.
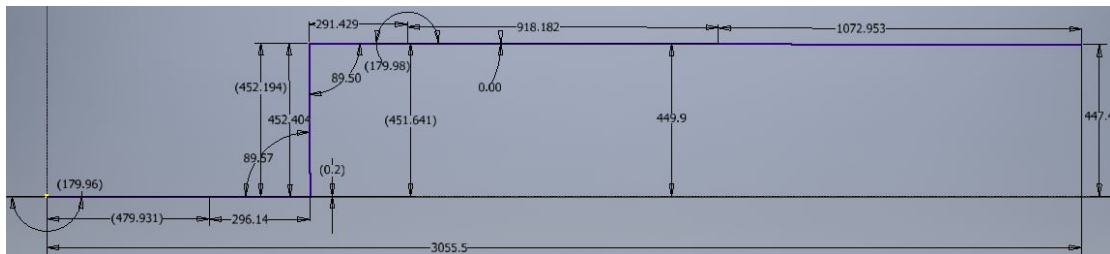

Figure A.9.3: Geometric model of piping system and compensator angles (center line) at 350 °C, ideal pretension.

Improved insulation

The interpretation of the measurement results of the temperature response validation experiments suggests that sensor temperature is crucial to guaranteeing a sufficiently small measurement uncertainty. The experience made shows that the sensor temperature has to be monitored and limited in order to protect the sensor against too high temperatures.

It has to be expected that the sensor in the original configuration will reach temperatures beyond 70 °C, which is the upper limit for valid results. Eventually temperatures would even rise above 85 °C, which is the maximum allowed temperature. The goal is therefore to minimize the heat flow from the upper stainless steel plate to the lower steel plate and to the dynamo-meter.

Before addressing more complex, maintenance intensive, expensive and failure endangered active cooling solutions, passive possibilities, i.e. better insulation were addressed. To evaluate possible improvements to the sensor insulation, a simplified static heat transfer model has been created, assuming a representative worst-case scenario: We assume that the bearing and the upper stainless steel plate have constant 200 °C, while the bottom steel plate and dynamo-meter have a constant 40 °C. This constitutes a very conservative estimation, as the stainless steel plate will actually be colder than the bearing and the lower steel plate will be warmer than the dynamo-meter. Assuming a greater temperature difference however ensures that the heat flow derived can be seen as an upper limit. As another conservative step, we neglect natural any heat exchange with the environment, such as natural convection and heat radiation. Finally, we assume that the temperature distribution in hot and cold reservoir is homogeneous and does not change over time.

Figure A.9.4 depicts the static heat flow model before and after the insulation. The screws are assumed to be placed in the perfect center of their boreholes, which in reality will be difficult to obtain. However, changes to heat flow should be small if bolt and steel plate touch as the contact area of two round shapes with different diameters is infinitely small in theory.

Before the insulation, the heat flow (red) is assumed to pass from the bearing to the bolt (via steel washer and air gap) and to the lower steel plate, as well as through the insulation board. The heat flow between insulation board and bolt as well as heat radiation inside the air gap is not considered. After the insulation, the heat flow is assumed to pass from the bearing to the bolt (via steel plate and bearing) and to the lower steel plate (via steel plate and air gap), as well as through the remaining insulation board. Radiation (blue) between upper and lower steel plate is assumed, but again not inside the air gaps between bolts and lower steel plate or bearing. Heat transfer due to forced convection (green) from both steel plates to air passing between the plates is indicated.

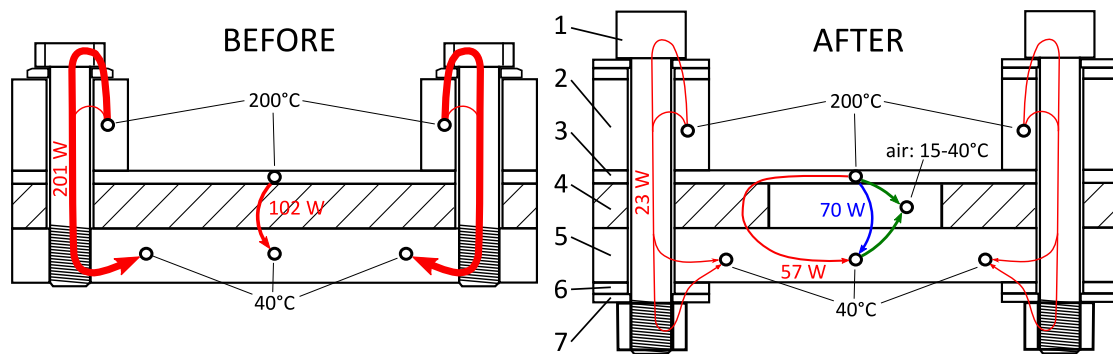These were the four steps taken. Please compare figures A.9.5 and A.9.4.

Figure A.9.4: Static heat flow model: Thickness of lines represents amount of heat flow, all numbers represent totals for the whole bearing (e.g. all four bolts). 1) bolt, 2) bearing, 3) stainless steel plate, 4) insulation board (Promat MONOLUX-800), 5) lower steel plate/ dynamo-meter connection plate, 6) insulation washer (K-Therm®-AS 600M), 7) steel washer (square shape).

1. Increase **diameter of all boreholes** from 16 mm vs holes: 17.5 mm in order to remove thread and prevent bolt from touching lower steel plate.

2. Cut **insulation board** as small as possible while still guaranteeing that it can withstand maximum compressive loads (nominal loads of dynamo-meter plus bolt forces at nominal torque) with a security factor of 2. This means that 56 % of the material had to remain to support double the maximum loads. The insulation material used is Promat MONOLUX-800 with a cold compressive strength of $27\,\text{N/mm}^2$. The thermal conductivity is $0.22\,\text{W/(m K)}$ at $200\,°\text{C}$ and, $0.24\,\text{W/(m K)}$ at $400\,°\text{C}$.

3. Introduce **insulation washers** made from K-Therm®-AS 600M, 30 mm x 40 mm with center holes of 16.5 mm diameter. Insulation washers are designed to withstand double the bolt forces at nominal torque. The heat conductivity is $0.28\,\text{W/(m K)}$ and the cold compressive strength is $250\,\text{N/mm}^2$ both at $200\,°\text{C}$.

4. Add **square shaped steel washers** to uniformly distribute compression loads on insulation washers.

As we can see in figure A.9.4, the reduction of the heat flow because of the changes applied is significant. Total heat flow reduces from 303 W to 140 W, which is a decrease of 54 %. As indicated, the combined effects of heat flow and radiation after insulation are actually greater than the heat flow through the insulation board before. However, the differences are in the range of a few W only, but the possibility of very effective active cooling through ventilation is introduced.
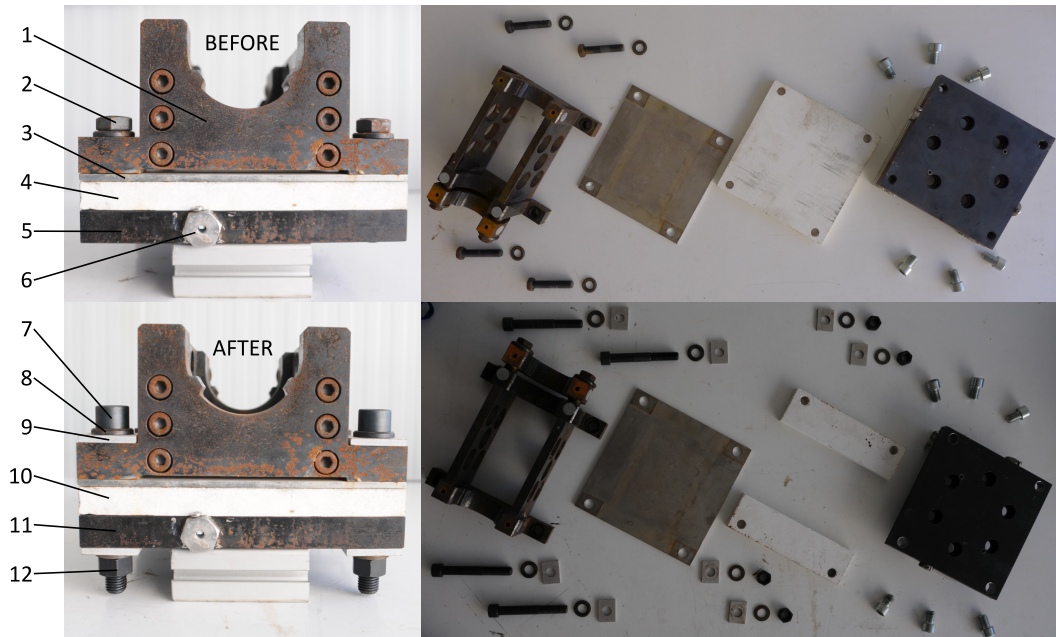
Figure A.9.5: Changes to dynamo-meter bearing due to improved insulation: top - before, bottom - after insulation. Parts: 1) Fix bearing (floating bearing on other side); 2) hexagon bolt ISO 4017 - M16x80 - 10.9; 3) stainless steel plate, $5 \times 230 \times 235$ mm with four 17.5 mm holes; 4) Promat MONOLUX-800 plate, $5 \times 230 \times 235$ mm with four 17.5 mm holes; 5) dynamo-meter connection plate, $23 \times 230 \times 235$ mm with four M16 screw threads; 6) One of two sockets for PT1000 temperature sensors; 7) bolt M16x110 - 10.9; 8) steel washer, later replaced through $4 \times 30 \times 40$ mm steel plates with 17.5 mm holes (not in photo, both sides); 9) insulation washer made from K-Therm®-AS 600M, $5 \times 30 \times 49$ mm; 10) Promat MONOLUX-800 plate, cut (compare picture on right); 11) dynamo-meter connection plate, $23 \times 230 \times 235$ mm with four 17.5 mm holes; 12) M16 nut, 12.9

(a) Before insulation

(b) After insulation

Figure A.9.6: Left, Dynamo-meter temperatures before (temperature response validation experiment no. 8) and right, after insulation (experiment no. 9). The graph shows the measurements of the four type-K thermoelements and the two PT1000 that are placed in the dynamo-meter connection plate. Please compare the description of the experiment setup in chapter 6.1 for details. The measurements of the thermoelements are assumed to have an uncertainty of 5 K, which is indicated.

Active cooling

Although improvements from the better insulation of the dynamo-meter bearing were significant, longer experiments still led to a dangerous increase of the dynamo-meter temperature. As we can see in figure A.9.8, even though ambient temperatures were low, the temperatures monitored by the two PT1000 in the connection plate rose to 50 °C after less than 3 hours of operation. Please keep in mind, that later test-rig operation will be for a continued time of several months at even higher pipe temperatures.

Sensor cooling is therefore mandatory. The first attempt with a simple ventilator, as shown in figure A.9.7 already yielded good results. An additional guide plate was used to redirect the air stream to the sensor, actively keeping its temperature below at a steady 40 °C, as we can see in figure A.9.8.

Figure A.9.7: Photo of ventilator and guide plate. The air stream produced by the ventilator is redirected by the "guide plate" (german: *Leitblech*) in order to cool the sensor but not the pipe and pass through the open space between stainless steel plate and dynamo-meter connection plate.

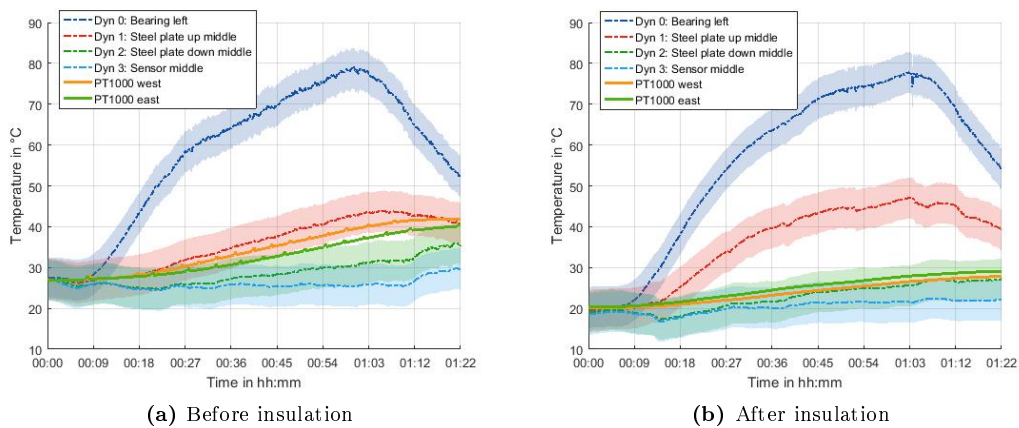**(a)** Before ventilation   **(b)** After ventilation
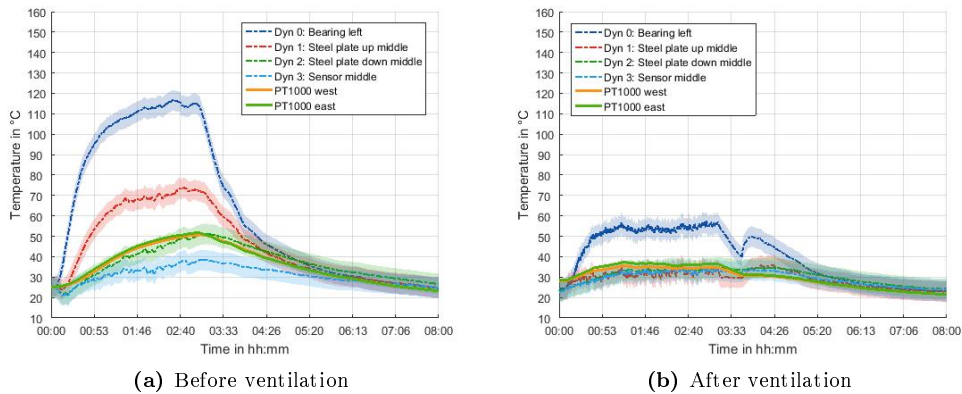
Figure A.9.8: Left, Dynamo-meter temperatures before (temperature response validation experiment no. 13) and right, after ventilation (experiment no. 14). The graph shows the measurements of the four type-K thermoelements and the two PT1000 that are placed in the dynamo-meter connection plate. Please compare the description of the experiment setup in chapter 6.1 for details. The measurements of the thermoelements are assumed to have an uncertainty of 5 K, which is indicated.

Pipe insulation design specifications

As described in chapter 6.1, one result of the temperature response validation experiments was that the insulation material may not entirely cover the the compensators not to hinder their movement and introduce parasitic forces. The insulation was therefore executed as depicted in figure A.9.9. To decrease heat losses, additional heat shields (german: *Wärmeschutzbleche*) should be considered, to decrease heat losses through convection and irradiation. Again, these should not be connected on both sides of the compensator at the same time. The same applies for the insulation of the part of the piping system inside the bearing. During temperature response validation experiments, the dynamo-meter reading F_{dyn} proved to be very sensitive to anything touching the dynamo-meter bearing. Here, increased insulation may be tried if proven necessary.
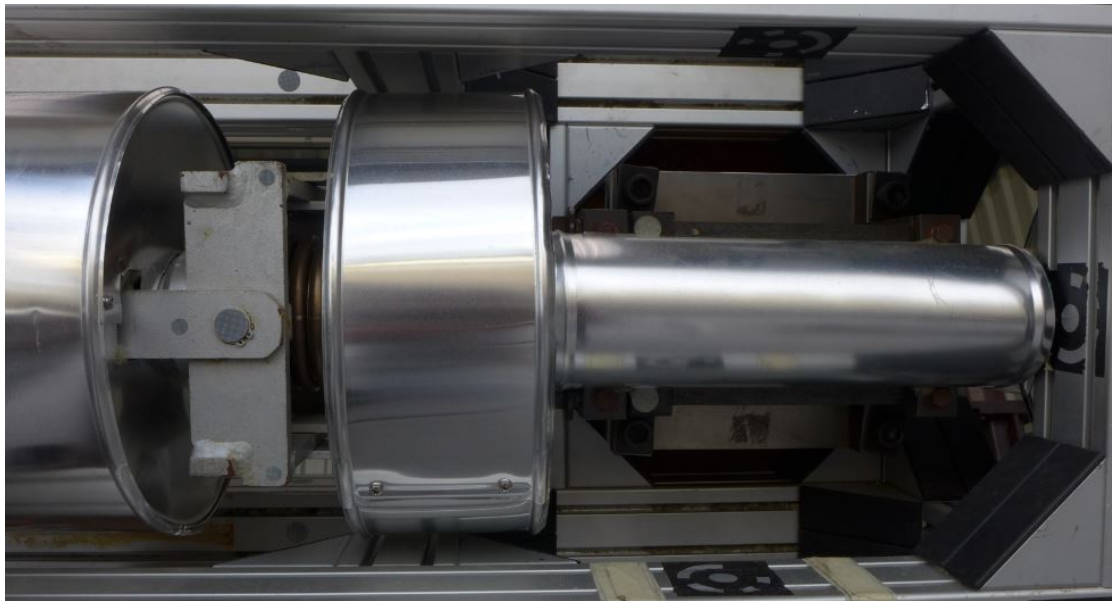
Figure A.9.9: Long Caption.

A.10 REPA translation due to thermal dilatation
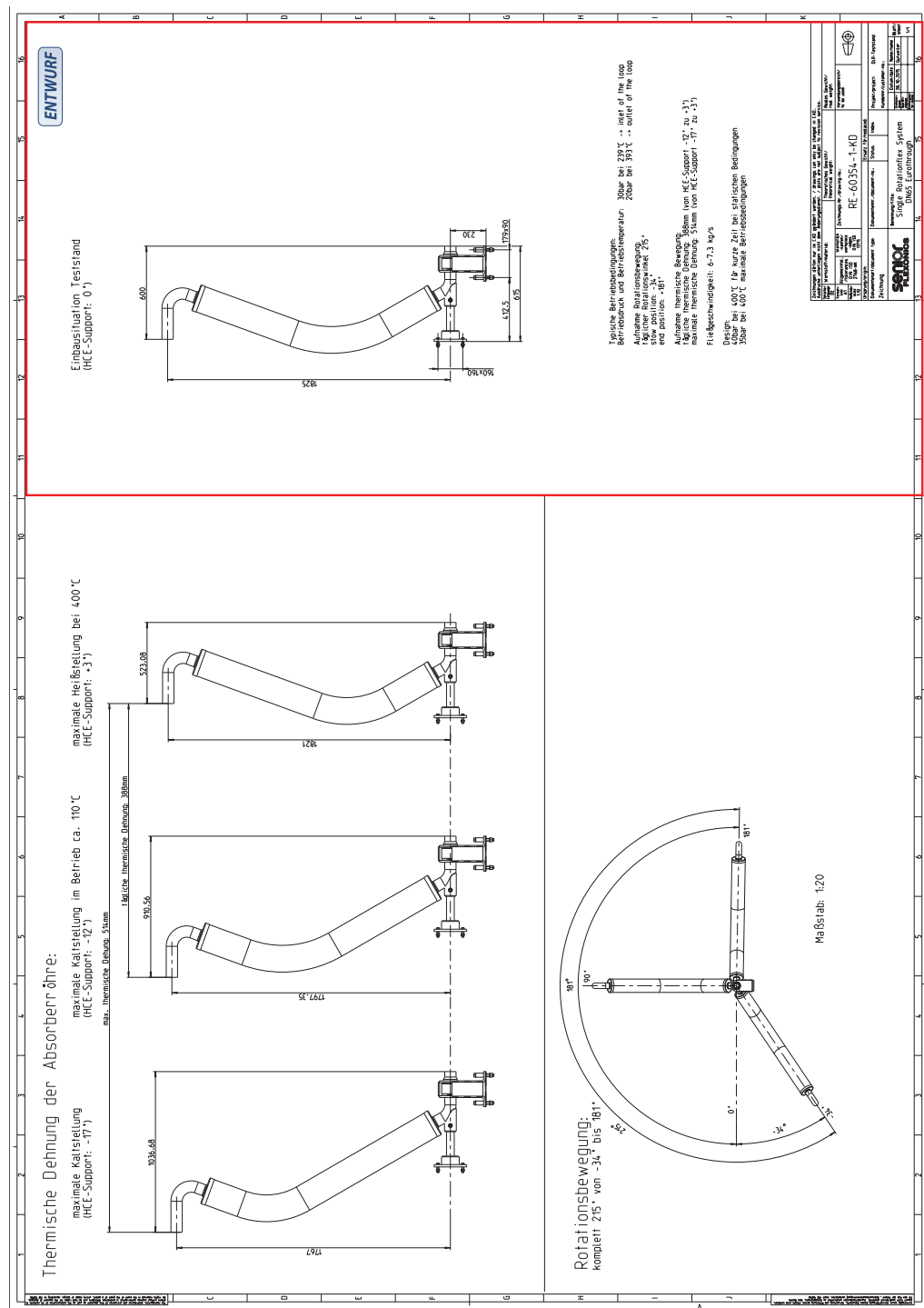
Figure A.10.1: REPA translation due to thermal dilatation of the absorber tubes. A document provided by Senior Flexonics. The REPA test-rig was designed on the basis of this document.

B   Data sheets and certificates

1. Data-sheet dynamo-meter K6D175 10kN/1kNm

2. Calibration certificate: original calibration

3. Calibration certificate: re-calibration and first temperature test
   !!! Important: Temperature test; value for 'Kanal 3' and 80 degC has to be 0.00077 instead of 0.0077. This is due to a reading error of ME-Messsysteme !!!

Mehrachsen-Kraft-Momentensensor K6D175

Messbereiche	Fx /kN	Fy /kN	Fz /kN	Mx /kNm	My /kNm	Mz /kNm
K6D175 10kN/1kNm	10	10	20	1	1	2
K6D175 20kN/2kNm	20	20	50	2	2	5
K6D175 50kN/5kNm	50	50	100	5	5	10

Beschreibung

Der Mehrachsen Sensor K6D eignet sich für die Kraft- und Drehmomentmessung in drei zueinander senkrechten Achsen.

Die Messbereiche für die Kräfte und Momente lassen sich werksseitig in einem weiten Bereich anpassen. Der K6D175 wurde speziell für folgende Anwendungen entwickelt:
1. Robotik
2. Messungen in der Automatisierungstechnik

Die Auswertung der Kraft- und Momentenbelastung erfolgt z.B. mit einem Messverstärker GSV-1A8USB..Die Berechnung der 6 Lastgrößen ist z.B. über eine Windows-DLL oder über Labview möglich mit Hilfe eines bereitgestellten digitalen Kalibrierdokuments. Das Kalibrierdokument enthält die individuellen Kalibrierfaktoren und Fehlerkorrekturen des Sensors.

Abmessungen

Zentrierbund Ø120 H8

Anschraubfläche Stator

Ø175
Ø164
Ø140
Ø120 H8 ⍌ 4

6x M16x2 ⍌ 25
2x Ø10 E7 ⍌ 25

45°
60°

110
1,7
1,7
46

176 +3

Zentrierbund Ø120 H8

Anschraubfläche Messplattform

2x Ø10 E7 ⍌ 25
6x M16x2 ⍌ 25

Ø175
Ø164
Ø140
Ø120 H8 ⍌ 4

60°
45°
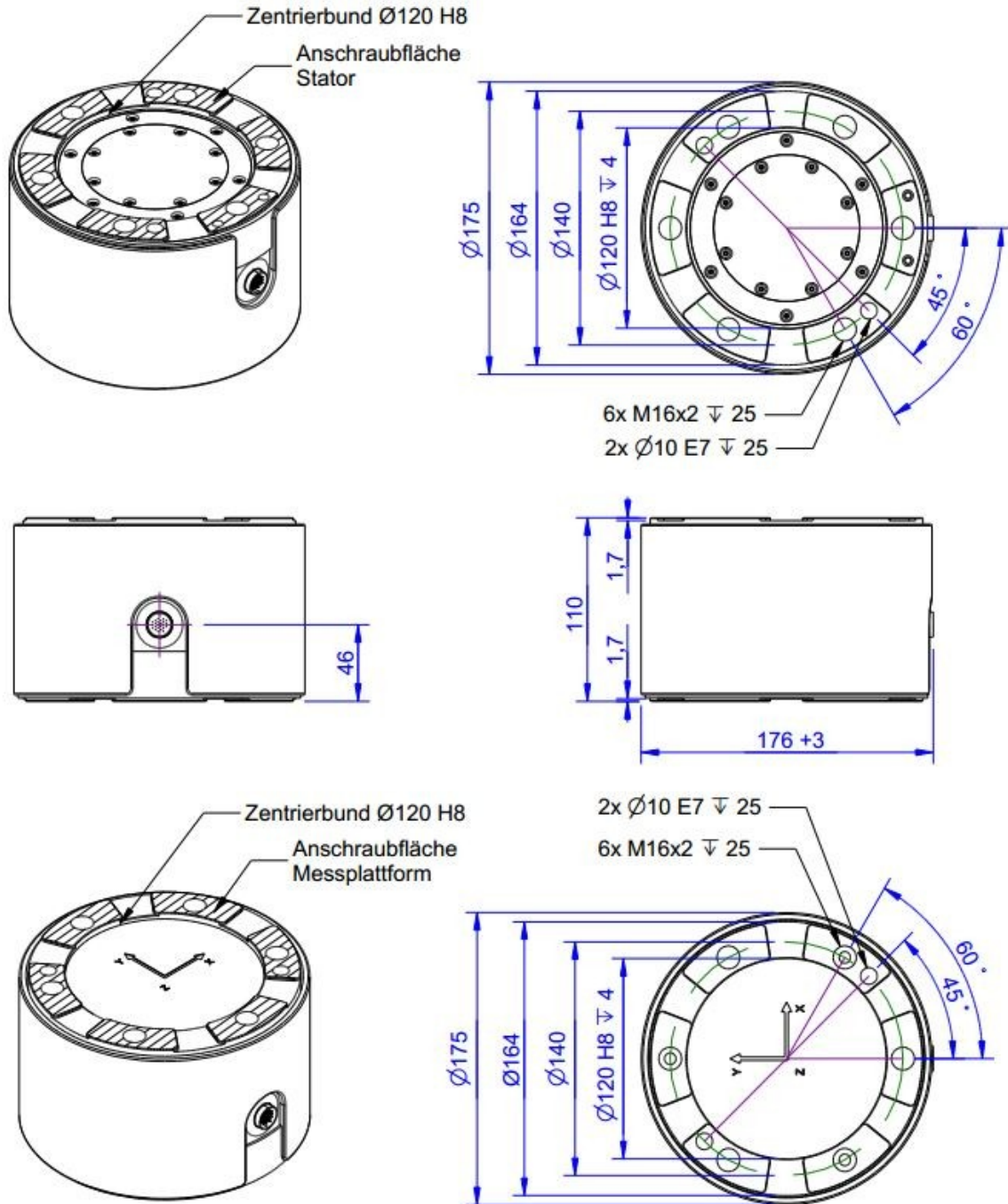
Technische Daten

Maße / Material		
Bauform		Messplattform
Material		Edelstahl 1.4542
Abmessungen	mm x mm	Ø175 x 110
Krafteinleitung		6x M16
mechanische Daten		
Nennkräfte (FS) Fx, Fy, Fz	kN	10, 20, 50
Nennmomente (FS) Mx, My, Mz	kNm	1, 2, 5
Gebrauchslast	%FS	150
Bruchlast	%FS	300
Messweg bei FS 1)	mm	ca. 0,1
Verdrillung bei FS 1)	rad	ca. 0,01
elektrische Daten		
Nennkennwert 2)	mV/V @ FS	ca. 0,5
Nullsignal	mV/V	<2
max. Speisespannung	V	5
Eingangswiderstand	Ohm	350 ±10
Ausgangswiderstand	Ohm	350 ±10
Isolationswiderstand	Ohm	>2 10^9
Steckverbinder, 24-polig, M16, Serie 723		09-0497-00-24
Genauigkeit		
rel. Spannweite 3)	%FS	0,5
rel. Linearitätsabweichung	%FS	<0,1
rel. Umkehrspanne	%FS	<0,1
Temperatureinfluss auf das Nullsignal	%FS/K	<0,1
Temperatureinfluss auf den Kennwert	%RD/K	<0,05
rel. Kriechen (30 min)	%FS	<0,1
Temperatur / Umwelt		
Nenntemperaturbereich	°C	-10… +70
Gebrauchstemperaturbereich	°C	-10 … +85
Lagertemperaturbereich	°C	-10 … +85
Schutzart		IP67

Abkürzungen: RD: Istwert („Reading"); FS: Endwert („Full Scale");

1) Messweg bei einachsiger Belastung Fx oder Fy oder Fz;

2) Vergleichswert bei einachsiger Belastung Fz;

3) Wiederholbarkeit bei gleicher Einbaulage und mehrachsiger Belastung;

Werkszertifikat 20543306

Kalibriergegenstand:	Mehrkomponenten-Sensor:, Typ K6D175 10kN/1kNm S/N: 15401935 Messverstärker: GSV-1A16USB K6D/M16 SN:15156211/15356132
Kalibrierlabor:	ME-Meßsysteme GmbH Neuendorfstr. 18a 16761 Hennigsdorf
Auftraggeber:	Deutsches Zentrum f. Luft- u. Raumfahrt
Auftragsnummer:	20543306
Ort der Kalibrierung	Hennigsdorf
Anzahl Seiten	5
Umgebungsbedingungen	21,0 °C ±1,5°C

Kalibrierverfahren

Der Mehrkomponenten-Sensor Typ K6D175 wurde in Reihe mit einem Referenzkraftsensor 1) in einer Referenzvorrichtung 4) belastet. Die Richtung der Referenzkräfte und Referenzmomente auf den Mehrkomponenten-Sensor wurde durch unterschiedliche Montagepositionen des Mehrkomponenten-Sensors in der Referenzvorrichtung sichergestellt.

Als Anzeige wurde der Messverstärker GSV-1A16USB K6D/M16 (15156211/15356132) verwendet.

Zur Ermittlung der Kalibriermatrix wurden aus 48 Messreihen 6 linear unabhängige Lastvektoren mit Hilfe des Referenzvorrichtung, des Referenzhebels und einer Belastungseinrichtung aufgebracht.

Zur Ermittlung der Kalibriermatrix dienen drei Kräfte in drei zueinander rechtwinkligen Richtungen, sowie drei Momente um drei zueinander rechtwinklige Achsen. Es werden die Lastvektoren (Fx,0,0,0,0,0), (0, Fy,0,0,0,0, (0,0, Fz,0,0,0), (0,0,Fz, Mx,0,0), (0,0,Fz,0,My,0) und (Fx,0,00,0,Mz) verwendet.

Zur Bestimmung der Matrix der relativen Spannweiten wird die Kalibriermatrix in gleicher Einbaulage des Mehrkomponenten-Sensors angewendet.

Vor jeder Belastung mit einem Lastvektor wird ein Nullabgleich durchgeführt.

Prüfnormale

1	Referenz-Maschine/Kraftsensor	Werkstoffprüfmaschine, ZD20EDC, SN:04/M06. 13-09.1726
2	Referenz Kraftsensor	KD9363s 1t/C3, Kalibrierzeichen 62305911 ME 2015-7 KD9363s 1t/C3, Kalibrierzeichen 62255133 ME 2015-7
3	Referenz Platte	$\varnothing$ 296 mm x 70mm
4	Referenz Hebel	$\varnothing$ 58 mm x 852mm

Zustand der Kalibriergegenstände

Messmittel	Typ	S/N	Zustand
Mehrkomponenten-Sensor	K6D175 10kN/1kNm	15301453	Neu /Erstkalibrierung
Messverstärker	GSV-1A16USB K6D/M16	15156211 15356132	Neu /Erstkalibrierung

Nullpunkterfassung

Kanal	1	2	3	4	5	6
mV/V	0,0047	0,0050	0,0022	0,0114	0,0047	-0,0003

Kalibriermatrix

Die Kalibriermatrix beschreibt den Zusammenhang zwischen den angezeigten Spannungen des Messverstärkers an den Kanälen 1 bis 6 (Bezeichner „ai0" bis „ai5") und den Komponenten 1 bis 6 (Fx, Fy, Fz, Mx, My, Mz) des Lastvektors.

Referenz		Kanal					
		1	2	3	4	5	6
Fx in N / V		-4,94	1987,29	-1942,62	1,02	1952,86	-2044,15
Fy in N / V		-2186,25	1160,60	1140,62	-2339,92	1139,83	1171,18
Fz in N / V		-3164,33	-3057,03	-3225,61	-3162,95	-3207,57	-3154,80
Mx in Nm / V		-114,53	-103,25	-112,21	-122,35	238,17	235,81
My in Nm / V		-194,06	-200,09	206,67	196,83	-0,58	11,69
Mz in Nm / V		125,94	-137,18	140,15	-130,11	128,32	-143,87

Abbildung 1: Kalibriermatrix in N/ V und Nm/V

Ursprung

Der Ursprung des Koordinatensystems befindet sich im Zentrum des Sensors auf der Oberfläche der oberen Seite. An der Stelle des Ursprungs ist eine Gravierung vorhanden.
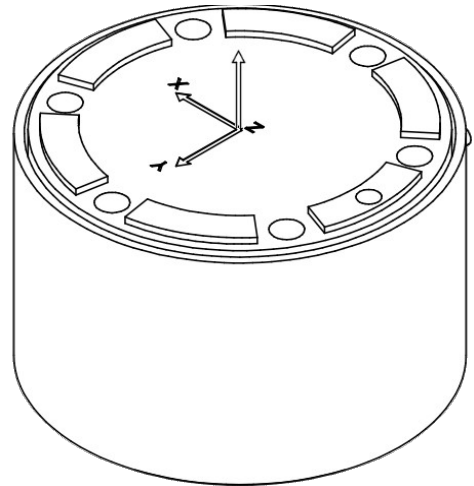

Abbildung 2: Ursprung des Koordinatensystems

Matrix der relativen Spannweiten

Die Matrix der relativen Spannweiten („Reproduzierbarkeit") beschreibt die Abweichung der angezeigten Kräfte und Momente in Prozent vom jeweiligen Endwert bei einachsiger Belastung mit den Lastvektoren (Fx,0,0,0,0,0), (0, Fy,0,0,0,0, (0,0, Fz,0,0,0), (0,0,0,Mx,0,0), (0,0,0,0,My,0),(0,0,0,0,0,Mz);

Messunsicherheit

Mit einer Wahrscheinlichkeit von 95% besitzen die Messergebnisse folgende Unsicherheit.

	Fx	Fy	Fz	Mx	My	Mz
Nennlast	10kN	10kN	20kN	1kNm	1kNm	2kNm
Messunsicherheit	±30N	±70N	±80N	±8Nm	±6Nm	±16Nm

Einzelergebnisse der Prüfung

Merkmal	Istwert	Sollwert	Ergebnis
Isolationswiderstand @5V	> 2GOhm	>2 GOhm	in Ordnung
Messunsicherheit	<2%	<2%	in Ordnung

Wir erklären hiermit, dass alle für das Produkt relevanten Prüfungen auf Einhaltung der Spezifikationen mit Messmitteln durchgeführt wurden, die auf nationale und internationale Normale rückführbar sind. Die regelmäßige Überprüfung durch die zertifizierten und akkreditierten Institutionen sichert, dass die Rückführbarkeit aufrecht erhalten wird.

Prüfer *Testing Engineer*	Datum *date*	
Künstner	15.10.15	

K6D-CalibrationMatrix HL

Kalibriergegenstand:	System bestehend aus: 6-Achsen Kraft-Momentensensor und Messverstärker
Hersteller:	ME-Meßsysteme GmbH Neuendorfstr. 18a 16761 Hennigsdorf
Typ:	Sensor: K6D175 10kN/1kNm SN:15401935 Messverstärker: GSV-1A8USB K6D/M16 SN:15156211
Auftraggeber:	Deutsches Zentrum für Luft und Raumfahrt Geb. Plataforma Solar de Almeria (DLR-PSA), Raum 1 Ctra. de Senés s/n ES-04200 Tabernas/Almeria
Auftragsnummer:	20547788
Anzahl der Seiten des Kalibrierscheins	4

Die Kalibrierung erfolgte unter Berücksichtigung der Anforderungen der DIN EN ISO/IEC 17025 mit Messmitteln die im Sinne der DIN EN ISO 9001 und DIN EN ISO 10012 auf Nationale Normale rückführbar sind. Die regelmäßige Überprüfung durch die zertifizierten und akkreditierten Institutionen sichert, dass die Rückführbarkeit aufrecht erhalten wird.

Prüfer: T.Künstner

Datum: 03.01.2017

Kalibriereinrichtung / Prüfnormale

1	Referenzgewicht	Gewichtssatz von 2,5 g – 10 kg, Klasse M1, SN:4840416, 73118-D-K-15192-01-00-2016-4
		Gewichtssatz von 2,5 g – 10 kg, Klasse M1, SN:4840416, 73119-D-K-15192-01-00-2016-4
		Gewichtssatz 100g – 10 kg, Klasse M1, SN: 4900416, 73120-D-K-15192-01-00-2016-04
		Gewichtssatz 100g – 10 kg, Klasse M1, SN: 4910416, 73121-D-K-15192-01-00-2016-04
2	Werkstoffprüfmaschine	ZD20EDC, SN:04/M06, 5759-D-K-17452-01-01, 2016-10

Angaben zur Kalibrierung

Umgebungstemperatur   21 °C± 1,5 °C

Kalibrierverfahren /Messbedingungen

Der 6-Achsen Kraft-Momentensensor Typ K6D175 wurde in Reihe mit einem Referenzgewicht sowie mit einer Werkstoffprüfmaschine belastet. Die Richtung der Referenzkräfte und Referenzmomente auf den Sensor wurde durch unterschiedliche Montagepositionen des Mehrkomponenten-Sensors in der Kalibriervorrichtung sichergestellt.

Als Anzeige wurde der Messverstärker GSV-1A8USB K6D/M16 (15156211) verwendet.

Zur Ermittlung der Kalibriermatrix wurden aus 48 Messreihen 6 linear unabhängige Lastvektoren mit Hilfe des Kalibriervorrichtung aufgebracht.

Vor jeder Belastung mit einem Lastvektor wird ein Nullabgleich durchgeführt.

Zustand der Kalibriergegenstände

Gegenstand	Typ	S/N	Zustand
6-Achsen Kraft-Momentensensor	K6D175 10kN/1kNm	15401935	Gebraucht/Rekalibrierung
Messverstärker	GSV-1A8USB K6D/M16	15156211	Gebraucht/Rekalibrierung

Nullpunkterfassung

Kanal	1	2	3	4	5	6
mV/V	0,0075	0,0160	0,0146	0,0037	0,0141	0,0063

Kalibriermatrix

Die Kalibriermatrix beschreibt den Zusammenhang zwischen den angezeigten Spannungen des Messverstärkers an den Kanälen 1 bis 6 (Bezeichner „ai0" bis „ai5") und den Komponenten 1 bis 6 (Fx, Fy, Fz, Mx, My, Mz) des Lastvektors.

		Kanal					
		1	**2**	**3**	**4**	**5**	**6**
Referenz							
Fx in N/V		6,10	1988,56	-1971,82	8,49	1954,07	-2055,73
Fy in N/V		-2161,41	1223,06	1196,94	-2338,29	1204,39	1231,05
Fz in N/V		-3175,05	-3057,37	-3257,57	-3212,60	-3216,90	-3174,84
Mx in Nm/V		-115,66	-115,22	-123,88	-124,54	226,16	222,88
My in Nm/V		-194,49	-193,88	200,39	199,22	5,30	8,36
Mz in Nm/V		128,81	-136,12	131,60	-137,26	131,52	-138,73

Abbildung 1: Kalibriermatrix in N/V und Nm/V

		Kanal					
		1	**2**	**3**	**4**	**5**	**6**
Referenz							
Fx in N / mV/V		15,24	4971,41	-4929,54	21,22	4885,18	-5139,34
Fy in N / mV/V		-5403,52	3057,65	2992,35	-5845,72	3010,98	3077,63
Fz in N / mV/V		-7937,62	-7643,42	-8143,92	-8031,49	-8042,25	-7937,10
Mx in Nm / mV/V		-289,14	-288,05	-309,71	-311,34	565,39	557,21
My in Nm / mV/V		-486,21	-484,71	500,96	498,05	13,25	20,90
Mz in Nm / mV/V		322,03	-340,30	329,00	-343,15	328,81	-346,83

Abbildung 2: Kalibriermatrix in N/mV/V und Nm/mV/V

Koordinatenursprung

Der Ursprung des Koordinatensystems befindet sich im Zentrum des Sensors auf der Oberfläche der oberen Seite. An der Stelle des Ursprungs ist eine Gravierung vorhanden.
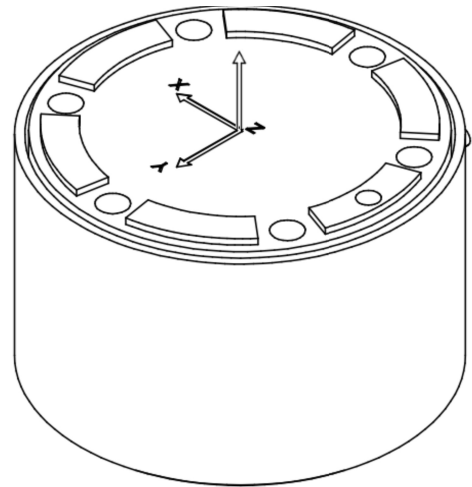

Abbildung 3: Ursprung des Koordinatensystems

Messunsicherheit

Mit einer Wahrscheinlichkeit von 95% besitzen die Messergebnisse folgende Unsicherheit.

	Fx	Fy	Fz	Mx	My	Mz
Nennlast	2350 N	800 N	2050 N	400 Nm	400 Nm	300 Nm
Messunsicherheit	±6N	±12N	±40N	±3,0Nm	±1,5Nm	±2,0Nm

Temperaturtest

	Nullpunktsignal in mV/V					
Temperatur	**Kanal 1**	**Kanal 2**	**Kanal 3**	**Kanal 4**	**Kanal 5**	**Kanal 6**
20 °C	0,0000	0,0000	0,0000	0,0000	0,0000	0,0000
80 °C	-0,0072	-0,0108	0,0077	-0,0109	-0,0085	-0,0256
20 °C	-0,0001	-0,0012	0,0003	-0,0036	-0,0021	0,0013